Aus dem Institut für Vegetative Anatomie
der Medizinischen Fakultät Charité – Universitätsmedizin Berlin

DISSERTATION

Epoxyeicosatriensäuren sind Ziel der durch das antidiuretische Hormon induzierten Signalgebung im Nierenmark

zur Erlangung des akademischen Grades
Doctor medicinae (Dr. med.)

vorgelegt der Medizinischen Fakultät
Charité – Universitätsmedizin Berlin

von

Tom Röschel

aus Berlin

Datum der Promotion: 4. März 2022

Inhaltsverzeichnis

8.

1. Zusammenfassung der Dissertation

1.1. Abstrakt (englisch)

Maintenance of the osmotic homeostasis by arginin-vasopressin (AVP) mediated antidiuresis requires the coordinated action of renal epithelial and vascular structures. In the thick ascending limb of the loop of Henle, AVP increases the transport activity of the Na^+, K^+, $2Cl^-$ cotransporter (NKCC2), thereby enabling the generation of the osmotic gradient necessary for urine concentration. AVP also reduces renal medullary blood flow by causing vasoconstriction of glomerular arterioles and descending vasa recta in order to control the gradient. Locally produced epoxyeicosatrienoic acid (EET) regioisomers inhibit TAL transport activity and cause vasodilation of the renal microvasculature to counteract the effects of AVP. We hypothesized that AVP has a regulatory function in determining renal EET levels. To this end we used Brattleboro rats with central diabetes insipidus (DI) due to a hereditary loss-of-function mutation in the AVP-gene. Animals were treated for 3 days with the selective AVP type-2 receptor agonist desmopressin (dDAVP; 5ng/h) to study medullary EET levels by mass spectrometry-based lipidome analysis. Medullary gene expression was analyzed by an Affymetrix mRNA microarray. Treatment of DI rats with dDAVP resulted in the expected drop in urine flow along with increased NKCC2 mRNA (+130 ± 7 %, $p<0,05$) and protein (+70 ± 5%, $p<0,05$) levels. Regioisomers of EET were decreased (5,6-EET, -56 ± 3%; 11,12-EET, -50 ± 3,4%; and 14,15-EET, -60 ± 3,7%; $p<0,05$). Calcium-independent group VIA phospholipase A_2 (iPLA2), which reflects EET synthesis, was significantly reduced (mRNA, -30 ± 3; protein, -65 ± 7%; $p<0,05$), and soluble epoxide hydrolase (sEH), the primary EET-degrading enzyme, was increased (mRNA, +160 ± 37%; protein, +120 ± 26%; $p<0,05$). The presence of both enzymes in ADH-sensitive nephron segments was confirmed by immunolocalization studies. Functional relevance of 14,15-EET for TAL transport activity was demonstrated in microperfusion studies of isolated murine TAL segments. Administration of 14,15-EET (1µmol/l) resulted in a significant reduction of transport activity as a function of ambient chloride concentration (-30% at 147 mmol/l Cl, -70% at 30 mmol/l Cl). Furthermore, treatment of cultured rat TAL cells with selective iPLA2 inhibitor (S)-bromoenol lactone (S-BEL; 5µmol/l 1h) increased phosphorylation (+189 ± 6%, $p<0,05$) and membrane insertion of NKCC2. In sum, these results demonstrate an inhibitory effect of AVP on renal EET levels which may result

from their decreased synthesis and augmented degradation. Downregulation of iPLA2 and activation of sEH may therefore contribute to ADH-mediated antidiuresis.

1.2. Abstrakt (deutsch)

Die Aktivierung der Harnkonzentrierung durch das antidiuretische Hormon (ADH) erfordert die Koordination renaler, epithelialer und vaskulärer Strukturen. Im dicken aufsteigenden Ast der Henle Schleife (TAL) stimuliert ADH die Transportaktivität des Na^+, K^+, $2Cl^-$ Kotransporters (NKCC2). Dadurch wird in der Medulla der Aufbau eines osmotischen Gradienten im Interstitium ermöglicht, welcher die treibende Kraft für die anschließende Wasserresorption im Sammelrohr darstellt. ADH bewirkt weiterhin eine Vasokonstriktion der glomerulären Arteriolen und absteigenden Vasa recta. Die resultierende Reduktion des medullären Blutflusses verhindert ein Auswaschen des osmotischen Gradienten. Lokal generierte Regioisomere der Epoxyeicosatriensäure (EET) können antagonistische Effekte zu ADH entfalten, indem sie die Transportaktivität des TAL hemmen und eine Vasodilatation renaler Widerstandsgefäße auslösen. Hier wurde die Hypothese geprüft, dass ADH eine regulierende Funktion für die lokalen EET-Spiegel ausübt. Ratten mit hereditärem zentralen Diabetes insipidus (DI) wurden für 3 Tage mit dem ADH V2-Rezeptoranalog Desmopressin (dDAVP; 5ng/h) behandelt. Die Messung medullärer EET-Gewebekonzentrationen erfolgte mittels Massenspektrometrie. Die medulläre Genexpression wurde durch Affymetrix mRNA-*Microarray* untersucht. Die Behandlung von DI-Ratten mit dDAVP führte zur Reduktion der Diurese. Gleichzeitig war die Expression von NKCC2 auf mRNA (+130 ± 7 %, $p<0,05$) und Proteinebene (+70 ± 5%, $p<0,05$) erhöht. Die EET-Gewebekonzentration war dagegen signifikant reduziert (5,6-EET: -56 ± 3%; 11,12-EET: -50 ± 3,4%; 14,15-EET: -60 ± 3,7%; $p<0,05$). Die *Microarray* Analyse zeigte eine signifikante Reduktion der Kalzium-unabhängigen Phospholipase A2 Gruppe VIA (iPLA2). Dies konnte über *Real time* PCR (-30 ± 3%, $p<0,05$) und *Western blot* (-65 ± 7%, $p<0,05$) bestätigt werden. Epoxidhydrolase (sEH), die den EET-Abbau katalysiert, war gesteigert (mRNA: +160 ± 37%, Protein: +120 ± 26%; $p<0,05$). Beide Enzyme wurden immunhistochemisch in ADH-sensitiven Nephronsegmenten lokalisiert. Der Einfluss von 14,15-EET auf die TAL-Transportaktivität wurde durch Mikroperfusionsstudien an isolierten TAL-Segmenten der Maus untersucht. Hier führte

die Behandlung mit 14,15-EET (1µmol/l, 30 min) zu einer signifikanten Reduktion der Transportaktivität in Abhängigkeit von der umgebenen Chloridkonzentration (-30% bei 147 mmol/l Cl, -70% bei 30 mmol/l Cl). Eine selektive Inhibition von iPLA2 mit S-Bromoenol Lacton (S-BEL; 5µmol/l 1h) in kultivierten medullären TAL-Zellen der Ratte führte zu einer Zunahme der aktivierenden Phosphorylierung von NKCC2 (+189 ± 6%, $p<0,05$) und bewirkte die Membraninsertion des Proteins. Zusammenfassend zeigen diese Befunde zum ersten Mal einen inhibitorischen Effekt von ADH auf die Gewebekonzentration von EET. Die Reduktion von EET ist dabei sowohl auf eine verminderte Synthese als auch auf einen vermehrten Abbau zurückzuführen. Die ADH-abhängige Regulation von iPLA2 und sEH stellt damit einen neuen Mechanismus der ADH-induzierten Harnkonzentrierung dar.

1.3. Einführung und Zielstellung

Die Regulation der Harnkonzentrierung durch das antidiuretische Hormon (ADH) ermöglicht eine bedarfsgerechte Steuerung der renalen Wasserausscheidung und ist damit essentiell für die osmotische Homöostase des Körpers. Fehlregulationen im ADH-Signalweg führen zu spezifischen Krankheitsbildern wie dem Syndrom der inadäquaten Antidiurese oder dem Diabetes insipidus (1,2) und sind an der Entstehung der arteriellen Hypertonie, dem kardiorenalen Syndrom und der diabetischen Nephropathie beteiligt (3,4,5,6).

Strukturelle Grundlage für den Prozess der Harnkonzentrierung ist die enge räumliche und funktionelle Beziehung zwischen epithelialen und vaskulären Strukturen der renalen Medulla. Die Stimulation basolateraler, membranständiger V2R Rezeptoren in der dicken aufsteigenden Henle‘schen Schleife (TAL) bewirkt eine aktivierende Phosphorylierung des Na^+, K^+, $2Cl^-$ Kotransporters (NKCC2) und steigert damit den transepithelialen Salztransport (7). Die resultierende Akkumulation von NaCl im Interstitium der Medulla stellt die treibende Kraft für die Gegenstrommultiplikation von Osmolyten und der nachfolgenden medullären Wasserresorption durch das Sammelrohr dar (8,9). Gleichzeitig wird über vaskuläre Rezeptoren der medulläre Blutfluss durch Kontraktion der absteigenden Vasa recta reduziert, um ein Auswaschen des osmotischen Gradienten zu verhindern. Die Kombination aus aktiven, energieverbrauchenden Transportprozessen bei gleichzeitig reduzierter Durchblutung

führt zu einer physiologisch geringen Sauerstoffkonzentration im Nierenmark. Beteiligte Gewebe sind daher bei Hypoxie durch pathophysiologische Belastung gefährdet und können akut oder chronisch geschädigt werden (10,11).

Mechanismen, die eine lokale Modulation der systemischen ADH-Signale und eine Koordination der unterschiedlichen ADH-Signalwege ermöglichen, werden daher intensiv erforscht. Von besonderem Interesse sind dabei lokal produzierte Eicosanoide wie Prostaglandin E2 (PGE2), 20-Hydroxeicosatetraensäure (20-HETE) und Epoxyeicosatriensäuren (EET) (12,13,14). Diese werden in einer Multienzymkaskade aus Arachidonsäure (AA) gebildet. Als geschwindigkeitsbestimmende Schrittmacherenzyme dieser Kaskade gelten Phospholipasen, welche die Freisetzung von AA aus Lipiden der Zellmembran katalysieren (15). Die freigesetzte AA wird im Anschluss durch verschiedene Oxygenasen kompetitiv in spezifische Eicosanoide metabolisiert (16). Der Abbau der Eicosanoide erfolgt entweder spontan oder wird ebenfalls enzymatisch reguliert (16,17). Die beteiligten Enzyme können dabei sowohl auf transkriptioneller als auch auf posttranslationaler Ebene reguliert werden. Aufgrund der Vielzahl der biologisch aktiven Metabolite und der an ihrer Produktion beteiligten Enzyme entstehen ausgesprochen komplexe Regelkreise, welche durch die isolierte Untersuchung einzelner Metabolite und Enzyme nur unzureichend verstanden sind.

Ziele der vorliegenden Arbeit waren die Charakterisierung der ADH-abhängigen Regulation von Lipidmediatoren durch Massenspektroskopie-basierte Lipidomik und die Erfassung der an ihrer Bildung beteiligten Enzyme durch *Microarray*-basierte Genexpressionsanalyse (18,19).

1.4. Methodik

Tierversuche und Gewebeaufbereitung

Zur Untersuchung ADH-vermittelter Effekte im TAL wurde ein etabliertes Rattenmodell (Diabetes insipidus [DI]-Ratten mit zentralem ADH Mangel) verwendet, dessen Zulassung durch die Tierversuchskommission des Landes Berlin (LaGeSo) genehmigt war (G006-02/05 und G0285/10). Adulte DI-Ratten, wurden für drei Tage mit dem ADH-Analogon dDAVP (5ng/h) oder mit 0,9% NaCl via subkutan implantierter osmotischer Minipumpen (Alzet-minipump, Model 2001, Charles River) behandelt (20). Am Ende des Behandlungszeitraums wurden ein Teil der Tiere anästhesiert (intraperitoneale

Injektion mit Pentobarbital 0.06 mg/g Körpergewicht) und die Nieren mittels retrograder Perfusionsfixierung fixiert für die Proteinvisualisierung durch Immunfluoreszenz. Die retrograde Perfusionsfixierung erfolgte nach einem etablierten Protokoll, nach welchem ein Katheter in der abdominalen Aorta unterhalb der Nierenarterien fixiert wird und anschließend mit einem Druck von 230 cm H_20 die Perfusion mit 3% Paraformaldehyd (PFA) erfolgt (21). Die Nieren wurden im Anschluss herauspräpariert, die Nierenkapsel wurde stumpf entfernt und das Gewebe anschließend für 24 Stunden bei 4°C in Sucrose-PBS Puffer belassen bevor es in Isopentan bei -80°C gelagert wurde. Die restlichen Tiere wurden mittels tiefer Narkose und Genickbruch getötet. Hierbei wurden die Nieren sofort herauspräpariert, in Cortex, innere- und äußere Medulla separiert und in flüssigem Stickstoff schockgefroren.
Weitere Nierengewebe stammten von auf gleiche Art PFA-perfundierten C57BL/6 und BALB/c Mäusen und Sprague Dawley (SD) Ratten (18,19,22). Humanes Nierengewebe wurde nach schriftlicher Einwilligung der Patienten aus dem Resektat einer Tumornephrektomie gewonnen und verwendet; dieses Gewebe wurde in 3% Paraformaldehyd immersionsfixiert (7). Zur Herstellung von Kryostatschnitten wurden alle Gewebe nach Immersion in Sucrose in Isopentan eingefroren und bei -26°C an einem Kryostat-Mikrotom (Leica CM3050 S, Wetzlar, Deutschland) mit einer Dicke von 5µm geschnitten und auf Glasobjektträger aufgezogen.

Direkte Eicosanoidmessung

EET und andere ungesättigte Fettsäure-Derivate wurden über Flüssigchromatographie (Agilent 1200) mit Massenspektrometriekopplung (Agilent 6410) durch die Firma Lipidomix GmbH am Campus Berlin-Buch gemessen. Das Nierenmark der DI-Ratten wurde hierfür in einer Wasser-Methanol Suspension gelöst und bei pH 6 gepuffert. Die Lösung wurde in eine Bond-Elut-Certify-II-Feststoffextraktionssäule (Phenomenex, Torrance, USA) überführt und die erhaltenen Fettsäure-Derivate dann aufgereinigt.
Vorrangig wurden hieraus Eicosanoide und Linolsäurederivate (Epoxyoctadeca-Monoensäuren [EPOME] und Dihydroxyoctadecensäuren [DiHOME]) bestimmt, welche als etablierter Marker für die Enzymaktivität der sEH Verwendung finden (23).

Microarray zur ADH-Wirkung an DI-Ratten

Um neue Regulationsmechanismen der ADH-vermittelten Antidiurese zu identifizieren, wurde eine Microarray-Genexpressionsstudie an dDAVP-behandelten DI-Ratten

durchgeführt. mRNA aus Ratten-Nierenmark wurde mittels Quiagen RNeasy mini kit isoliert. cDNA und cRNA wurden nach dem Affymetrix Standardprotokoll hergestellt. Die Analyse wurde am Zentrum für Medizinische Forschung der Universität Mannheim mittels GenChip® Rat Genome 230 2.0 Array (Affymetrix, Santa Clara, USA) fertiggestellt. Die erhobenen Daten wurden in die *Gene Expression Omnibus Database* hochgeladen (GEO Zugangsnummer: GSE34225).

real-time PCR und Western blot

Zur Validierung der Microarray Daten wurden *Real-time* PCR und *Western blot* eingesetzt. Extrahierte RNA aus Rattenniere wurde mit dem cDNA Synthese Kit (Applied Biosystems, Darmstadt, Deutschland) über *reverse* Transkription in cDNA umgeschrieben. Quantitative TaqMan *real-time* PCR wurde im 7500 fast real-time PCR System (Applied Biosystems) nach Herstelleranleitung durchgeführt. TaqMan Sonden wurden von Applied Biosystems (iPLA2: Rn.01485101, sEH: Mm.00514706, NKCC2: Rn.01504428, GAPDH: 4352338E) generiert (18,19), GAPDH mRNA Spiegel wurden parallel bestimmt und dienten als Beladungskontrolle. mRNA Spiegel wurden mithilfe der $2^{-\Delta\Delta CT}$ Methode berechnet.

Antigen	**Verdünnung**	**Hersteller**	**Seriennummer**
NKCC2	1:500	Ellison*	(2.1)
phosphoNKCC2	1:5000	Pineda**	(pT2)
β-Aktin	1:20000	Sigma	A 5441
iPLA2	1:500	Sigma	HPA 001171
sEH	1:500	Sigma	HPA 023094

Tabelle 1: Primärantikörper zur Proteinquantifizierung mittels Western blot
Angegeben sind die verwendeten Primärantikörper für: Na^+, K^+, $2Cl^-$ Kotransporter (NKCC2), phosphorylierter Na^+, K^+, $2Cl^-$ Kotransporter (phosphoNKCC2), β-Aktin, Ca-unabhängige Phospholipase A_2 Typ VI A (iPLA2) und die lösliche Epoxidhydrolase (sEH) mit der eingesetzten Verdünnung im *Western blot* und den Seriennummern der Hersteller.* 2.1 Antikörper zur Detektion von NKCC2 wurde in Zusammenarbeit mit dem Labor von Prof. Ellison entwickelt und publiziert (23). ** pT2 Antikörper zur Detektion von phosphoNKCC2 wurde durch die Arbeitsgruppe von Prof. Bachmann, in Zusammenarbeit mit Pineda Antikörper-Service (Berlin, Deutschland) entwickelt und publiziert (7).

Proteindetektion und -quantifizierung mittels *Western blot* erfolgte nach dem laborinternen Standard. Unter konstanter Kühlung wurde das Gewebe zerkleinert und in Homogenisierungspuffer (250 mM Saccharose, 10 mM Triethanolamin, Complete

Protease Inhibitor Cocktail Tabl. (Roche, Mannheim)) gelöst. Das Zellhomogenat wurde mittels kurzer Ultraschallimpulse lysiert und die Zellkerne wurden bei 800g abzentrifugiert. Gel-Elektrophorese wurde in 10% SDS-Polyacrylamid Gel durchgeführt, anschließend erfolgte der Elektrotransfer auf eine Nitrozellulosemembran. Proteindetektion erfolgte mit den entsprechenden Primärantikörpern (siehe Tabelle 1) Densitometrische Auswertungen erfolgten mit der Alpha Imager Software (Cell Biosciences, Santa Clara, USA). Alle Ergebnisse wurden gegen β-Aktin normalisiert.

Immunfluoreszenz

Die Lokalisationsstudien für iPLA2 und sEH erfolgten mittels indirekter Immunfluoreszenz. Primärantikörper wurden in 5% entfettetem Milchpulver in PBS für 2 Stunden auf den histologischen Präparaten belassen. Sekundärantikörper waren Carbocyanin (CY2) und Indocarbocyanin (CY3) gekoppelt. Alle Sekundärantikörper wurden von Jackson Research Labs (West Grove, USA) erworben und in einer Verdünnung von 1:250 verwendet. Bei der Doppelimmunfärbung wurden zwei Primärantikörper unterschiedlicher Wirtsspezies und zwei Sekundärantikörper verwendet. Die verwendeten Primärantikörper sind in der Tabelle 2 aufgeführt.

Antigen	**Verdünnung**	**Hersteller**	**Seriennummer**
NKCC2	1:2000	Ellison*	(2.1)
phsophoNKCC2	1:5000	Pineda**	(pT2)
NCC	1:100	Ellison***	
AQP2	1:100	Santa Cruz	SC 9882
COX2	1:200	Santa Cruz	SC 1746
Calbindin	1:1000	Santa Cruz	SC 9848
iPLA2	1:50	Sigma	HPA 001171
sEH	1:50	Sigma	HPA 023094

Tabelle 2: Primärantikörper zur Proteindetektion mittels Immunfluoreszenz
Angegeben sind die verwendeten Primärantikörper für: Na^+, K^+, $2Cl^-$ Kotransporter (NKCC2), phosphorylierter Na^+, K^+, $2Cl^-$ Kotransporter (phosphoNKCC2), Na-Cl-Kotransporter (NCC), Aquaporin-2 (AQP2), Cyclooxygenase-2 (COX2), Calbindin, Ca-unabhängige Phospholipase A_2 Typ VI A (iPLA2) und die lösliche Epoxidhydrolase (sEH), die eingesetzten Verdünnungen in der Immunhistochemie und die Seriennummern der Hersteller. * 2.1 Antikörper zur Detektion von NKCC2 wurde in Zusammenarbeit mit dem Labor von Prof. Ellison entwickelt und publiziert (23). ** pT2 Antikörper zur Detektion von phosphoNKCC2 wurde durch die Arbeitsgruppe von Prof. Bachmann, in Zusammenarbeit mit Pineda Antikörper-Service (Berlin, Deutschland) entwickelt und publiziert (7). *** Antikörper zur Detektion von NCC wurde in Zusammenarbeit mit dem Labor von Prof. Ellison entwickelt und publiziert (22,25).

Zellnuklei wurden mit dem Fluoreszenzfarbstoff 4',6-Diamidin-2-phenylindol (DAPI) markiert. Auswertung der Immundoppelmarkierung erfolgte konfokal am Zeiss LSM Exciter confocal microscope und der ZEN 2008 Software (Carl Zeiss, Jena) (18,19,22).

Zellkulturversuche

Ein bereits etabliertes Zellmodell mit immortalisierten Zellen aus den medullären Anteilen der dicken aufsteigenden Henle'schen Schleife (mTAL), wurde für unsere Versuche benutzt. Eine detaillierte Beschreibung erfolgte durch Ferreri et al. Die mTAL-Zellen exprimieren das TAL-spezifische Tamm-Horsfall Glykoprotein und den Bumetanid sensitiven NKCC2 (26). Eine Stimulation der mTAL-Zellen mit ADH führte zu einer signifikanten Steigerung der Phosphorylierung von NKCC2.

Zellen wurden bei 37°C und 5% CO2 bis zur Konfluenz in Petrischalen und zur Mikroskopie auf Aminosilan beschichteten Glasscheiben belassen und mit Renal Epithelial Growth Cell Medium (PromoCell GmbH, Heidelberg, Deutschland) inkubiert. Das verwendete Medium wurde 48-stündlich erneuert. Die mTAL Zellen wurden mit dem iPLA2 spezifischen Inhibitor, dem S-Enantiomer des Bromoenol Lacton (S-BEL) (CAS 478288-94-7, Cayman Chemicals) in einer Konzentration von 5µmol/l für eine Stunde behandelt (18). Kontrollen wurden mit dem Lösungsmittel Dimethylsulfoxid (DMSO) behandelt.

Zur Proteinextraktion wurden die geernteten Zellen unter Kühlung in Triethanolamin-haltigem Homogenisierungspuffer homogenisiert und unter der Anwendung von Ultraschall lysiert. Das weitere Prozedere erfolgte analog zum *Western blot* Protokoll.

Die Lokalisation des NKCC2 bzw. des phosphorylierten NKCC2 (phosphoNKCC2) wurde mittels Immunfluoreszenz bestimmt. Hierfür wurden die auf Glas gewachsenen mTAL Zellen in 3% PFA fixiert. Das Standardprotokoll für Immunfluoreszenz wurde angewandt.

Mikroperfusionsstudien an isolierten TAL-Segmenten der Maus

Um einen funktionellen Nachweis zwischen lokaler EET und der Transportaktivität im TAL zu liefern, kooperierten wir mit der Arbeitsgruppe von Prof. M. Bleich am Kiel Marine Science der Christian-Albrechts-Universität zu Kiel. Kortikale TAL Segmente von C57/BL6 Mäusen wurden präpariert und in 1 µmol/l 14,15-EET (Cayman Chemicals, Ann Arbor, USA), 1µmol/l 14,15-Dihydroxyeicosatriensäuren (DHET) (Cayman Chemicals) oder dem Lösungsmittel Ethanol für 30 Minuten belassen. Die

Tubuli wurden in eine doppelläufige Perfusionspipette eingespannt und isoliert perfundiert. Über den einen Schenkel wurde das transepitheliale Potential gegenüber dem Umgebungsmedium gemessen und über den zweiten Schenkel ein definierter Strompuls appliziert. Hieraus wurde der transepitheliale Widerstand berechnet während, die Chloridkonzentration im Medium zuerst basolateral und dann luminal reduziert wurde (19,27). Eine Veränderung im transepithelialen Widerstand spiegelt eine veränderte Transportkapazität durch NKCC2 wieder (19,28).

1.5. Ergebnisse

dDAVP Behandlung in DI-Ratten

Zur Untersuchung metabolisch aktiver Fettsäuremetabolite und deren Synthese und Abbau bestimmender Enzyme wurden DI-Ratten für drei Tage mit dem ADH-Analogon dDAVP behandelt. Erwartungsgemäß war hierdurch die Urinmenge der Tiere signifikant reduziert (-94 ± 24 %, $p < 0.05$). Zudem kam es zu einer Verringerung der Plasmaosmolarität, einer gesteigerten Urinosmolarität, sowie zu einem Anstieg der Kreatininclearance (10). Gleichzeitig konnte eine signifikante Zunahme sowohl an NKCC2 mRNA (+70 ± 5%, $p < 0.05$) als auch an NKCC2 Proteingehalt (+130 ± 7%, $p < 0.05$) detektiert werden (18). Des Weiteren konnte ein signifikanter Anstieg von phosphoNKCC2, welches die transportaktive Form des NKCC2 darstellt (7), im *Western blot* der äußeren Medulla gezeigt werden (+130 ± 32%, $p < 0.05$) (18). Diese Ergebnisse verdeutlichen, dass es unter dDAVP-Gabe zu einer Natriumretention im TAL und, als Folge, zur Antidiurese im Tiermodell kam. Dieses zuvor schon validierte Modell eignete sich dementsprechend für die Untersuchungen zur ADH-abhängigen Regulation aktiver Fettsäuremetabolite bei der Harnkonzentrierung (29).

Massenspektrometrie ungesättigter Fettsäuren unter dDAVP Therapie

DDAVP Gabe in DI-Ratten führte zu einem signifikanten Abfall der Spiegel von 5,6-EET (12.8 ± 3.2 ng/g vs. 35.7 ± 9.5 ng/g, $p < 0.05$), 11,12-EET (16.7 ± 3.3 ng/g vs. 38.4 ± 9.7 ng/g, $p < 0.05$) und 14,15-EET (11.2 ± 3 ng/g vs. 34.7 ± 9.2 ng/g, $p < 0.05$) im Nierenmark (19). Die Reduktion der 8,9-EET Spiegel war nicht siginifikant (17.4 ± 4 ng/g vs. 44 ± 13.7 ng/g, $p = 0.08$) (19). Die Spiegel der Linolsäurederivate waren ebenfalls reduziert (9,10-EPOME: 69 ± 14 ng/g vs. 254 ± 60 ng/g; 12,13-EPOME: 36 ±

11 ng/g vs. 166 ± 44 ng/g; $p < 0.05$) (19). Ihre Abbauprodukte waren nicht signifikant verändert (9,10-DIHOME: 52 ± 8.8 ng/g vs. 47 ± 8.7 ng/g, $p = 0.7$; 12,13-DIHOME: 85 ± 25 ng/g vs. 56 ± 14 ng/g; $p = 0.4$) (19). Das Verhältnis zwischen DIHOMEs und EPOMEs war sowohl für 9,10 DIHOME / 9,10 EPOME (0.85 vs. 0.23; $p < 0.05$), als auch für 12,13 DIHOME / 12,13 EPOME (2.54 vs. 0.43; $p < 0.05$) in den DI-Ratten nach dDAVP-Gabe erhöht (19). Es kommt also zu einem aktiven Abbau der renalen EET und EPOME unter dDAVP-Gabe, vermutlich auf Grund einer Aktivierung der sEH (19,30). Erwartungsgemäß waren PGE2 Spiegel erhöht, während Thromboxan und 20-HETE nicht nachgewiesen werden konnten (19).

Microarray Daten

Die Genexpressionsanalyse der 3 Tage lang mit dDAVP behandelten DI-Ratten verdeutlichte, dass eine Vielzahl an Enzymen des Fettsäurestoffwechsels durch ADH reguliert werden. mRNA-Mengen diverser Phospholipasen waren unter dem Einfluss von dDAVP reguliert; so war die Phospholipase A2 Gruppe IVA (cPLA2) heraufreguliert und die Kalzium-unabhängige Phospholipase A2 Gruppe VIA (iPLA2) herabreguliert (18). Die an der EET Synthese beteiligten Cytochrom P450 (CYP) Monooxygenasen waren nicht verändert (19). sEH und Cyclooxygenase 2 (COX2) mRNA-Mengen waren signifikant gesteigert (siehe Tabelle 3) (19).

Gen	**x-fache Expression**	**p-Wert**
Phospholipase A_2 Gruppe IV A	1,98	< 0.05
Kalzium-unabhängige Phospholipase A_2 Typ VIA	0,77	< 0.05
Cytochrom P450 Familie 2, Unterfamilie c, Isoenzym 11	1,3	0,68
Cytochrom P450 Familie 2, Unterfamilie c, Isoenzym 23	0,97	0,52
Cytochrom P450 Familie 2, Unterfamilie j, Isoenzym 3	0,99	0,8
Cytochrom P450 Familie 2, Unterfamilie j, Isoenzym 4	0,78	< 0.05
Cyclooxygenase 2	2,2	< 0.05
Lösliche Epoxidhydrolase	2,45	< 0.05

Tabelle 3: Microarray Daten diverser Enzyme aus dem Fettsäuremetabolismus
Angegeben sind Veränderungen der mRNA-Mengen von Enzymen des Fettsäuremetabolismus nach dDAVP-Gabe in DI-Ratten, ausgedrückt als das x-fache der Kontrolltiere.

iPLA2 und sEH unter dem Einfluss von dDAVP

Im *Western blot* wurde eine Reduktion der iPLA2 (-65 ± 7%, $p < 0.05$) und eine Zunahme der sEH (+120 ± 26%, $p < 0.05$) im Vergleich zu den Kontrolltieren nachgewiesen (18,19). In Einklang mit diesen Ergebnissen waren in den dDAVP behandelten Tieren die iPLA2 mRNA Konzentration reduziert (-30 ± 3%, $p < 0.05$) und die sEH mRNA Konzentration gesteigert (+160 ± 37%, $p < 0.05$) (18,19).

Lokalisation der iPLA2

Western blot Analysen an homogenisierten Nieren von Sprague-Dawley Ratten zeigten immunreaktive iPLA2-Produkte vorrangig bei 70 kDa neben weiteren Banden bei 85, 63, 52 und 48 kDa (18). Bei Trennung von Mark und Rinde waren die 70 kDa Isoform dabei vorrangig in der äußeren Medulla und die 85 kDa Isoform hauptsächlich in der inneren Medulla nachweisbar (18). In den kortikalen Anteilen war nur ein schwaches iPLA2 Signal nachweisbar (18).

Das zelluläre Verteilungsmuster der iPLA2 wurde mittels Immunfluoreszenz in Nieren von Mensch, Maus und Ratte weiter untersucht. Es zeigte sich ein vorrangig zytoplasmatisches Verteilungsmuster distal in den Henle'schen Schleifen der äußeren Medulla (18). Zellen des proximalen Tubus und Endothelzellen zeigten kein iPLA2 Signal (18). Eine Doppelimmunfärbung mit dem TAL-spezifischen Transporter NKCC2 belegte die Expression der iPLA2 im medullären und kortikalen TAL mit Ausnahme der Macula densa (MD) (18). Weiter wurde in der Pars convoluta des distalen Tubulus (DCT) die Kolokalisation von iPLA2 mit dem Thiazid-sensitivem Natrium Chlorid Kotransporter (NCC) nachgewiesen (18). Das Kalziumtransportprotein Calbindin, welches im DCT-2, Verbindungstubulus (CNT) und frühen Sammelrohr (CD) lokalisiert ist, ließ sich mit anti-iPLA2 ebenfalls doppelmarkieren; die Schaltzellen waren hiervon ausgenommen (18).

Die Spezifität des iPLA2 Antikörpers wurde im *Western blot* im Gewebe von iPLA2 *knockout*- Mäusen bestätigt (18).

Lokalisation der sEH

Western blot Analysen an präparierten Nieren von Sprague-Dawley Ratten zeigte eine dominante Bande der sEH bei ca. 63 kDa, welche im Nierenkortex, der äußeren- und der inneren Medulla nachweisbar war (19). Vergleichend wies die innere Medulla ein

stärkeres Signal auf, wobei nur hier auch zwei weitere Banden bei 50 kDa und 48 kDa gezeigt werden konnten (19). Immunhistochemisch konnte in der Rattenniere die Verteilung der sEH in allen Nierenzonen nachgewiesen werden (19). Proximale und distale Nephronsegmente waren gefärbt (19). Doppelmarkierungen mit anti-Aquaporin 2 (AQP2) und anti-COX2 zeigten die Lokalisation von sEH in kortikalen Sammelrohrhauptzellen und in der MD (19). NKCC2-positive TAL und NCC-positive DCT Abschnitte wiesen kein sEH Signal auf (19). In der inneren Medulla, in der im *Western blot* das stärkste sEH Signal erschien, waren sowohl CD als auch dünne ab- und aufsteigende Schenkel der Henle Schleife sEH positiv (19). Ähnliche Verteilungsmuster konnten in humanem Nierengewebe gezeigt werden (19).

iPLA2 Inhibition im mTAL Zellkulturmodell

Die physiologische Relevanz einer modifizierten Eicosanoidsynthese wurde an einem mTAL-Zellkulturmodel weiter untersucht. mTAL Zellen wurden mit einem spezifischen Hemmstoff der iPLA2, dem S-BEL behandelt (5µmol/l, 1 Stunde) und die NKCC2 und phosphoNKCC2 Proteinspiegel quantifiziert. Die resultierende Inhibition der iPLA2-abhängigen Arachidonsäurefreisetzung führte im Zellmodell zu einem statistisch signifikanten Anstieg von phosphoNKCC2 (+189 ± 6%, $p < 0.05$) bei unverändertem NKCC2 (18). Immunhistochemisch konnte gezeigt werden, dass es unter der Behandlung mit S-BEL zu einer Verschiebung des phosphoNKCC2 Signals vom Zytosol in Richtung auf die Zellmembran kam (18).

14,15-EET vermittelte TAL-Transportkapazität isolierter Tubuli

Isolierte Tubuli wurden mit 14,15-EET und dem physiologisch inaktiven 14,15-DHET behandelt, um einen direkten Zusammenhang zwischen lokaler Eicosanoidwirkung und TAL Transportkapazität zu untersuchen. Diese ist maßgeblich von der Phosphorylierung und damit der Membraninsertion von NKCC2 abhängig und durch die luminale Chloridkonzentration begrenzt (31,32). Der gemessene Kurzschlussstrom (I'_{sc}) in $\mu A/cm^2$ dient hierbei als Parameter für Transportaktivität und wurde bei 30 mmol/l Cl, entsprechend dem EC_{50} von NKCC2 sowie bei 147 mmol/l Cl untersucht, um die maximale Transportkapazität des Transporters zu erfassen. Eine 30-minütige Behandlung mit 14,15-EET resultierte in einer Reduktion des I'_{sc} auf 70% bei 147 mmol/l Cl, und auf 30% bei 30 mmol/l Cl im Vergleich zu unbehandelten Tubuli (19). Mit dem metabolisch inaktiven 14,15-DHET trat keine Änderung im I'_{sc} ein (19).

Diese Daten belegen eine funktionelle Verbindung zwischen dem antidiuretischem Hormon und den Eicosanoid auf- und abbauenden Enzymen iPLA2 und sEH; ADH erniedrigt somit über ihre Steuerung die medullären Eicosanoidspiegel (18,19).

1.6. Diskussion

Die Konservierung von freiem Wasser durch die ADH-vermittelte Produktion eines konzentrierten Urins gehört zu den essentiellen Aufgaben der Niere und erfordert eine enge Koordination epithelialer und vaskulärer Strukturen. Die Mechanismen und Mediatoren, die diese Koordination vermitteln sind bisher nur unvollständig verstanden.
Ergebnisse früherer Studien zeigten jedoch, dass lokal produzierte Eicosanoide wie PGE2, 20-HETE und EET-Regioisomere die Transportprozesse in zentralen ADH-Zielstrukturen wie TAL, CNT und CD beeinflussen (12,13,14) und dadurch die Effekte der systemischen ADH-Signale modulieren können. Die Bedeutung dieser lokalen Modulation ist bisher nur unzureichend verstanden. Ziel der vorliegenden Arbeit war, die Mechanismen der ADH-abhängigen Regulation des Eicosanoidmetabolismus in der renalen Medulla systematisch zu untersuchen.
Bisherige Arbeiten zur Eicosanoidsynthese im Kontext des renalen Konzentrierungsmechanismus waren vorrangig auf COX2-abhängig gebildete Prostaglandine fokussiert (33). Auch die Ergebnisse der hier vorliegenden Studie zeigen erhöhte Gewebekonzentrationen von PGE2 und eine stimulierte Genexpression von COX2 in der Medulla der dDAVP-behandelten Tiere und bestätigen damit die Ergebnisse früherer Studien (34,35). Zusätzlich konnten signifikant verringerte Spiegel der EET-Regioisomere unter dDAVP-Stimulation im Nierenmarksgewebe gezeigt werden, während deren metabolisch inaktive Abbauprodukte, DHET, vermehrt nachweisbar waren (19). Unsere *Microarray*-Genexpressionsanalyse zeigte passend dazu eine reduzierte Expression von iPLA2 und eine gesteigerte Expression des EET-abbauenden Enzyms sEH und damit Evidenz für eine koordinierte Regulation von Schrittmacherenzymen des EET-Stoffwechsels (18,19).
Die physiologischen Effekte von EET im Herz-Kreislauf-System und in der Niere sind gut untersucht (36). So bewirken sie in ihrer Funktion als *endothelial derived hyperpolarizing factor* eine Vasodilatation von Widerstandsgefäßen (37). In der Niere fungieren 11,12- und 14,15-EET zudem als potente Inhibitoren des epithelialen

Natriumkanals (ENaC) im CNT und CD und bewirken damit eine Salurese (38,39). Die Kombination dieser Effekte führt zu einer kräftigen Blutdrucksenkung und hat damit antagonistische Effekte zum ADH (40).

Im Gegensatz zu den Effekten im CNT und CD sind die Auswirkungen von EET auf die Transportaktivität des TAL weniger gut belegt. He et al. konnten in kultivierten murinen MD-Zellen einen inhibitorischen Effekt von 14,15 EET auf die NKCC2-Transportaktivität nachweisen (41). In Übereinstimmung mit dieser Arbeit zeigen unsere Mikroperfusionsstudien an isolierten murinen TAL-Segmenten einen inhibitorischen Effekt von 14,15-EET auf die Transportaktivität von NKCC2, während 14,15-DHET, das sEH-abhängig gebildete Abbauprodukt von 14,15-EET, keinen Effekt hatte (19). Im Gegensatz zu den hier dargestellten Ergebnissen konnten Grider et al. keinen Effekt von 5,6-EET auf die Transportaktivität von isolierten Ratten-TAL-Segmenten zeigen (42); hier war jedoch die verwendete Dosis von 5,6-EET deutlich geringer als die von uns massenspektrometrisch erfassten Gewebskonzentrationen in den DI-Ratten. Der fehlende Effekt mag daher auf einem Dosisproblem beruhen. Zusammenfassend zeigen die Mikroperfusionsstudien eine inhibitorische Wirkung von EET auf die Transportaktivität im TAL und legen damit einen funktionellen Antagonismus zwischen EET und ADH nahe.

Die primär geschwindigkeitsbestimmenden Enzyme im Syntheseweg aller Eicosanoide sind Phospholipasen, welche die hydrolytische Freisetzung von AA aus Membranphospholipiden katalysieren. Die *Microarray*-Analyse von über 30 bekannten Phospholipasen zeigte eine signifikante Steigerung der Abundanz von cPLA2 mRNA. Studien von Downey et al. charakterisieren die cPLA2 als Schlüsselenzym im PGE2 Metabolismus (43). Da die Bedeutung von COX-2 und PGE2 für den Prozess der Harnkonzentrierung bereits umfassend belegt ist, wurde dieser Punkt in der Arbeit nicht weiter vertieft (43).

Bisher nicht beschrieben war dagegen der inhibitorische Effekt von dDAVP auf die Expression von iPLA2. Die Lokalisation von iPLA2 und die Regulation durch dDAVP wurde daher weiter mittels TaqMan *real-time* PCR, *Western Blot* und Immunlokalisation untersucht (18). In der Rattenniere konnten wir dabei ein ADH-abhängig reguliertes 70 kDa großes Hauptisoenzym nachweisen (18,44). Das Verteilungsmuster der iPLA2 in der Niere von Mensch, Maus und Ratte betraf das distale Nephron und die Sammelrohre; dies stellt einen neuartigen Befund dar (18). Die zuvor beschriebene COX2 abhängige Prostaglandinsynthese in der MD scheint - vom betroffenen Zelltyp

her - anhand dieser Daten als iPLA2 unabhängig (18). Eine weitere Arbeit berichtet von einer Expression der iPLA2 im proximalen Tubulus des Kaninchens, doch konnten wir dies immunhistochemisch nicht bestätigen, möglicherweise aufgrund einer quantitativen Problematik (45).

Zur Bestätigung der funktionellen Relevanz von iPLA2 für die NKCC2-Transportaktivität wurden Zellkulturstudien mit dem selektiven iPLA2-Inhibitor S-BEL durchgeführt. Hier zeigten sich eine gesteigerte Proteinbiosynthese, Phosphorylierung und Membraninsertion von NKCC2 nach Inkubation der Zellen mit dem Inhibitor (18). Mehrere Studien von Gimenez et al. und aus dem Labor von S. Bachmann haben gezeigt, dass Mechanismen, welche mit einer vermehrten Phosphorylierung von NKCC2 einhergehen, auch die NKCC2 Transportaktivität steigern (7,31,46). Die Zellkulturstudien belegen eine inhibitorische Wirkung von iPLA2 auf den TAL-Transport. Ein Zusammenhang zwischen iPLA2 und dem Transport im TAL wurde zuvor im Kontext der Dopamin-vermittelten Salurese beschrieben (47). Interessanterweise konnten Zhang et al. zeigen, dass die blutdrucksenkenden und saluretischen Effekte von Dopamin in der Niere durch EET vermittelt werden (48).

Zusammenfassend zeigen diese Studien eine inhibitorische Wirkung von iPLA2 auf die Transportaktivität von NKCC2 (18). Eine verminderte iPLA2-Enzymaktivität in den dDAVP-behandelten Tieren führt daher vermutlich zu einer Aktivierung von NKCC2 und unterstützt damit die Harnkonzentrierung.

Die Oxidation von AA zu 5,6-, 8,9-, 11,12- und 14,15-EET wird durch CYP Monooxygenasen katalysiert (49,50). Diverse CYP Isoformen (CYP 2C11, 2C23, SJ3 und SJ4) wurden im Kontext der renalen EET Synthese beschrieben (50,51). In Ratten gilt die CYP SC23 als die wichtigste Monooxygenase im renalen EET Metabolismus (52). Basierend auf den Ergebnissen des *Microarray* wurden CYP Monooxygenasen nur marginal durch ADH reguliert (19). Sie sind daher in diesem Zusammenhang eher nicht limitierend in der Regulation der lokalen EET Spiegel und wurden dementsprechend in dieser Arbeit nicht weiter untersucht.

Der Abbau der EET erfolgt entweder über die Beta-Oxidation oder, quantitativ relevanter, enzymatisch durch sEH-vermittelte Hydrolyse (53). Die bei der Hydrolyse entstehenden DHET sind im Vergleich zu ihren Ausgangssubstanzen biologisch deutlich weniger aktiv (54). Gleichzeitig sind sie durch die hydrophile Modifikation deutlich besser wasserlöslich und werden dadurch mit dem Blutstrom aus der Medulla

entfernt (55). Dementsprechend wird die Aktivität von sEH als Hauptdeterminante der EET-Bioverfügbarkeit gewertet (53).
Lokalisationsstudien zur intrarenalen sEH Verteilung haben in der Literatur unterschiedliche Ergebnisse produziert. So haben Weiss et al. an humanem Nierengewebe die sEH vorrangig in afferenten Arteriolen nachgewiesen und eine Regulation des renalen Blutflusses durch EET sowie einen Einfluss auf Blutdruck und Salzhomöostase über juxtaglomeruläre Regulation vermutet (56). Fleming et al. hingegen konnten an murinem Gewebe die sEH vorrangig in den distalen Tubulusepithelien nachweisen, während Gefäßendothelien keine sEH aufwiesen (57). Beide Arbeitsgruppen haben jedoch bei den Lokalisationsstudien auf Doppelmarkierungen mit distal-tubulären Zielstrukturen verzichtet. Mit dieser Methode konnten wir die sEH dezidiert in dünnen absteigenden und aufsteigenden Schenkeln der Henle Schleife, in der MD und im CD, nicht jedoch im TAL von murinem und humanem Nierengewebe nachweisen (19). Durch den anatomischen Aufbau der äußeren Medulla der Säugetierniere besteht jedoch eine enge räumliche Beziehung zwischen TAL und CD-Profilen (58,59). Eine ADH-abhängig vermehrte Expression von sEH im CD kann daher die EET-Gewebekonzentration lokal absenken und damit die inhibitorische Wirkung der EET auf die Transportaktivität des TAL reduzieren (19). Weitere Studien sind notwendig, um diese Hypothese zu bestätigen.

Zusammenfassend konnte in den vorliegenden Arbeiten erstmalig eine ADH-vermittelte Reduktion der renalen EET-Gewebekonzentration und die funktionelle Bedeutung von EET für den renalen Konzentrierungsmechanismus beschrieben werden (19). Weiterhin konnten die für die Reduktion der EET-Spiegel relevanten Enzyme identifiziert werden (18,19). Diese Studien erweitern damit grundlegend unser Verständnis der Mechanismen der ADH-induzierten Harnkonzentrierung (18,19).

1.7. Literaturverzeichnis

1. Ball SG. Vasopressin and disorders of water balance: the physiology and pathophysiology of vasopressin. Ann Clin Biochem. 2007;44:417-31.

2. Ellison DH, Berl T. Clinical practice. The syndrome of inappropriate antidiuresis. N Engl J Med. 2007;356(20):2064-72.

3. Bardoux P, Martin H, Ahloulay M, Schmitt F, Bouby N, Trinh-Trang-Tan MM, Bankir L. Vasopressin contributes to hyperfiltration, albuminuria, and renal hypertrophy in diabetes mellitus: study in vasopressin-deficient Brattleboro rats. Proc Natl Acad Sci U S A. 1999;96(18):10397-402.

4. Perico N, Zoja C, Corna D, Rottoli D, Gaspari F, Haskell L, Remuzzi G. V1/V2 Vasopressin receptor antagonism potentiates the renoprotection of renin-angiotensin system inhibition in rats with renal mass reduction. Kidney Int. 2009;76(9):960-7.

5. Schrier RW, Masoumi A, Elhassan E. Role of vasopressin and vasopressin receptor antagonists in type I cardiorenal syndrome. Blood Purif. 2009;27(1):28-32.

6. Roussel R, Velho G, Bankir L. Vasopressin and diabetic nephropathy. Curr Opin Nephrol Hypertens. 2017;26(4):311-318.

7. Mutig K, Paliege A, Kahl T, Jöns T, Müller-Esterl W, Bachmann S. Vasopressin V2 receptor expression along rat, mouse, and human renal epithelia with focus on TAL. Am J Physiol Renal Physiol. 2007;293(4):F1166-77.

8. Koertenoeven MLA, Pedersen NB, Rosenbaek LL, Fenton RA. Vasopressin regulation of sodium transport in the distal nephron and collecting duct. Am J Physiol Renal Physiol. 2015;309:F280-F299.

9. Knepper MA, Kwon TH, Nielsen S. Molecular physiology of water balance. N Engl J Med. 2015 Apr 2;372(14):1349-58.

10. Dietrich A, Mathia S, Kaminski H, Mutig K, Rosenberger C, Mrowka R, Bachmann S, Paliege A. Chronic activation of vasopressin V2 receptor signalling lowers renal medullary oxygen levels in rats. Acta Physiol. 2013;207(4):721-31.

11. Eckardt KU, Bernhardt WM, Weidemann A, Warnecke C, Rosenberger C, Wiesener MS, Willam C. Role of hypoxia in the pathogenesis of renal disease. Kidney Int Suppl. 2005 Dec;(99):S46-51.

12. Culpepper RM, Andreoli TE. Interactions among prostaglandin E2, antidiuretic hormone, and cyclic adenosine monophosphate in modulating Cl- absorption in single mouse medullary thick ascending limbs of Henle. J Clin Invest. 1983;71(6):1588-601.

13. Amlal H, Legoff C, Vernimmen C, Paillard M, Bichara M. Na(+)-K+(NH4+)-2Cl- cotransport in medullary thick ascending limb: control by PKA, PKC, and 20-HETE. Am J Physiol. 1996 Aug;271(2 Pt 1):C455-63.

14. He H, Podymow T, Zimpelmann J, Burns KD. NO inhibits Na+-K+-2Cl- cotransport via a cytochrome P-450-dependent pathway in renal epithelial cells (MMDD1). Am J Physiol Renal Physiol. 2003 Jun;284(6):F1235-44.

15. Bonventre JV. Phospholipase A2 and signal transduction. J Am Soc Nephrol. 1992 Aug;3(2):128-50.

16. Roman RJ. P-450 metabolites of arachidonic acid in the control of cardiovascular function. Physiol Rev. 2002 Jan;82(1):131-85.

17. Imig JD. Epoxides and soluble epoxide hydrolase in cardiovascular physiology. Physiol Rev. 2012 Jan;92(1):101-30.

18. Paliege A, Roeschel T, Neymeyer H, Seidel S, Kahl T, Daigeler AL, Mutig K, Mrowka R, Ferreri NR, Wilson BS, Himmerkus N, Bleich M, Bachmann S. Group VIA phospholipase A2 is a target for vasopressin signaling in the thick ascending limb. Am J Physiol Renal Physiol. 2012;302(7):F865-74.

19. Boldt C, Röschel T, Himmerkus N, Plain A, Bleich M, Labes R, Blum M, Krause H, Magheli A, Giesecke T, Mutig K, Rothe M, Weldon SM, Dragun D, Schunck WH, Bachmann S, Paliege A. Vasopressin lowers renal epoxyeicosatrienoic acid levels by activating soluble epoxide hydrolase. Am J Physiol Renal Physiol. 2016;311(6):F1198-F1210.

20. Valtin H., Schroeder HA. Familial hypothalamic diabetes insipidus in rats (Brattleboro strain). American Journal of Physiology. 1964;206(2):425-430.

21. Paliege A, Rosenberger C, Bondke A, Sciesielski L, Shina A, Heyman SN, Flippin LA, Arend M, Klaus SJ, Bachmann S. Hypoxia-inducible factor-2alpha-expressing interstitial fibroblasts are the only renal cells that express erythropoietin under hypoxia-inducible factor stabilization. Kidney Int. 2010;77(4):312-8.

22. Hoorn EJ, Walsh SB, McCormick JA, Fürstenberg A, Yang CL, Roeschel T, Paliege A, Howie AJ, Conley J, Bachmann S, Unwin RJ, Ellison DH. The calcineurin inhibitor tacrolimus activates the renal sodium chloride cotransporter to cause hypertension. Nat Med. 2011;17(10):1304-9.

23. Frömel T, Jungblut B, Hu J, Trouvain C, Barbosa-Sicard E, Popp R, Liebner S, Dimmeler S, Hammock BD, Fleming I. Soluble epoxide hydrolase regulates hematopoietic progenitor cell function via generation of fatty acid diols. Proc Natl Acad Sci U S A. 2012;109(25):9995-10000.

24. Schmitt R, Klussmann E, Kahl T, Ellison DH, Bachmann S. Renal expression of sodium transporters and aquaporin-2 in hypothyroid rats. Am J Physiol Renal Physiol. 2003;284(5):F1097-104.

25. Bostanjoglo M, Reeves WB, Reilly RF, Velázquez H, Robertson N, Litwack G, Morsing P, Dørup J, Bachmann S, Ellison DH. 11Beta-hydroxysteroid dehydrogenase, mineralocorticoid receptor, and thiazide-sensitive Na-Cl cotransporter expression by distal tubules. J Am Soc Nephrol. 1998;9(8):1347-58.

26. Eng B, Mukhopadhyay S, Vio CP, Pedraza PL, Hao S, Battula S, Sehgal PB, McGiff JC, Ferreri NR. Characterization of a long-term rat mTAL cell line. Am J Physiol Renal Physiol. 2007;293(4):F1413-22.

27. Greger R. Cation selectivity of the isolated perfused cortical thick ascending limb of Henle's loop of rabbit kidney. Pflugers Arch. 1981;390(1):30-7.

28. Borschewski A, Himmerkus N, Boldt C, Blankenstein KI, McCormick JA, Lazelle R, Willnow TE, Jankowski V, Plain A, Bleich M, Ellison DH, Bachmann S, Mutig K. Calcineurin and Sorting-Related Receptor with A-Type Repeats Interact to Regulate the Renal Na^+-K^+-$2Cl^-$ Cotransporter. J Am Soc Nephrol. 2016;27(1):107-19.

29. Ecelbarger CA, Kim GH, Wade JB, Knepper MA. Regulation of the abundance of renal sodium transporters and channels by vasopressin. Exp Neurol. 2001;171(2):227-34.

30. Ulu A, Davis BB, Tsai HJ, Kim IH, Morisseau C, Inceoglu B, Fiehn O, Hammock BD, Weiss RH. Soluble epoxide hydrolase inhibitors reduce the development of atherosclerosis in apolipoprotein e-knockout mouse model. J Cardiovasc Pharmacol. 2008;52(4):314-23.

31. Giménez I, Forbush B. Short-term stimulation of the renal Na-K-Cl cotransporter (NKCC2) by vasopressin involves phosphorylation and membrane translocation of the protein. J Biol Chem. 2003;278(29):26946-51.

32. Greger R, Oberleithner H, Schlatter E, Cassola AC, Weidtke C. Chloride activity in cells of isolated perfused cortical thick ascending limbs of rabbit kidney. Pflugers Arch. 1983;399(1):29-34.

33. Harris RC Jr. Cyclooxygenase-2 inhibition and renal physiology. Am J Cardiol. 2002;89(6A):10D-17D.

34. Zhang MZ, Sanchez Lopez P, McKanna JA, Harris RC. Regulation of cyclooxygenase expression by vasopressin in rat renal medulla. Endocrinology. 2004;145(3):1402-9.

35. Yang T, Schnermann JB, Briggs JP. Regulation of cyclooxygenase-2 expression in renal medulla by tonicity in vivo and in vitro. Am J Physiol. 1999;277(1):F1-9.

36. Imig JD. Epoxides and soluble epoxide hydrolase in cardiovascular physiology. *Physiol Rev*. 2012;92(1):101-130.

37. Campbell WB, Fleming I. Epoxyeicosatrienoic acids and endothelium-dependent responses. Pflügers Archiv. 2010;459:881–895.

38. Capdevila J, Wang W. Role of cytochrome P450 epoxygenase in regulating renal membrane transport and hypertension. Curr Opin Nephrol Hypertens. 2013 Mar;22(2):163-9.

39. Pidkovka N, Rao R, Mei S, Gong Y, Harris RC, Wang WH, Capdevila JH. Epoxyeicosatrienoic acids (EETs) regulate epithelial sodium channel activity by extracellular signal-regulated kinase 1/2 (ERK1/2)-mediated phosphorylation. J Biol Chem. 2013;288(7):5223-31.

40. Bankir L, Bichet DG, Bouby N. Vasopressin V2 receptors, ENaC, and sodium reabsorption: a risk factor for hypertension? Am J Physiol Renal Physiol. 2010;299(5):F917-28.

41. He H, Podymow T, Zimpelmann J, Burns KD. NO inhibits Na+-K+-2Cl- cotransport via a cytochrome P-450-dependent pathway in renal epithelial cells (MMDD1). Am J Physiol Renal Physiol. 2003;284(6):F1235-F1244.

42. Grider JS, Falcone JC, Kilpatrick EL, Ott CE, Jackson BA. P450 arachidonate metabolites mediate bradykinin-dependent inhibition of NaCl transport in the rat thick ascending limb. Can J Physiol Pharmacol. 1997;75(2):91-96.

43. Downey P, Sapirstein A, O'Leary E, Sun TX, Brown D, Bonventre JV. Renal concentrating defect in mice lacking group IV cytosolic phospholipase A(2). Am J Physiol Renal Physiol. 2001;280(4):F607-F618.

44. Larsson Forsell PK, Kennedy BP, Claesson HE. The human calcium-independent phospholipase A2 gene multiple enzymes with distinct properties from a single gene. Eur J Biochem. 1999;262(2):575-85.

45. Portilla D, Shah SV, Lehman PA, Creer MH. Role of cytosolic calcium-independent plasmalogen-selective phospholipase A2 in hypoxic injury to rabbit proximal tubules. J Clin Invest. 1994;93(4):1609-15.

46. Giménez I, Forbush B. Regulatory phosphorylation sites in the NH2 terminus of the renal Na-K-Cl cotransporter (NKCC2). Am J Physiol Renal Physiol. 2005;289(6):F1341-5.

47. Grider J, Kilpatrick E, Ott C, Jackson B. Effect of dopamine on NaCl transport in the medullary thick ascending limb of the rat. Eur J Pharmacol. 1998;342(2-3):281-284.

48. Zhang MZ, Wang Y, Yao B, Gewin L, Wei S, Capdevila JH, Harris RC. Role of epoxyeicosatrienoic acids (EETs) in mediation of dopamine's effects in the kidney. Am J Physiol Renal Physiol. 2013;305(12):F1680-6.

49. Roman RJ. P-450 metabolites of arachidonic acid in the control of cardiovascular function. Physiol Rev. 2002;82(1):131-185.

50. El-Sherbeni AA, Aboutabl ME, Zordoky BN, Anwar-Mohamed A, El-Kadi AO. Determination of the dominant arachidonic acid cytochrome p450 monooxygenases in rat heart, lung, kidney, and liver: protein expression and metabolite kinetics. AAPS J. 2013;15(1):112-122.

51. Enayetallah AE, French RA, Thibodeau MS, Grant DF. Distribution of soluble epoxide hydrolase and of cytochrome P450 2C8, 2C9, and 2J2 in human tissues. J Histochem Cytochem. 2004;52(4):447-454.

52. Kaergel E, Muller DN, Honeck H, Theuer J, Shagdarsuren E, Mullally A, Luft FC, Schunck WH. P450-dependent arachidonic acid metabolism and angiotensin II-induced renal damage. Hypertension. 2002;40(3):273-9.

53. Yu Z, Xu F, Huse LM, Morisseau C, Draper AJ, Newman JW, Parker C, Graham L, Engler MM, Hammock BD, Zeldin DC, Kroetz DL. Soluble epoxide hydrolase regulates hydrolysis of vasoactive epoxyeicosatrienoic acids. Circ Res. 2000;87(11):992-8.

54. Imig JD, Navar LG, Roman RJ, Reddy KK, Falck JR. Actions of epoxygenase metabolites on the preglomerular vasculature. J Am Soc Nephrol. 1996;7(11):2364-2370.

55. VanRollins M, Kaduce TL, Knapp HR, Spector AA. 14,15-Epoxyeicosatrienoic acid metabolism in endothelial cells. J Lipid Res. 1993;34(11):1931-42.

56. Yu Z, Davis BB, Morisseau C, Hammock BD, Olson JL, Kroetz DL, Weiss RH. Vascular localization of soluble epoxide hydrolase in the human kidney. Am J Physiol Renal Physiol. 2004;286(4):F720-6.

57. Jung O, Brandes RP, Kim IH, Schweda F, Schmidt R, Hammock BD, Busse R, Fleming I. Soluble epoxide hydrolase is a main effector of angiotensin II-induced hypertension. Hypertension. 2005;45(4):759-65.

58. Lemley KV, Kriz W. Anatomy of the renal interstitium. Kidney Int. 1991;39(3):370-81.

59. Kaissling B, Hegyi I, Loffing J, Le Hir M. Morphology of interstitial cells in the healthy kidney. Anat Embryol (Berl). 1996;193(4):303-18.

2. Eidesstattliche Versicherung

„Ich, Tom Röschel, versichere an Eides statt durch meine eigenhändige Unterschrift, dass ich die vorgelegte Dissertation mit dem Thema: Epoxyeicosatriensäuren sind Ziel der durch das antidiuretische Hormon induzierten Signalgebung im Nierenmark (Epoxyeicosatrienoic acids are a target for vasopressin signalling in the renal medulla), selbstständig und ohne nicht offengelegte Hilfe Dritter verfasst und keine anderen als die angegebenen Quellen und Hilfsmittel genutzt habe.
Alle Stellen, die wörtlich oder dem Sinne nach auf Publikationen oder Vorträgen anderer Autoren/innen beruhen, sind als solche in korrekter Zitierung kenntlich gemacht. Die Abschnitte zu Methodik (insbesondere praktische Arbeiten, Laborbestimmungen, statistische Aufarbeitung) und Resultaten (insbesondere Abbildungen, Graphiken und Tabellen) werden von mir verantwortet.

[Ich versichere ferner, dass ich die in Zusammenarbeit mit anderen Personen generierten Daten, Datenauswertungen und Schlussfolgerungen korrekt gekennzeichnet und meinen eigenen Beitrag sowie die Beiträge anderer Personen korrekt kenntlich gemacht habe (siehe Anteilserklärung). Texte oder Textteile, die gemeinsam mit anderen erstellt oder verwendet wurden, habe ich korrekt kenntlich gemacht.

Meine Anteile an etwaigen Publikationen zu dieser Dissertation entsprechen denen, die in der untenstehenden gemeinsamen Erklärung mit dem/der Erstbetreuer/in, angegeben sind. Für sämtliche im Rahmen der Dissertation entstandenen Publikationen wurden die Richtlinien des ICMJE (International Committee of Medical Journal Editors; www.icmje.og) zur Autorenschaft eingehalten. Ich erkläre ferner, dass ich mich zur Einhaltung der Satzung der Charité – Universitätsmedizin Berlin zur Sicherung Guter Wissenschaftlicher Praxis verpflichte.

Weiterhin versichere ich, dass ich diese Dissertation weder in gleicher noch in ähnlicher Form bereits an einer anderen Fakultät eingereicht habe.

Die Bedeutung dieser eidesstattlichen Versicherung und die strafrechtlichen Folgen einer unwahren eidesstattlichen Versicherung (§§156, 161 des Strafgesetzbuches) sind mir bekannt und bewusst.“

Datum Unterschrift

3. Anteilserklärung an den erfolgten Publikationen

Tom Röschel hatte folgenden Anteil an den folgenden Publikationen:

Publikation 1

Boldt C*, **Roeschel T***, Himmerkus N, Plain A, Bleich M, Labes R, Blum M, Krause H, Magheli A, Giesecke T, Mutig K, Rothe M, Weldon SM, Dragun D, Schunck WH, Bachmann S, Paliege A, *Vasopressin lowers renal epoxyeicosatrienoic acid levels by activating soluble epoxide hydrolase,* Am J Physiol Renal Physiol., 2016
*geteilte Erstautorschaft

Impact Factor: 3,09

Beitrag im Einzelnen: Entwurf von Versuchsprotokollen, Therapie und Pflege der dDAVP behandelten DI-Ratten, Implantation der subkutanen osmotischen Minipumpen, Präparation und Perfusionsfixierung von Nierengewebe, Lokalisationsstudien mittels indirekter Immunfluoreszenz und Auswertung am Konfokalmikroskop in Nieren von Mensch, Maus und Ratte, Durchführung molekularbiologischer Arbeitstechniken, Auswertung und Interpretation der Ergebnisse, Mitarbeit beim Verfassen des Manusskripttextes, Literaturrecherche

Die von mir erhobenen Daten sind als *Figure* 3, 4, 5, 7, 8 und 11 in die Publikation eingegangen.

Publikation 2

Paliege A, **Roeschel T**, Neymeyer H, Seidel S, Kahl T, Daigeler AL, Mutig K, Mrowka R, Ferreri NR, Wilson BS, Himmerkus N, Bleich M, and Bachmann S, *Group VIA phospholipase A_2 is a target for vasopressin signaling in the thick ascending limb,* Am J Physiol Renal Physiol., 2012

Impact Factor: 3,09

Beitrag im Einzelnen: Entwurf von Versuchsprotokollen, Pflege und Therapie immortalisierter Zelllinien im Zellkulturlabor, Lokalisationsstudien mittels indirekter Immunfluoreszenz und Auswertung am Konfokalmikroskop, Durchführung molekularbiologischer Arbeitstechniken, Auswertung und Interpretation der Ergebnisse

Die von mir erhobenen Daten sind als *Figure* 1, 2, 3, 5, 6, 7 und 8 in die Publikation eingegangen.

Publikation 3

Hoorn EJ, Walsh SB, McCormick JA, Fürstenberg A, Yang CL, **Roeschel T**, Paliege A, Howie AJ, Conley J, Bachmann S, Unwin RJ, Ellison DH, *The calcineurin inhibitor tacrolimus activates the renal sodium chloride cotransporter to cause hypertension,* Nature Medicine, 2011

Impact Factor: 28,95

Beitrag im Einzelnen: retrograde Perfusionsfixierung der Versuchstiere, Lokalisationsstudien mittels indirekter Immunfluoreszenz und Immunhistochemie, Auswertung und am Konfokalmikroskop

Die von mir erhobenen Daten sind als *Figure* 2A in die Publikation eingegangen.

Unterschrift, Datum und Stempel des betreuenden Hochschullehrers
Prof. Dr. Sebastian Bachmann

_____

Unterschrift des Doktoranden
Tom Röschel

_____

4. Druckexemplare der ausgewählten Publikationen

4.1. Vasopressin lowers renal epoxyeicosatrienoic acid levels by activationg soluble epoxide hydrolase

Am J Physiol Renal Physiol 311: F1198–F1210, 2016.
First published September 28, 2016; doi:10.1152/ajprenal.00062.2016.

Vasopressin lowers renal epoxyeicosatrienoic acid levels by activating soluble epoxide hydrolase

Christin Boldt,[1]* Tom Röschel,[1]* Nina Himmerkus,[2] Allein Plain,[2] Markus Bleich,[2] Robert Labes,[1] Maximilian Blum,[3] Hans Krause,[4] Ahmed Magheli,[4] Torsten Giesecke,[1] Kerim Mutig,[1] Michael Rothe,[5] Steven M. Weldon,[6] Duska Dragun,[7,8] Wolf-Hagen Schunck,[3] Sebastian Bachmann,[1] and Alexander Paliege[7,8]

[1]*Department of Anatomy, Charité-Universitätsmedizin Berlin, Berlin, Germany;* [2]*Department of Physiology, Christian-Albrechts-University, Kiel, Germany;* [3]*Max Delbrueck Center for Molecular Medicine, Berlin, Germany;* [4]*Department of Urology, Charité-Universitätsmedizin Berlin, Berlin, Germany;* [5]*Lipidomix, Berlin, Germany;* [6]*Boehringer Ingelheim Pharmaceuticals, Ridgefield, Connecticut;* [7]*Department of Nephrology, Charité-Universitätsmedizin Berlin, Berlin, Germany; and* [8]*Berlin Institute of Health, Berlin, Germany*

Submitted 29 January 2016; accepted in final form 19 September 2016

Boldt C, Röschel T, Himmerkus N, Plain A, Bleich M, Labes R, Blum M, Krause H, Magheli A, Giesecke T, Mutig K, Rothe M, Weldon SM, Dragun D, Schunck WH, Bachmann S, Paliege A. Vasopressin lowers renal epoxyeicosatrienoic acid levels by activating soluble epoxide hydrolase. *Am J Physiol Renal Physiol* 311: F1198–F1210, 2016. First published September 28, 2016; doi:10.1152/ajprenal.00062.2016.—Activation of the thick ascending limb (TAL) Na^+-K^+-$2Cl^-$ cotransporter (NKCC2) by the antidiuretic hormone arginine vasopressin (AVP) is an essential mechanism of renal urine concentration and contributes to extracellular fluid and electrolyte homeostasis. AVP effects in the kidney are modulated by locally and/or by systemically produced epoxyeicosatrienoic acid derivates (EET). The relation between AVP and EET metabolism has not been determined. Here, we show that chronic treatment of AVP-deficient Brattleboro rats with the AVP V2 receptor analog desmopressin (dDAVP; 5 ng/h, 3 days) significantly lowered renal EET levels (−56 ± 3% for 5,6-EET, −50 ± 3.4% for 11,12-EET, and −60 ± 3.7% for 14,15-EET). The abundance of the principal EET-degrading enzyme soluble epoxide hydrolase (sEH) was increased at the mRNA (+160 ± 37%) and protein levels (+120 ± 26%). Immunohistochemistry revealed dDAVP-mediated induction of sEH in connecting tubules and cortical and medullary collecting ducts, suggesting a role of these segments in the regulation of local interstitial EET signals. Incubation of murine kidney cell suspensions with 1 μM 14,15-EET for 30 min reduced phosphorylation of NKCC2 at the AVP-sensitive threonine residues T96 and T101 (−66 ± 5%; $P < 0.05$), while 14,15-DHET had no effect. Concomitantly, isolated perfused cortical thick ascending limb pretreated with 14,15-EET showed a 30% lower transport current under high and a 70% lower transport current under low symmetric chloride concentrations. In summary, we have shown that activation of AVP signaling stimulates renal sEH biosynthesis and enzyme activity. The resulting reduction of EET tissue levels may be instrumental for increased NKCC2 transport activity during AVP-induced antidiuresis.

urine concentration mechanism; thick ascending limb; NKCC2

WATER CONSERVATION BY THE mammalian kidney is achieved by the tightly controlled, coordinate action of epithelial and vascular components. The hypothalamic antidiuretic hormone (arginine vasopressin, AVP) plays a dominant role herein. It stimulates luminal insertion of water channels along the connecting tubule and collecting duct epithelia, as well as the insertion of urea transporters into medullary portion of the collecting duct (37). The thick ascending limb (TAL) is sensitive to AVP as well, since abundance, phosphorylation, and surface expression of the furosemide sensitive Na^+-K^+-$2Cl^-$ cotransporter (NKCC2) are stimulated by the hormone (37). At the vascular level, AVP causes vasoconstriction of preglomerular arterioles and descending vasa recta and, thereby, reduces medullary blood flow. The combination of an augmented solute transport activity and a reduced perfusion facilitates efficient countercurrent multiplication but also results in a marked hypoxia of key medullary structures (17), which may promote the development of renal disease (5). The renal effects of AVP are modulated by locally produced arachidonic acid derivates such as 20-hydroxyeicosatetraenoic acid (20-HETE), epoxyeicosatrienoic acid (EET), and prostaglandin E_2 (PGE_2) which inhibit TAL transport activity (1, 15, 26, 31, 57) and increase medullary perfusion (4, 74). While the regulation of 20-HETE and PGE_2 during AVP-induced antidiuresis has been studied in considerable detail (59, 73, 77), less is known regarding the mechanisms that determine synthesis and metabolism of EET in this setting. EETs exist as four regioisomers: 5,6-EET, 8,9-EET, 11,12-EET, and 14,15-EET, which are synthesized by the cytochrome *P*-450 (CYP450) monooxygenases (18, 57). CYP450 isoforms 2C9/10, 2C11, 2C23, 2J3, and 2J4 have all been shown to contribute to renal EET synthesis (18, 19, 34). In rats, 2C23 is considered the principal renal isoform to generate EET in rat kidney (34). EETs are metabolically degraded mainly by soluble epoxide hydrolase (sEH), which hydrolyzes EET to their corresponding, less active dihydroxyeicosatrienoic acid isomers (DHETs) (31, 57). The preferred substrates for sEH are 14,15-EET, 11,12-EET, and 8,9-EET, whereas the affinity of the enzyme toward 5,6-EET is low (30). The kidney shows substantial sEH activity, but the site of its synthesis and regulation within the renal parenchyma has not been unequivocally clarified (19, 33, 38, 48, 75). Earlier, microarray-based gene expression studies have provided evidence for AVP-dependent activation of sEH in the kidney (17, 51), prompting us to study the effects of AVP on renal medullary EET metabolism in greater detail.

* C. Boldt and T. Röschel contributed equally to this article.
Address for reprint requests and other correspondence: A. Paliege, Dept. of Nephrology, Charité-Universitätsmedizin Berlin, Berlin, Philippstr. 12, D-10115, Germany (e-mail: alexander.paliege@charite.de).

In the present study, we found that sEH is abundantly expressed in the segments of human and rat nephrons and collecting duct system. Chronic AVP treatment induced sEH biosynthesis in AVP-deficient Brattleboro rats, which was associated with a reduction of renal EET levels. Functional studies in isolated TAL segments demonstrated an inhibitory effect of 14,15-EET on NKCC2 phosphorylation and transport activity. Induction of sEH by AVP may, therefore, be an essential mechanism for the maintenance of sustained antidiuresis.

MATERIALS AND METHODS

Animal studies and tissue preservation. Animal studies were performed according to National Institutes of Health's guidelines after approval from the Berlin Council on Animal Care (permission numbers G006-02/05, G0285/10, and O0124/96). For localization studies, adult Sprague-Dawley (SD) rats ($n = 3$) were perfusion-fixed via the abdominal aorta, using a fixative containing 3% paraformaldehyde (Merck, Darmstadt, Germany) dissolved in PBS, as previously described (52). Kidneys were harvested and processed for cryostat and paraffin sectioning using established methodology (51). For Western blot analysis of zonal sEH distribution, additional SD rats ($n = 3$) were killed by cervical dislocation. Kidneys were carefully removed and dissected into cortex, outer medulla, and inner medulla using sterile razor blades and a stereotactic microscope. Samples were subsequently snap frozen in liquid nitrogen, and stored at −80°C until further use. Human kidney samples ($n = 3$) were obtained from the healthy parts of tumor nephrectomy specimen after written consent of the patients. Tissue blocks were immersion-fixed for 12 h using 3% paraformaldehyde in PBS and subsequently processed for paraffin embedding (46). Detailed protocols for treatment of Brattleboro rats with 1-desamino-8-D-Arg vasopressin (dDAVP) have been published before (51). Briefly, Brattleboro rats aged 2–3 mo ($n = 26$) were treated with normal saline as vehicle or dDAVP ($n = 13$ each; 5 ng/h for 3 days; Sigma Aldrich, Munich, Germany) via subcutaneous infusion using osmotic minipumps (ALZET osmotic minipump, model 2001; Charles River, Sulzfeld, Germany). At the end of the treatment period, animals for microarray ($n = 3$ per group) and biochemical studies ($n = 5$ per group) were killed by cervical dislocation. Kidneys were carefully removed and processed at 4°C. Samples were snap frozen in liquid nitrogen, and stored at −80°C until further use. Animals for morphological studies ($n = 5$ per group) were perfusion fixed as detailed above. sEH-deficient mice were originally obtained from Boehringer Ingelheim Pharmaceutical (Ridgefield, CT) and bred in the animal facility of the Max Delbrück Center for Molecular Medicine in Berlin. A detailed description for the establishment of gene deletion and genotyping has been published (41, 62). Animals were back-crossed into FVB/N background for at least six generations (28). At 3 mo of age, kidneys of male knockout and wild-type mice ($n = 4$ for each genotype) were harvested for biochemical analysis or fixed overnight using 3% paraformaldehyde in PBS and processed for histological studies. Microdissection of murine TAL segments was performed as previously described (9) using a total of six male C57/BL6 mice (Charles River, Sulzfeld, Germany).

Microarray studies. Gene expression profiling studies were conducted in the microarray facility at the Zentrum für Medizinische Forschung of the University Mannheim (Mannheim, Germany), as previously described (17, 51). Affymetrix rat genome 230 2.0 arrays and a custom CDF version 9 annotation with Unigene-based gene definitions (http://brainarray.mbni.med.umich.edu/Brainarray/Database/CustomCDF/CDF_download_v9.asp) were used for the analysis. Raw and normalized data were deposited in the Gene Expression Omnibus database (http://www.ncbi.nlm.nih.gov/geo/; GEO accession number: GSE34225).

Quantification of renal outer medullary lipid levels. Free tissue lipid levels were determined by mass spectrometry in kidney samples of dDAVP-treated Brattleboro rats and controls. Samples were powdered in liquid nitrogen, dissolved in a 50/50 vol/vol mixture of water and methanol supplemented with 0.01% butylhydroxytoluol, mixed with 10 μl internal standard solution (0.5 μg/ml), and buffered at pH 6 with 2 ml SPE-buffer (0.1 mol/l aqueous sodium acetate solution, pH 6). Solid-phase extraction was performed using a Bond-Elut-Certify-II-Column (Phenomenex, Torrance, CA). Eicosanoids were eluted with 2 ml n-hexane/ethylacetate (25/75 vol/vol) with 1% acetic acid. The solvent was evaporated with a gentle stream of N_2 at 40°C. Residues were resuspended in 100 μl methanol/water mixture and processed for measuring. Liquid chromatography-mass spectrometry (LC-MS/MS) was performed at the mass spectrometry facility of Lipidomix, as previously described (Lipidomix, Berlin, Germany) (2). Free tissue levels of EET isomers and of the linoleic acid epoxides 9,10-EPOME and 12,13-EPOME and their respective diols 9,10-DIHOME and 12,13-DIHOME were determined in parallel. Since the formation of these diols is also catalyzed by sEH, the ratio of DIHOME and EPOME isomers can be used as a measure for sEH tissue activity (20, 68).

Real-time PCR. mRNA was isolated from whole kidney homogenates using Roti-Aqua phenol-chloroform extraction kit, according to the manufacturer's protocol (Carl Roth, Karlsruhe, Germany). After digestion of genomic DNA by DNase 1 treatment (Qiagen, Hilden, Germany) cDNA was generated by reverse transcription using the Applied Biosystems cDNA synthesis kit (Applied Biosystems, Darmstadt, Germany). TaqMan quantitative RT-PCR for sEH was performed using the Applied Biosystems probe Mm00514706 and the 7500 Fast real-time PCR system (Applied Biosystems) following the manufacturer's instructions. The mRNA levels of GAPDH were determined in parallel and served as a loading control (catalog no. 4352338E; Applied Biosystems). Expression levels were calculated using the $2^{-\Delta\Delta CT}$ method and were expressed as a percentage of control (40).

Primary antibodies. For detection of sEH, we used an Affinity-purified rabbit antibody against human sEH (1:500, HPA023094; Atlas Antibodies, Stockholm, Sweden). Antibodies against total and phospho-(p)-T96/T101-NKCC2 were generated in our laboratory and have been described before (46). Antibodies for cyclooxygenase 2 (COX-2; sc-1746) and aquaporin 2 (AQP2; sc-9882) were obtained from Santa Cruz Biotechnology (Dallas, TX). Antibody against the Na^+-Cl^--cotransporter NCC was provided by D. Ellison (Oregon Health & Science University, Portland, OR) and served as a marker for the distal convoluted tubule (51). Antibody for the proximal tubule marker megalin was a kind gift of T. Willnow (MDC, Berlin, Germany) and has been described before (3). The antibody against mouse α-smooth muscle actin was obtained from DAKO (Hamburg, Germany); the antibody for β-actin was obtained from Sigma-Aldrich.

Immunoblotting. Samples for Western blot analysis were prepared as previously described (71). Briefly, tissues were ground in liquid nitrogen using sterile mortar and pestle and subsequently dissolved in homogenization buffer containing 250 mM sucrose, 10 mM triethanolamine, and protease inhibitors (cOmplete protease inhibitor cocktail; Roche Diagnostics, Indianapolis, IN). Nuclei were removed by centrifugation (1,000 *g* for 10 min). Protein concentration of post-nuclear homogenates was determined using bicinchoninic acid protein assay following the manufacturer's instructions (ThermoFisher Scientific, Bonn, Germany). Samples were subsequently separated by SDS-PAGE in a 10% gel (50 μg protein/lane) and electrophoretically transferred to nitrocellulose membranes. Primary antibodies were applied after blocking of nonspecific protein binding sites with 5% nonfat dry milk in PBS. Membranes were incubated for 1 h at room temperature followed by an overnight incubation at 4°C. Bound antibody was detected using the appropriate HRP-conjugated secondary antibodies and chemiluminescence. Developed X-ray films were scanned and densitometrically evaluated using the Alpha Imager software (Cell Biosci-

Table 1. *Microarray analysis of dDAVP effects on outer medullary mRNA levels of soluble epoxide hydrolase and cytochrome P-450 monooxygenases*

Gene Title	Gene Symbol	mRNA Accession	Probe Set ID	*x*-Fold of Control	*P*
Epoxide hydrolase 2, cytoplasmic	EPHX2	NM_022936	Rn.54495_at	2.45	0.04*
Cytochrome *P*-450, family 2, subfamily c, polypeptide 11	Cyp2c11	NM_019184	1387328_at	1.3	0.68
Cytochrome *P*-450, family 2, subfamily c, polypeptide 23	Cyp2c23	NM_031839	1367988_at	0.97	0.52
Cytochrome *P*-450, family 2, subfamily j, polypeptide 3	Cyp2j3	NM_175766	1370706_a_at	0.99	0.8
Cytochrome *P*-450, family 2, subfamily j, polypeptide 4	Cyp2j4	NM_023025	Rn.44992_at	0.78	0.003*
Cytochrome *P*-450, family 2, subfamily j, polypeptide 10	Cyp2j10	NM_001134980	Rn.34638_at	0.95	0.26

Analysis of published microarray data of kidney extracts from dDAVP-treated Brattleboro rats shows strong induction of sEH mRNA levels, as compared to vehicle-treated controls, whereas the mRNA abundance of the principal cytochrome *P*-450 monooxygenases, Cyp2c11, Cyp2c23, Cyp2j3, and Cyp2j10 are unaltered. Cyp2j4 mRNA shows a modest decrease which, however, could not be reproduced by an alternative technology. Data are derived from (51) and are presented as *x*-fold of vehicle-treated controls. $*P < 0.05$; $n = 3$ per group.

ences, Santa Clara, CA). Expression levels were normalized to the expression of the housekeeping gene β-actin.

Immunostaining. Immunofluorescence and immunoperoxidase staining were carried out as previously described (51). Briefly, 4-μm paraffin sections were deparaffinized, rehydrated, and subjected to antigen retrieval by boiling in 0.1 M sodium citrate buffer using a pressure cooker. Nonspecific binding sites were blocked by incubation with 5% dry milk in PBS. Renal localization of sEH was studied by immunofluorescence staining on 4-μm paraffin sections of human and rat kidneys using the rabbit anti-sEH antibody in a 1:100 dilution. Immunoreactive nephron segments were characterized by double labeling with the established segment-specific antibodies to NKCC2 (1:5,000 dilution) for TAL, COX-2 (1:100 dilution) for macula densa, NCC (1:100 dilution) for distal convoluted tubule, and AQP2 (1:100 dilution) for connecting tubule and collecting duct, respectively. Bound antibodies were detected with the appropriate Alexa Fluor 488 or Cy3-labeled secondary antibodies (Dianova, Hamburg, Germany). Stained sections were examined by confocal microscopy using a Zeiss LSM Exciter confocal microscope and ZEN 2008 software (Carl Zeiss, Jena, Germany). Sections for immunoperoxidase staining were prepared as detailed above. Tissue peroxidases were blocked with 3% hydrogen peroxide in methanol prior to application of the primary antibodies. Signal was developed using HRP-labeled donkey anti-rabbit secondary antibody (Dianova) and 3,3′-diaminobenzidine containing 0.3% hydrogen peroxide (Sigma-Aldrich); samples were processed synchronously with standardized incubation times to ensure comparability of the measurements.

Validation of sEH antibody. Antibody specificity was verified by immunoblotting in sEH knockout tissue and by peptide blockade in rat kidney sections. To this end, we performed Western blot analysis on total kidney homogenates from sEH-deficient mice and their respective controls. Peptide blockade studies were conducted using the immunizing peptide (APrEST76223, Atlas Antibodies, Stockholm, Sweden). sEH antibody was diluted in 5% nonfat dry milk in PBS and incubated at 37°C for 30 min with different amounts of blocking peptide prior to application to rat kidney sections. Western blot analysis and immunostainings were performed as described above.

Renal tubule perfusion. Freshly isolated cortical thick ascending limb segments of 10 male C57/BL6 mice (Charles River, Sulzfeld, Germany) were incubated with either 0.34% ethanol (control) or with 1 μM 14,15-EET (Cayman Chemicals, Ann Arbor, MI) in 0.32% ethanol or 1 μM 14,15-DHET (Cayman Chemicals) in 0.34% ethanol for 30–40 min at 30°C in incubation solution (140 mmol/l NaCl, 0.4 mmol/l KH_2PO_4, 1.6 mmol/l K_2HPO_4, 1 mmol/l $MgCl_2$, 10 mmol/l Na-acetate, 1 mmol/l α-ketoglutarate, 1.3 mmol/l Ca-gluconate, 3.75 mg/ml glycine, 0.48 mg/ml trypsin inhibitor, 0.25 mg/ml DNase I, and 5 mg/ml albumin, at pH 7.4). All chemicals were obtained from Merck (Darmstadt, Germany) unless indicated otherwise. Preincubated cortical thick ascending limbs (cTALs) were then transferred into the bath on a heated microscope stage. The bath was heated to 37°C, and continuous bath perfusion at 3–5 ml/min with control solution (140 mmol/l NaCl, 0.4 mmol/l KH_2PO_4, 1.6 mmol/l K_2HPO_4, 1 mmol/l $MgCl_2$, 5 mmol/l glucose, 1.3 mmol/l Ca-gluconate, at pH 7.4) was obtained by gravity perfusion. Tubules were held and perfused by a concentric glass pipette system. The perfusion pipette was double-barreled, and *barrel 1* was used for voltage measurement and perfusion (perfusion rate 10–20 nl/min; 7.6 ± 0.3 μm inner diameter) with control solution. *Barrel 2* was used for constant current injection (13 nA) and perfusion with low Cl^- solution (28 mmol/l NaCl, 0.4 mmol/l KH_2PO_4, 1.6 mmol/l K_2HPO_4, 1 mmol/l $MgCl_2$, 5 mmol/l glucose, 1.3 mmol/l Ca-gluconate, 51 mmol/l mannitol, 62 mmol/l $NaSO_4$, at pH 7.4). After an equilibration period under symmetric control conditions, first the basolateral and then the luminal solution was changed to low Cl^-. Cable equations were used to calculate transepithelial resistance R_{te}, as described previously (21). Equivalent short-circuit current I'_{sc} was calculated from R_{te} and V_{te}, according to Ohms law, for both conditions, respectively. The percentage of I'_{sc} under low Cl^- in relation to the I'_{sc} under high Cl^- (V_{max}) was calculated as the measure of Cl^- affinity of the transporter (9). The effects of the EET isomers on NKCC2 phosphorylation were determined using mouse kidney cell suspensions. To this end, kidneys of adult male C57/BL6N mice were flushed with incubation solution to remove the blood. Kidneys were subsequently incubated for 10 min in incubation solution containing 1 mg/ml collagenase 2 (Sigma-Aldrich) for collagenase digestion. After complete digestion, the cells were pelleted by centrifugation at 1000 *g* for 10 min, collagenase solution was discarded, and the pellet resuspended in fresh incubation solution containing 100 nM dDAVP to induce NKCC2 phosphorylation. Aliquots of the resulting cell sus-

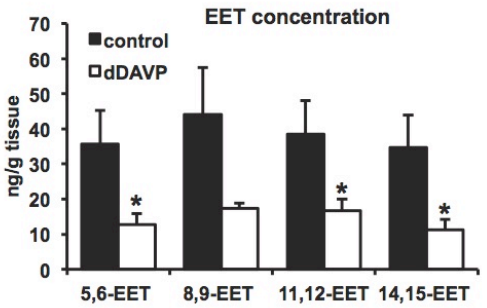

Fig. 1. Effect of AVP V2 receptor analog desmopressin (dDAVP) treatment on outer medullary free epoxyeicosatrienoic acid (EET) levels in Brattleboro rats. Quantification of outer medullary free EET concentrations reveals significantly lower levels of 5,6-EET, 11,12-EET, and 14,15-EET upon 5 ng/h dDAVP for 3 days compared with vehicle-treated controls. 8,9-EET reduction failed to be significant ($P = 0.08$). Data are expressed as means ± SE; $*P < 0.05$; $n = 7$ or 8 per group.

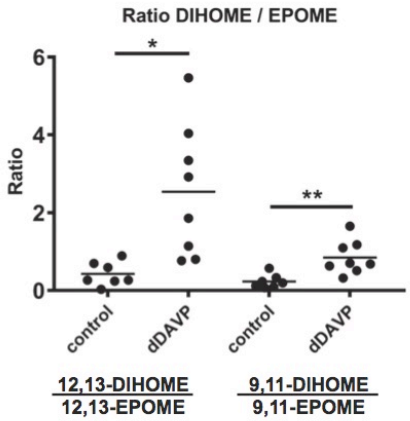

Fig. 2. Effect of dDAVP treatment on outer medullary levels of linoleic acid derivates in Brattleboro rats. Quantification of outer medullary levels of epoxide (EPOME)- and dihydroxy (DIHOME)-derivatives of linoleic acid reveals an increased DIHOME/EPOME ratio; this suggests increased activity of soluble epoxide hydrolase (sEH) (61). *$P < 0.05$; **$P < 0.01$; $n = 7$ or 8 per group.

pension were treated for 30 min at 37°C with 5,6-EET, 8,9-EET, 11,12-EET, 14,15-EET, and 14,15-DHET (1 μM final concentration; Cayman Chemicals) or with ethanol as vehicle. After the treatment, cells were pelleted at 1000 *g* for 10 min and prepared for Western blot analysis as described above.

Statistical analysis. All values are given as means ± SE. Statistical analysis was performed using unpaired Student's *t*-test or ANOVA with post hoc Tukey's test. Null hypothesis was excluded when P was <0.05.

RESULTS

Effect of dDAVP on medullary expression of EET-metabolizing enzymes. Screening of Affymetrix microarray results from kidney extracts of dDAVP- or vehicle-treated Brattleboro rats revealed constant mRNA levels for the CYP monooxygenases in CYP2C11, CYP2C23, CYP2J3, and Cyp2J10 (Table 1). Abundance of CYP2J4 mRNA was reduced by 20% relative to the vehicle-treated controls ($P < 0.05$), but subsequent real-time PCR verification studies in a separate set of animals ($n = 5$ per group) failed to confirm differential regulation (data not shown). mRNA levels for sEH were significantly induced (+145% relative to controls; $P < 0.05$) and in the real-time PCR verification studies (+160 ± 37%, $P < 0.05$).

Effect of dDAVP on renal-free EET tissue levels. Mass spectrometry analysis of renal lipid levels in dDAVP-treated Brattleboro rats revealed a reduced abundance of 5,6-EET (12.8 ± 3.2 ng/g vs. 35.7 ± 9.5 ng/g; $P < 0.05$), 11,12-EET (16.7 ± 3.3 ng/g vs. 38.4 ± 9.7 ng/g; $P < 0.05$), and 14,15-EET (11.2 ± 3 ng/g vs. 34.7 ± 9.2 ng/g; $P < 0.05$) relative to controls. Levels of the 8,9-isomer showed a strong trend toward reduced levels (17.4 ± 4 ng/g vs. 44 ± 13.4 ng/g; $P = 0.08$) but failed to reach the level of statistical significance. Values are given as ng EET/g wet tissue weight in dDAVP and vehicle-treated animals with $n = 7$ to 8 animals per group (Fig. 1). It must be noted that 5,6-EET rapidly forms a lactone in aqueous solutions, which may differ from the

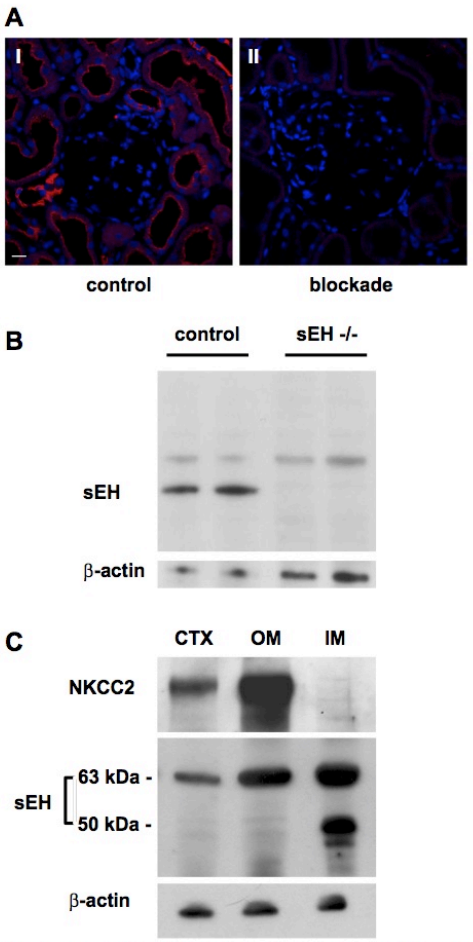

Fig. 3. Verification of anti-sEH antibody and distribution of sEH protein. *A*: representative micrographs documenting labeling of rat kidney sections with rabbit anti-sEH antibody (*I*) or with rabbit anti-sEH antibody following preincubation with the immunizing peptide (*II*). Abundant signal for sEH is present in the macula densa, proximal tubule, and collecting duct profiles *I*: preincubation of sEH antibody with the immunizing peptide results in a dose-dependent reduction of immunofluorescence signal. Blockade was maximal at 10-fold excess of the peptide *II*: immunofluorescence staining; bar indicates 20 μm. *B*: Western blot analysis of kidney homogenates of wild-type (*lanes 1* and *2*) and sEH-deficient mice (sEH-/-; *lanes 3* and *4*) showing a dominant band at 63 kDa in the wild-type animals, whereas no product is present in the sEH-/- kidneys, thus confirming the specificity of the antibody. *C*: Western blot analysis of the zonal distribution of sEH reveals a dominant immunoreactive band at ~63 kDa, which is present in all kidney zones. Samples from the inner medulla contain additional immunoreactive products at ~50 and 48 kDa, which probably represent splice variants of sEH (27). Western blot for NKCC2 shows abundant signal in the outer medulla, weaker signal in the cortex, and absence of signal in the inner medulla, thus confirming the adequate separation of the kidney zones. β-actin serves as a loading control.

parent molecule in its biological activity. During the tissue processing for our mass spectrometry assay, this lactone is converted back to 5,6-EET. Thus, the measured levels for the 5,6-EET regioisomer may be higher than the biologically active levels in the tissue.

We also determined the levels of the linoleic acid epoxides 9,10-EPOME (69 ± 14 ng/g vs. 254 ± 60 ng/g; $P < 0.05$) and 12,13-EPOME (36 ± 11 ng/g vs. 166 ± 44 ng/g; $P < 0.05$), as well as their respective diols 9,10-DIHOME [52 ± 8.8 ng/g vs. 47 ± 8.7 ng/g; $P = 0.7$, not significant (n.s.)] and 12,13-DIHOME (85 ± 25 ng/g vs. 56 ± 14 ng/g; $P = 0.4$ n.s.) in dDAVP-treated Brattleboro rats and control rats. The ratios for 9,10-DIHOME and 9,10-EPOME (0.85 vs. 0.23; $n = 7$ to 8 animals per group; $P < 0.05$) and 12,13-DIHOME and 12,13-EPOME (2.54 vs. 0.43; $n = 7$ or 8 animals per group; $P < 0.01$) were significantly increased in the dDAVP-treated animals, thus demonstrating increased sEH enzyme activity (Fig. 2).

Characterization of sEH antibody. Specificity of the sEH antibody was verified by peptide blockade and by immunoblotting on kidney samples of sEH-deficient mice. Preincubation of sEH antibody with the immunizing peptide caused a dose-dependent decrease in signal intensity in rat kidney sections. Blockade was maximal at 10-fold excess of the blocking peptide (Fig. 3*A*). Western blot analysis of kidney homogenates from wild-type mice revealed the presence of a dominant sEH-immunoreactive band at 63 kDa, which was absent in the homogenates of the sEH-deficient mice. An additional band was detected at 70 kDa. However, this band was also present in the sEH-deficient mice and was, therefore, considered unspecific (Fig. 3*B*).

Renal distribution of sEH. Zonal distribution of sEH was analyzed on rat kidney homogenates isolated from cortex and outer and inner medulla. Distribution of NKCC2 was determined in parallel and showed abundant signal in the outer medulla, weaker signal in the cortex, and absence of signal in

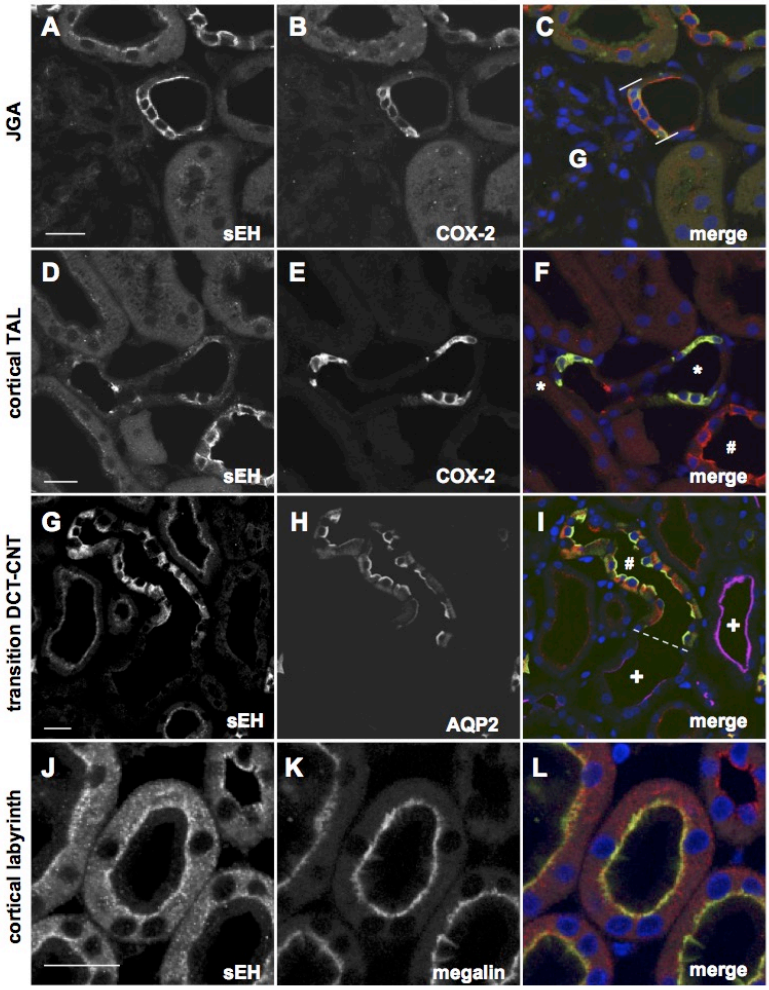

Fig. 4. Localization of sEH protein in Sprague-Dawley rat kidney. Representative micrographs documenting double labeling of rat kidney sections with rabbit anti sEH antibody (*A*, *D*, *G*, *J*) and cyclooxygenase 2 (COX-2; *B* and *E*) as a marker for the macula densa segment, the Na^+-Cl^--cotransporter NCC as a marker for the distal convoluted tubule (DCT; magenta in *I*), aquaporin 2 (AQP2) as a marker for the principal cells of the connecting tubule (CNT; *H*), and megalin as a marker for the proximal tubule (*K*). In the merged color images (*C*, *F*, *I*, *L*), red signal indicates sEH, and green signals mark COX-2 (*C* and *F*), AQP2 (*I*), and megalin (*L*). Magenta signal (*I*) marks NCC. Macula densa [between flanking lines in (C)] shows strong signal for sEH and COX-2 (*A*–*C*). sEH and COX-2 are also coexpressed in a subset of TAL cells distant to the juxtaglomerular apparatus (JGA; *D*–*F*). Abundant signal for sEH is present in the AQP2-immunoreactive CNT principal cells (*G*–*I*). DCT profiles are negative for sEH (*G*–*I*). Proximal convoluted tubule shows subapical sEH signal beneath megalin staining (*J*–*L*). Immunofluorescence staining: bars 20 μm. Blue nuclei are stained by DAPI. G denotes glomerulus in *C*; while * denotes TAL in *F*. Dashed line in *I* marks the transition from DCT (+) to CNT (#).

the inner medulla, thus confirming the adequate separation of the kidney zones. Western blot for sEH revealed a dominant immunoreactive band at ~63 kDa, which was present in all kidney zones. Samples from the inner medulla contained additional sEH-immunoreactive products at 50 and 48 kDa, which probably represent splice variants of the enzyme (Fig. 3*C*) (27).

Immunofluorescence labeling of rat and human kidney sections confirmed abundant expression of immunoreactive protein in all kidney zones (Figs. 3–6). In the cortex, strong cytosolic sEH signal was found in profiles of the macula densa, as indicated by the coexpression COX-2 (Fig. 4, *A–C*). Coexpression of sEH and COX-2 was further detected in a subset of cells in the cortical TAL (Fig. 4, *D–F*), whereas the remaining TAL was devoid of staining. Principal cells of the connecting tubule and the cortical collecting duct were identified by their expression of AQP2 and showed abundant sEH signal (Fig. 4, *G–I*). Triple labeling with the Na^+-Cl^--cotransporter NCC demonstrated the complete absence of sEH from the distal convoluted tubule (Fig. 4*I*). Profiles of the proximal tubule displayed subapical signal with intermediate intensity, which was localized directly below the megalin-immunoreactive brush-border membrane (Fig. 4, *J–L*). Signal intensity increased toward the end of the S3 segment and extended into the thin descending limb of the loop of Henle (Fig. 5, *A–C*). Profiles of the thin ascending limb of the loop of Henle stained positive as well (Fig. 5, *D–F*). Strong staining for sEH in the outer medulla was further detected in the collecting ducts, which were typically in close proximity with NKCC2-expressing profiles of the thick ascending limb, thus suggesting functional interaction (Fig. 5, *G–I*). Staining in the inner medulla was localized to tDLH, tALH, and to the principal cells of the inner medullary collecting duct, as indicated by the coexpression of AQP2 (Fig. 5, *J–L*). Since immunohistochemistry does not allow

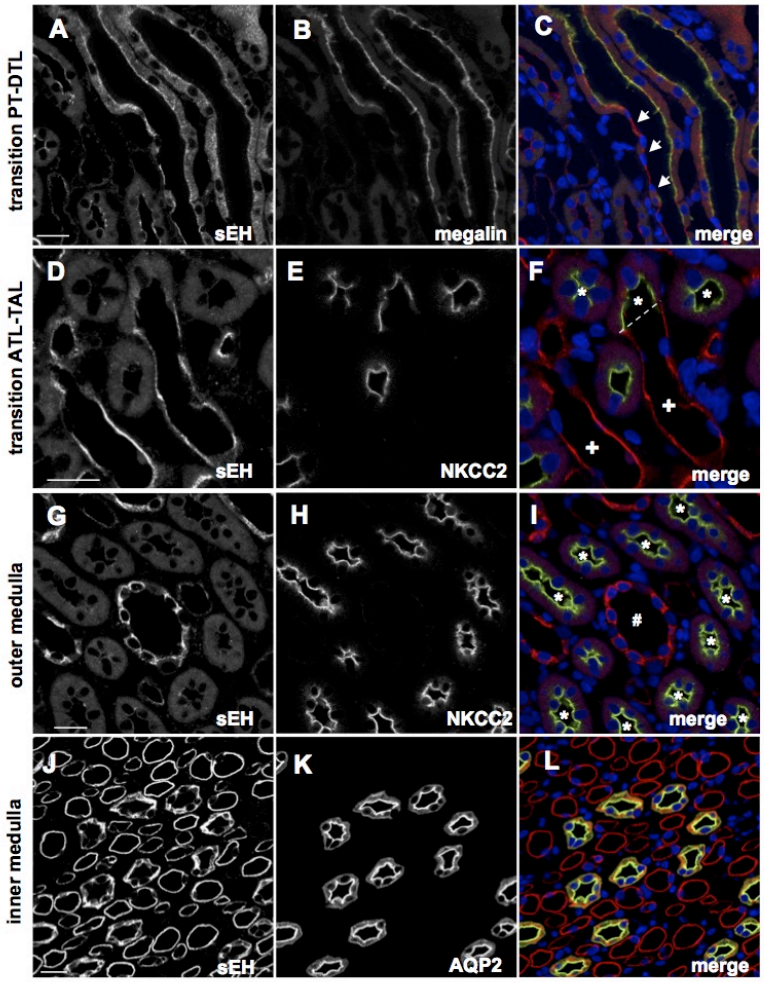

Fig. 5. Localization of sEH protein in Sprague-Dawley rat kidney (continued). Representative micrographs documenting double labeling of rat kidney sections with rabbit anti sEH antibody (*A*, *D*, *G*, *J*) and megalin (*B*) as a marker for the proximal tubule (PT), Na-K-2Cl-cotransporter NKCC2 (*E* and *H*) as a marker for the thick ascending limb (TAL), and aquaporin 2 (AQP2; *K*) as a marker for the medullary collecting duct. In the merged color images (*C*, *F*, *I*, *L*), red signal indicates sEH, and green signals mark megalin (*C*), NKCC2 (*F* and *I*), and AQP2 (*L*). PT sEH signal is localized subapically (*A–C*). Signal is stronger within terminal S3 and ensuing descending thin limb (DTL) portions (arrows in *C*) and continues to the ascending thin limb (ATL; + in *F*) until its transition to the negative TAL (* in *F* and *I*). Abundant sEH signal is present in the principal cells of the collecting duct in the outer (*G–I*) and inner medulla (*J–L*). Double labeling with NKCC2 shows the close local association between sEH-expressing collecting ducts (# in *I*) and profiles of the TAL in the outer medulla (*G–I*). In the inner medulla, sEH is abundantly expressed in DTL, ATL, and collecting ducts, with partial overlap to AQP2 in the latter (*J–L*). Immunofluorescence staining: bars 20 μm. Blue nuclei are stained by DAPI. The dashed line in *F* marks the transition from ATL to TAL.

the distinction between the full-length protein and the shorter products, the observed signals in the inner medulla reflect the sum of the full-length protein and the shorter variants.

The renal vasculature, as identified by the expression of α-smooth muscle actin in myocytes and pericytes of the vascular wall, was devoid of sEH staining (Fig. 6). Studies in human kidney samples confirmed the expression in the macula densa and in the collecting duct using the sEH antibody validated in rodent tissue together with NKCC2 or AQP2 costaining (Fig. 7).

Effect of chronic dDAVP treatment on renal sEH expression. The effects of a chronic activation of the urine-concentrating

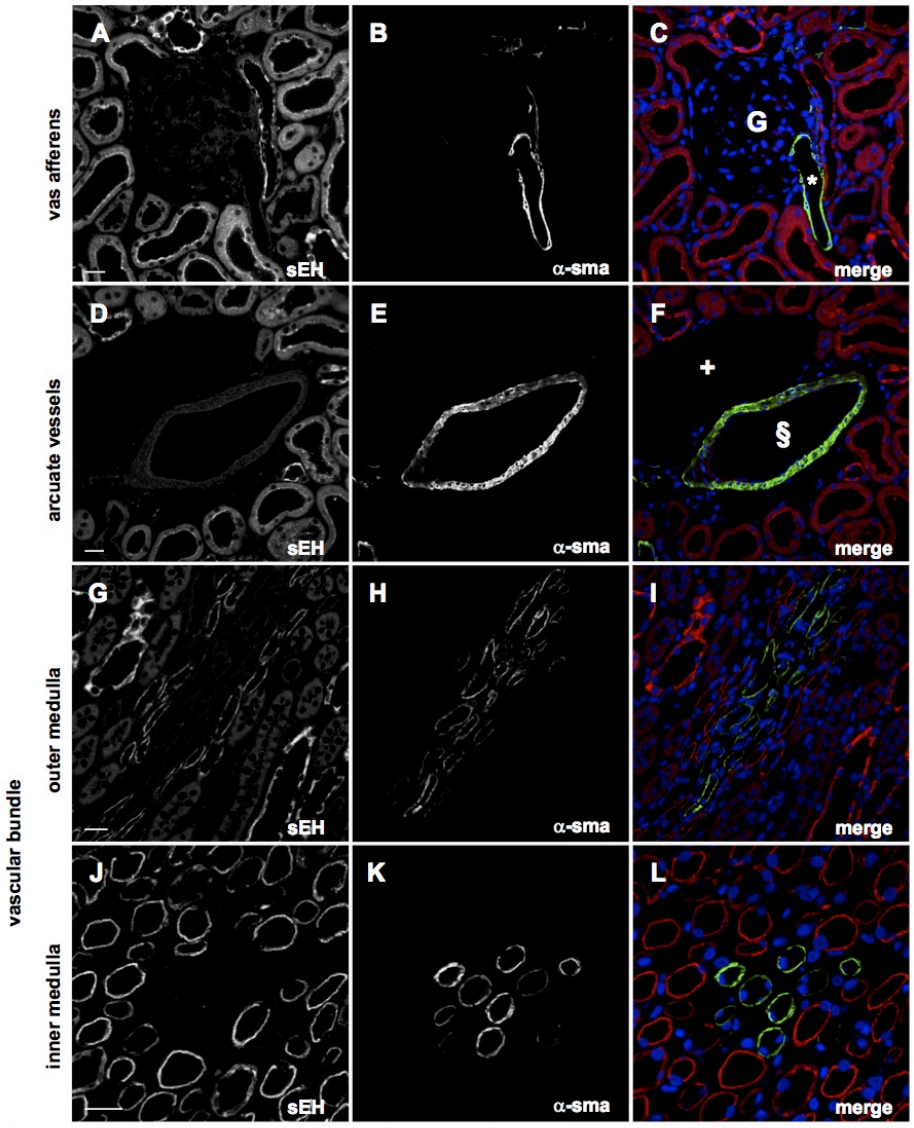

Fig. 6. Localization of sEH protein in the renal vasculature. Representative micrographs documenting double labeling of rat kidney sections with rabbit anti-sEH antibody (*A*, *D*, *G*, *J*) and α-smooth muscle actin (*B*, *E*, *H*, *K*; α-sma) as a marker for the vascular wall. In the merged color images (*C*, *F*, *I*, *L*), red signal indicates sEH, and green signals mark α-sma. There is complete separation of the two signals, demonstrating an absence of sEH from vascular smooth muscle and endothelial cells of afferent arterioles (*A–C*), arcuate vessels (*D–F*), vasa recta of outer (*G–I*), and inner medulla (*J–L*). Immunofluorescence staining: bars 20 μm. Blue nuclei are stained by DAPI. G denotes glomerulus, while * denotes afferent arteriole in *C*; + indicates the lumen of an arcuate vein, and § indicates the lumen of an arcuate artery in *F*.

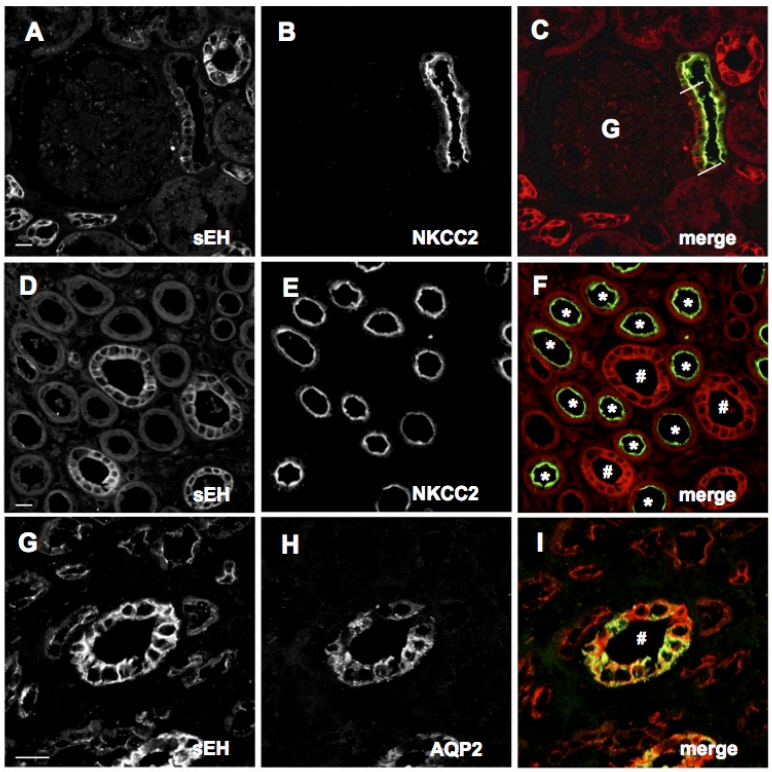

Fig. 7. Localization of sEH protein in the human kidney. Double labeling of human kidney sections with rabbit anti-sEH antibody (*A*, *D*, *G*) and antibodies against NKCC2 (*B* and *E*) or aquaporin 2 (AQP2; *H*). In the merged color images (*C*, *F*, *I*), red signal indicates sEH, and green signals mark NKCC2 (*C* and *F*) and AQP2 (*I*). Ample sEH protein is expressed in the macula densa (between flanking lines in (*C*), whereas the cells of the surrounding TAL are negative. Strong staining is also present in outer and inner medullary collecting duct profiles. Immunofluorescence staining: bars 20 μm. G denotes glomerulus in *C*, while * denotes TAL in *F*; and # shows the collecting ducts in *F* and *I*.

mechanism on renal sEH expression were studied in dDAVP-treated Brattleboro rats. Functional data for these animals demonstrating augmented urine concentration and induced levels of NKCC2 and aquaporin 2 have been reported before (17, 51). Immnuohistochemistry revealed increased sEH protein levels in the cortex and in the outer medulla of dDAVP-treated animals. Here sEH signal was strongly increased in connecting tubules and in the cortical and outer medullary collecting ducts. Protein levels in the inner medulla remained unchanged (Fig. 8*A*). Western blot analysis of total kidney homogenates confirmed increased levels of the 63 kDa (+65 ± 7% compared with controls; $P < 0.05$) and the 50 kDa (+65 ± 7% compared with controls; $P < 0.05$) variant of the protein in the dDAVP-treated animals (Fig. 8, *B* and *C*).

Effect of EET regioisomers on TAL transport activity and NKCC2 phosphorylation. The acute effects of the different EET regioisomers on the phosphorylation of NKCC2 were determined in murine kidney cell suspensions prestimulated with 100 nM dDAVP. Incubation of these cell suspensions with the individual EET regioisomers resulted in a significant reduction of pNKCC2 abundance for 5,6-EET, 8,9-EET and 14,15-EET compared with the vehicle-treated controls (−35 ± 14%, −53 ± 8%, and −66 ± 5%, respectively; $P < 0.05$). In contrast, 11,12-EET had no effect (+18 ± 15%, $P = 0.5$) (Fig. 9). To corroborate these results, we studied the effects of the 14,15-EET regioisomer in greater detail and also included the inactive metabolite 14,15-DHET. Phosphorylation of NKCC2 functionally changes the transport current by changing NKCC2 membrane trafficking, as well as by changing its Cl^- affinity, rate-limiting in the cortical TAL with already dilute luminal fluid (9, 22). To investigate the effect of 14,15-EET on TAL tubular transport, we, therefore, measured the equivalent short-circuit current I'_{sc} under two Cl^- concentrations, at 147 mmol/l to assess maximal transport velocity (V_{max}) of the transporter and at 30 mmol/l, a concentration close to the described EC_{50} of NKCC2 for Cl^- (22). Freshly isolated cTAL were incubated with either vehicle (control), 1 μmol/l 14,15 -EET or 1 μmol/l 14,15-DHET for 30–40 min. After this preincubation period isolated perfused cTALs of the three groups, Control, 14,15-EET, and 14,15-DHET, showed the typical lumen positive transport I'sc. Pretreatment with 14,15-EET reduced I'sc to 70% of the control I'_{sc} under high Cl^- concentrations and to ~30% under the low Cl^- concentration, respectively (Fig. 10*A*). To address the question of whether 14,15-EET only reduces the total amount of NKCC2 in the plasma membrane, thereby shifting the curve in the scheme (Fig. 10*B*) from 1 to 2, or also decreases its Cl^- affinity (*curve 3* in the scheme), we calculated the percentage of I'sc (low Cl^-) of the respective V_{max} (147 Cl^-) values (Fig. 10*B*). 14,15-EET treatment led to a 55% reduction, indicating a markedly reduced Cl^- affinity. In contrast, pretreatment with 14,15-DHET did not induce a change in any of the parameters. Treatment of murine kidney cell suspensions with 100 nM dDAVP and 14,15-EET at concentrations of 0.1 or 1 μM

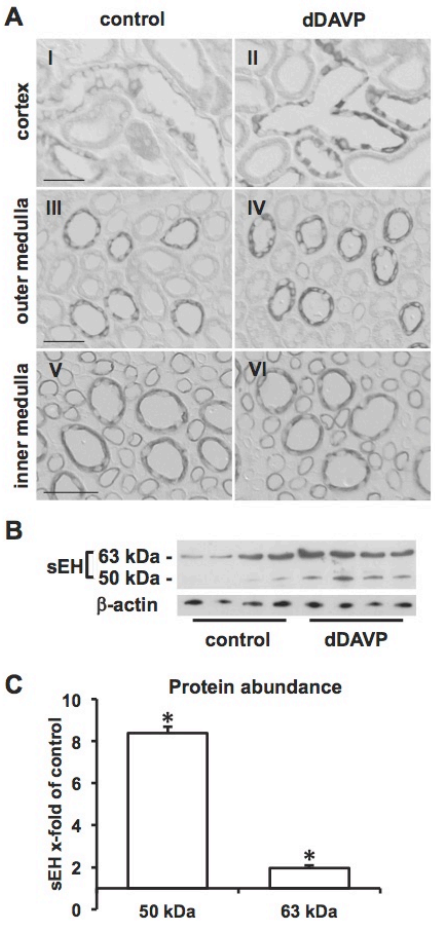

Fig. 8. Effect of chronic vasopressin V_2 receptor activation on sEH protein expression in Brattleboro rats. *A*: representative high-power micrographs showing sEH signal in the cortex (*I*, *II*), outer medulla (*III*, *IV*), and inner medulla of Brattleboro rats after vehicle (*I*, *III*, *V*; control) or dDAVP treatment (*II*, *IV*, *VI*; dDAVP). Treated animals show a stronger accumulation of immunoreactive sEH in the cortex and outer medulla compared with controls. Inner medullary sEH signals are not different. Immunoperoxidase staining: bars 100 μm; $n = 8$ per group. *B*: Western blot of kidney homogenates from Brattleboro rats treated with vehicle or dDAVP showing increased signal intensity for the 63- and 50-kDa sEH variants; β-actin served as a loading control. *C*: densitometric analysis of the signal confirms increased total abundance of sEH in the treated animals. Data are means ± SE; $*P < 0.05$; $n = 8$ per group.

resulted in a dose-dependent reduction of pNKCC2 levels compared with cell suspensions treated with 100 nM dDAVP and ethanol as vehicle (control). Treatment with 1 μM 14,15-DHET had no effect on the NKCC2 phosphorylation (Fig. 10*D*).

Effect of sEH gene disruption on NKCC2 phosphorylation. Analysis of outer medullary pNKCC2 abundance revealed greatly reduced levels in the sEH-deficient mice relative to the wild-type controls (Fig. 11), whereas total NKCC2 abundance was unchanged (data not shown).

DISCUSSION

The aim of the present study was to characterize the effects of AVP on the abundance and metabolism of EET isomers in the kidney. We have demonstrated markedly reduced tissue levels of EET isomers along with an increased abundance of the principal EET-metabolizing enzyme sEH in connecting tubules and collecting ducts of AVP-treated Brattleboro rat kidneys compared with vehicle-treated controls. EET isomers and AVP have been shown to exert opposing effects on essential renal sodium transporters. In connecting tubule (CNT) and collecting duct (CD), AVP activated the amiloride-sensitive epithelial sodium channel ENaC (5, 6), whereas 14,15-EET acted as a potent inhibitor of ENaC transport activity (13). In the TAL, AVP caused activation of NKCC2-dependent ion transport, in part, by increasing its phosphorylation (46). In the present study, we found a pronounced inhibitory effect of all EET regioisomers with the exception of 11,12-EET on NKCC2 phosphorylation. Parallel microperfusion studies on murine cortical TAL segments demonstrated an

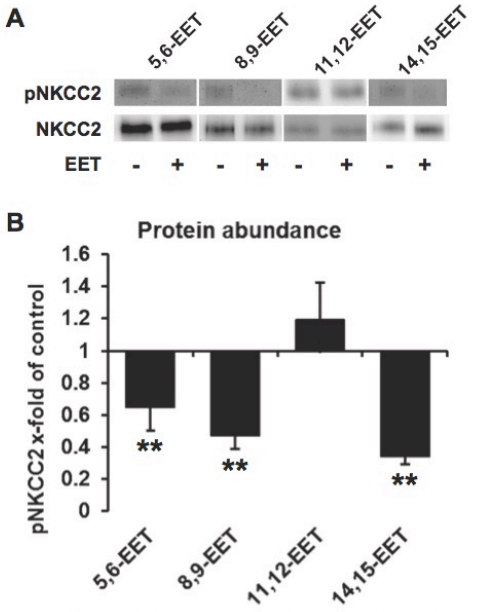

Fig. 9. Effect of EET regioisomers on NKCC2 phosphorylation. *A*: Western blots of murine kidney cell suspensions treated with 100 nM dDAVP as control (−) or with 100 nM dDAVP and 1 μM 5,6-EET, 8,9-EET, 11,12-EET, or 14,15-EET (+) for 30 min. Bands show lower levels of phosphorylated NKCC2 (pNKCC2) after treatment with 5,6-EET, 8,9-EET, and 14,15-EET; total NKCC2 abundance was determined in parallel and serves as loading control. *B*: Densitometric analysis of the signal intensity and normalization to total NKCC2 levels confirms reduced abundance of pNKCC2 after treatment with 5,6-EET, 8,9-EET, and 14,15-EET. No effect is detectable following treatment with 11,12-EET. Data are expressed as means ± SE; $**P < 0.01$; $n = 8$–10 per group. Samples were prepared from a total of six mice.

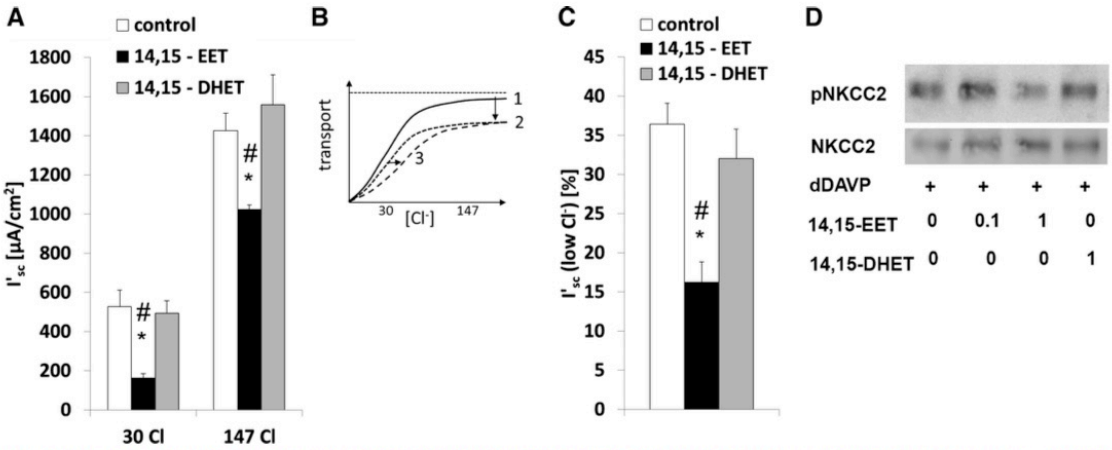

Fig. 10. Effects of 14,15-EET on TAL transport activity and NKCC2 phosphorylation. *A*: summarized data of the equivalent short-circuit current I'_{sc} of isolated perfused cTAL pretreated with vehicle (control; white bars), 1 μM 14,15-EET (black bars), or 1 μM 14,15-DHET (gray bars) under two symmetric Cl^- concentrations, 30 mmol/l Cl^- (30) and 147 mmol/l Cl^- (147). *B*: simplified scheme to illustrate enzyme kinetic like properties of NKCC2 (*curve 1*) with maximal transport rate (V_{max}, dashed line). Reduced number of NKCC2 in the membrane reduces V_{max} with unchanged EC_{50} (*curve 2*). Changes in Cl^- affinity of NKCC2 lead to an additional shift of EC_{50} to higher Cl^- concentrations (*curve 3*). *C*: I'_{sc} at low-chloride concentration expressed as a percentage of the respective V_{max} values; the 55% reduction after 14,15-EET pretreatment shows a markedly reduced Cl^- affinity. Treatment with 14,15-DHET has no detectable effect on I'_{sc}. Electrophysiological data are means ± SE; n = 8, 9, and 8 for control, 14,15-EET, and 14,15-DHET, respectively. *$P < 0.05$ control vs. 14,15-EET. #$P < 0.05$ 14,15-EET vs. 14,15-DHET. *D*: Western blot of dDAVP-stimulated murine kidney cell suspensions showing a dose-dependent reduction of phosphorylated NKCC2 (pNKCC2) after treatment with 0.1 μM and 1 μM 14,15-EET compared with the vehicle-treated control. Treatment of dDAVP-stimulated kidney cell suspensions with 14,15-DHET has no effect. Total NKCC2 abundance was determined in parallel and serves as a loading control. Representative example of n = 9 for vehicle-, EET-, and DHET, respectively. Samples were prepared from a total of six mice.

inhibitory effect of 14,15-EET on the chloride sensitivity of NKCC2 and overall TAL transport activity. In line with this, sEH-deficient mice, which display elevated tissue levels of EETs and 20-HETE (41, 62), showed markedly reduced phosphorylation of NKCC2. These findings agree with data by He et al. (26) on the inhibitory effects of 14,15-EET on NKCC2 transport activity in cultured murine macula densa cells. By contrast, Grider et al. (23) found no effect of 10^{-8} M 5,6-EET on transport activity in isolated rat TAL segments. However, the 5,6-EET concentration used in that study was well below the free tissue concentrations observed in our study and may, therefore, have been insufficient to inhibit NKCC2-dependent transport. Opposing effects of AVP and EETs have further been described for the renal vasculature. Here, AVP causes vasoconstriction either directly by activating vascular V_1 receptors or indirectly by its effects on epithelial V_2 receptors (8, 45, 67), whereas EETs may function as vasodilating mediators in afferent arterioles and interlobular arteries (reviewed in Ref. 30). The observed reduction of renal EET levels in response to AVP may, therefore, be instrumental for sodium retention and increase in renovascular resistance during AVP-mediated urine concentration.

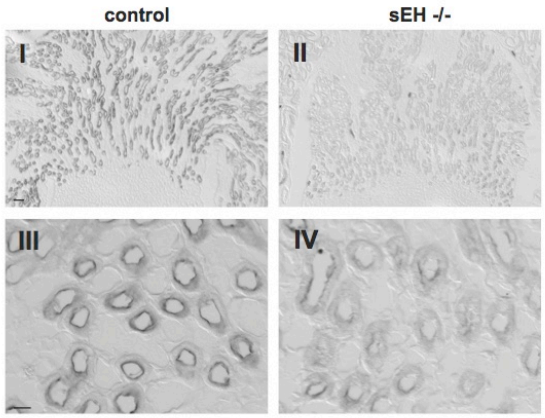

Fig. 11. Effect of sEH deficiency on outer medullary levels of phosphorylated NKCC2 (pNKCC2). Representative low- (*I* and *II*) and high- (*III* and *IV*) power micrographs showing reduced levels of immunoreactive pNKCC2 in the outer medulla of sEH-deficient mice (*II* and *IV*; sEH-/-) compared with wild-type controls (*I* and *II*). Immunoperoxidase staining: bars, 200 μm for *I* and *II*, and 20 μm for *III* and *IV*. n = 4 per group.

Cellular sources and regulation of renal EET synthesis during antidiuresis have not been clarified satisfactorily in previous work. The first rate-limiting step during the formation of EETs is the release of arachidonic acid from membrane phospholipids, which is typically catalyzed by a phospholipase A2 (PLA2) isoenzyme. The identity of the PLA2 isoenzyme involved in the synthesis of EETs has not been elucidated. However, in a previous study, we have shown that the calcium-independent isoform of PLA2 (iPLA2β) is abundantly expressed in the connecting tubule and medullary collecting duct and that chronic stimulation with dDAVP led to a reduction of iPLA2β biosynthesis, with the assumed consequence of reduced AA release (51). Since both connecting tubule and collecting duct have been identified as important sites for intrarenal EET production (65), reduced iPLA2 levels at these sites may likely have contributed to the reduced abundance of

EETs observed in the present study. Alternative pathways for arachidonic acid release have been described, but their relevance for renal EET synthesis remains to be determined (16, 36). The next step in the biosynthesis of EETs is catalyzed by a CYP monooxygenase isoenzyme; however, on the basis of the results of microarray studies CYP monooxygenase abundance was not affected by AVP. This finding argues against a relevant role of CYP monooxygenases as rate-limiting enzymes in EET metabolism under this condition. Here, we have, however, identified an additional mechanism for the regulation of EET levels in response to AVP, which centrally involves the function of sEH.

So far, ample evidence has linked sEH to the pathophysiology of cardiovascular and renal disease, and inhibitors of sEH have been shown to exert antihypertensive and renoprotective effects (33, 34, 38, 44, 53, 58). In spite of extensive studies performed on the renal expression of sEH, however, there is still no consensus regarding the intrarenal localization of the enzyme. Earlier reports range from an exclusively vascular localization (75) over interstitial (53) to preferentially glomerular (38) or tubular expression (33). In our study, we found widespread distribution of the protein with expression in proximal tubules, ascending and descending thin limbs of the loop of Henle, the macula densa, and in CNT and CD, whereas glomeruli, medullary TAL and DCT, and vascular structures were devoid of staining. Little is currently known regarding the function of sEH in individual nephron segments. In the proximal tubule, 5,6-EET and 14,15-EET have been shown to inhibit sodium transport (29, 39, 42, 64). Expression of sEH in the apical membrane of proximal tubules may, therefore, serve to deactivate EETs in the tubular fluid to avoid uncontrolled inhibition of transport. Another important finding of our study is the abundant expression of sEH in macula densa and cortical TAL and its colocalization with COX-2 at these sites. COX-2-derived prostaglandins cause vasodilation of the afferent arteriole and, thereby, play an important role for the maintenance of glomerular filtration during impaired renal perfusion (24). However, COX-2 is also capable of oxidizing 5,6-EET, and the resulting metabolites have been shown to cause vasoconstriction of the preglomerular vasculature (31). sEH activity in the macula densa and the cortical TAL may, therefore, reduce local EET levels and may, thus, prevent the formation of vasoconstrictive metabolites. Notably, we found high levels of sEH also in the inner medulla, where we and others had previously detected abundant COX-2 expression (12, 70, 73). Again, sEH may serve to prevent the formation of EET metabolites with unwanted properties at this site.

The dDAVP-treated Brattleboro rats revealed elevated sEH levels in CNT and CD, which corresponds to the established localization of the AVP V_2 receptor (46, 50, 60) and suggests a functional link between AVP signaling and sEH activation. Although a mechanism for this link has so far not been explored, the analysis of the sEH promotor sequence revealed the presence of several putative cAMP-response elements in our hands. AVP-dependent induction of sEH biosynthesis may, therefore, be mediated via the AVP V_2 receptor-dependent activation of adenylyl cyclase VI (56). Other mediators that have been shown to regulate sEH biosynthesis and may interfere with AVP signaling include ANG II (32, 69, 72, 78), steroid hormones (43, 55), and PPARγ agonists (25, 47).

The potential biological relevance of an AVP-dependent activation of sEH is illustrated by observations in several animal models for renal and cardiovascular disease. Along this line, spontaneously hypertensive rats displayed increased renal sEH activity compared with their normotensive Wistar-Kyoto counterparts (76), along with elevated plasma levels of AVP (11, 14), and an increased abundance of renal AVP receptors (66). Hypertension in these animals could be effectively reduced by treatment with antagonists for AVP (63) or sEH (35). Parallel protective effects of antagonists for AVP and sEH have also been described for DOCA-salt-induced hypertension (10, 49, 54), systolic heart failure (44), or diabetic nephropathy (7). On the basis of our findings, we, thus, suggest that the detrimental effects of AVP may, in part, be mediated by its effect on sEH synthesis and the resulting accelerated degradation of vasodilatory and transport-inhibiting EET.

In summary, we have shown that activation of AVP signaling causes upregulation of renal sEH biosynthesis and enzyme activity. The resulting reduction of EET tissue levels may facilitate increased transport activity and renal vasoconstriction to promote antidiuresis, but it may as well render the kidney susceptible to insult. Further characterization of the AVP-sEH-EET axis may, therefore, provide new targets for renoprotective therapeutic strategies.

ACKNOWLEDGMENTS

We thank F. Grams, K. Riskowsky, and C. Andrée for technical assistance and A. Drobbe for editorial support.

GRANTS

These studies were supported by the Deutsche Forschungsgemeinschaft (FOR667 and FOR1368).

DISCLOSURES

S. M. Weldon is employed by Boehringer Ingelheim Pharmaceuticals. M. Rothe is employed by Lipidomix.

AUTHOR CONTRIBUTIONS

C.B., T.R., M. Bleich, H.K., A.M., T.G., K.M., S.M.W., W.-H.S., S.B., and A. Paliege conceived and designed research; C.B., T.R., N.H., A. Plain, M. Blum, H.K., T.G., K.M., M.R., and A. Paliege performed experiments; C.B., T.R., M. Bleich, R.L., M. Blum, M.R., D.D., W.-H.S., and A. Paliege analyzed data; C.B., T.R., M. Blum, A.M., M.R., W.-H.S., S.B., and A. Paliege interpreted results of experiments; C.B., T.R., R.L., and A. Paliege prepared figures; C.B., T.R., N.H., A. Plain, M. Bleich, R.L., M. Blum, H.K., A.M., T.G., K.M., M.R., S.M.W., D.D., W.-H.S., S.B., and A. Paliege approved final version of manuscript; H.K., A.M., S.M.W., D.D., W.-H.S., and S.B. edited and revised manuscript; A. Paliege drafted manuscript.

REFERENCES

1. **Amlal H, Legoff C, Vernimmen C, Paillard M, and Bichara M.** Na^+-K^+(NH_4^+)-2Cl-cotransport in medullary thick ascending limb: control by PKA, PKC, and 20-HETE. *Am J Physiol Cell Physiol* 271: C455–C463, 1996.
2. **Arnold C, Markovic M, Blossey K, Wallukat G, Fischer R, Dechend R, Konkel A, von Schacky C, Luft FC, Muller DN, Rothe M, Schunck WH.** Arachidonic acid-metabolizing cytochrome P450 enzymes are targets of ω-3 fatty acids. *J Biol Chem* 285: 32,720–32,733, 2010.
3. **Bachmann S, Schlichting U, Geist B, Mutig K, Petsch T, Bacic D, Wagner CA, Kaissling B, Biber J, Murer H, Willnow TE.** Kidney-specific inactivation of the megalin gene impairs trafficking of renal inorganic sodium phosphate cotransporter (NaPi-IIa). *J Am Soc Nephrol* 15: 892–900, 2004.
4. **Badzynska B, Sadowski J.** Opposed effects of prostaglandin E_2 on perfusion of rat renal cortex and medulla: interactions with the renin-angiotensin system. *Exp Physiol* 93: 1292–1302, 2008.

5. **Bankir L, Bouby N, Ritz E.** Vasopressin: a novel target for the prevention and retardation of kidney disease? *Nat Rev Nephrol* 9: 223–239, 2013.
6. **Bankir L, Fernandes S, Bardoux P, Bouby N, Bichet DG.** Vasopressin-V_2 receptor stimulation reduces sodium excretion in healthy humans. *J Am Soc Nephrol* 16: 1920–1928, 2005.
7. **Bankir L, Roussel R, Bouby N.** Protein- and diabetes-induced glomerular hyperfiltration: role of glucagon, vasopressin, and urea. *Am J Physiol Renal Physiol* 309: F2–F23, 2015.
8. **Boertien WE, Meijer E, de Jong PE, Bakker SJ, Czerwiec FS, Struck J, Oberdhan D, Shoaf SE, Krasa HB, Gansevoort RT.** Short-term renal hemodynamic effects of tolvaptan in subjects with autosomal dominant polycystic kidney disease at various stages of chronic kidney disease. *Kidney Int* 84: 1278–1286, 2013.
9. **Borschewski A, Himmerkus N, Boldt C, Blankenstein KI, McCormick JA, Lazelle R, Willnow TE, Jankowski V, Plain A, Bleich M, Ellison DH, Bachmann S, Mutig K.** Calcineurin and sorting-related receptor with A-type repeats interact to regulate the renal Na^+-K^+-$2Cl^-$ cotransporter. *J Am Soc Nephrol* 27: 107–119, 2016.
10. **Brooks VL, Freeman KL, Qi Y.** Time course of synergistic interaction between DOCA and salt on blood pressure: roles of vasopressin and hepatic osmoreceptors. *Am J Physiol Regul Integr Comp Physiol* 291: R1825–R1834, 2006.
11. **Burrell LM, Risvanis J, Dean RG, Patel SK, Velkoska E, Johnston CI.** Age-dependent regulation of renal vasopressin V_{1A} and V_2 receptors in rats with genetic hypertension: implications for the treatment of hypertension. *J Am Soc Hypertens* 7: 3–13, 2013.
12. **Campean V, Theilig F, Paliege A, Breyer M, Bachmann S.** Key enzymes for renal prostaglandin synthesis: site-specific expression in rodent kidney (rat, mouse). *Am J Physiol Renal Physiol* 285: F19–F32, 2003.
13. **Capdevila J, Wang W.** Role of cytochrome P450 epoxygenase in regulating renal membrane transport and hypertension. *Curr Opin Nephrol Hypertens* 22: 163–169, 2013.
14. **Crofton JT, Share L, Shade RE, Allen C, Tarnowski D.** Vasopressin in the rat with spontaneous hypertension. *Am J Physiol Heart Circ Physiol* 235: H361–H366, 1978.
15. **Culpepper RM, Andreoli TE.** Interactions among prostaglandin E_2, antidiuretic hormone, and cyclic adenosine monophosphate in modulating Cl^- absorption in single mouse medullary thick ascending limbs of Henle. *J Clin Invest* 71: 1588–1601, 1983.
16. **Dichlberger A, Schlager S, Kovanen PT, Schneider WJ.** Lipid droplets in activated mast cells—a significant source of triglyceride-derived arachidonic acid for eicosanoid production. *Eur J Pharmacol* 785: 59–69, 2016.
17. **Dietrich A, Mathia S, Kaminski H, Mutig K, Rosenberger C, Mrowka R, Bachmann S, Paliege A.** Chronic activation of vasopressin V_2 receptor signaling lowers renal medullary oxygen levels in rats. *Acta Physiol* 207: 721–731, 2013.
18. **El-Sherbeni AA, Aboutabl ME, Zordoky BN, Anwar-Mohamed A, El-Kadi AO.** Determination of the dominant arachidonic acid cytochrome p450 monooxygenases in rat heart, lung, kidney, and liver: protein expression and metabolite kinetics. *AAPS J* 15: 112–122, 2013.
19. **Enayetallah AE, French RA, Thibodeau MS, Grant DF.** Distribution of soluble epoxide hydrolase and of cytochrome P450 2C8, 2C9, and 2J2 in human tissues. *J Histochem Cytochem* 52: 447–454, 2004.
20. **Fromel T, Jungblut B, Hu J, Trouvain C, Barbosa-Sicard E, Popp R, Liebner S, Dimmeler S, Hammock BD, Fleming I.** Soluble epoxide hydrolase regulates hematopoietic progenitor cell function via generation of fatty acid diols. *Proc Natl Acad Sci USA* 109: 9995–10,000, 2012.
21. **Greger R.** Cation selectivity of the isolated perfused cortical thick ascending limb of Henle's loop of rabbit kidney. *Pflügers Arch* 390: 30–37, 1981.
22. **Greger R, Oberleithner H, Schlatter E, Cassola AC, Weidtke C.** Chloride activity in cells of isolated perfused cortical thick ascending limbs of rabbit kidney. *Pflügers Arch* 399: 29–34, 1983.
23. **Grider JS, Falcone JC, Kilpatrick EL, Ott CE, Jackson BA.** P450 arachidonate metabolites mediate bradykinin-dependent inhibition of NaCl transport in the rat thick ascending limb. *Can J Physiol Pharmacol* 75: 91–96, 1997.
24. **Harris RC Jr.** Cyclooxygenase-2 inhibition and renal physiology. *Am J Cardiol* 89: 10D–17D, 2002.
25. **Harris TR, Hammock BD.** Soluble epoxide hydrolase: gene structure, expression and deletion. *Gene* 526: 61–74, 2013.
26. **He H, Podymow T, Zimpelmann J, Burns KD.** NO inhibits Na^+-K^+-$2Cl^-$ cotransport via a cytochrome P-450-dependent pathway in renal epithelial cells (MMDD1). *Am J Physiol Renal Physiol* 284: F1235–F1244, 2003.
27. **Hennebold JD, Mah K, Perez W, Vance JE, Stouffer RL, Morisseau C, Hammock BD, Adashi EY.** Identification and characterization of an ovary-selective isoform of epoxide hydrolase. *Biol Reprod* 72: 968–975, 2005.
28. **Hercule HC, Schunck WH, Gross V, Seringer J, Leung FP, Weldon SM, da Costa Goncalves A, Huang Y, Luft FC, Gollasch M.** Interaction between P450 eicosanoids and nitric oxide in the control of arterial tone in mice. *Arterioscler Thromb Vasc Biol* 29: 54–60, 2009.
29. **Houillier P, Chambrey R, Achard JM, Froissart M, Poggioli J, Paillard M.** Signaling pathways in the biphasic effect of angiotensin II on apical Na/H antiport activity in proximal tubule. *Kidney Int* 50: 1496–1505, 1996.
30. **Imig JD.** Epoxides and soluble epoxide hydrolase in cardiovascular physiology. *Physiol Rev* 92: 101–130, 2012.
31. **Imig JD, Navar LG, Roman RJ, Reddy KK, Falck JR.** Actions of epoxygenase metabolites on the preglomerular vasculature. *J Am Soc Nephrol* 7: 2364–2370, 1996.
32. **Imig JD, Zhao X, Capdevila JH, Morisseau C, Hammock BD.** Soluble epoxide hydrolase inhibition lowers arterial blood pressure in angiotensin II hypertension. *Hypertension* 39: 690–694, 2002.
33. **Jung O, Brandes RP, Kim IH, Schweda F, Schmidt R, Hammock BD, Busse R, Fleming I.** Soluble epoxide hydrolase is a main effector of angiotensin II-induced hypertension. *Hypertension* 45: 759–765, 2005.
34. **Kaergel E, Muller DN, Honeck H, Theuer J, Shagdarsuren E, Mullally A, Luft FC, Schunck WH.** P450-dependent arachidonic acid metabolism and angiotensin II-induced renal damage. *Hypertension* 40: 273–279, 2002.
35. **Kato Y, Fuchi N, Saburi H, Nishimura Y, Watanabe A, Yagi M, Nakadera Y, Higashi E, Yamada M, Aoki T.** Discovery of 2,8-diazaspiro[4.5]decane-based trisubstituted urea derivatives as highly potent soluble epoxide hydrolase inhibitors and orally active drug candidates for treating hypertension. *Bioorg Med Chem Lett* 23: 5975–5979, 2013.
36. **Kawaguchi H, Okamoto H, Saito H, Yasuda H.** Renal phospholipase C and diglyceride lipase activity in spontaneously hypertensive rats. *Hypertension* 10: 100–106, 1987.
37. **Knepper MA, Kwon TH, Nielsen S.** Molecular physiology of water balance. *N Engl J Med* 372: 1349–1358, 2015.
38. **Lee JP, Yang SH, Lee HY, Kim B, Cho JY, Paik JH, Oh YJ, Kim DK, Lim CS, Kim YS.** Soluble epoxide hydrolase activity determines the severity of ischemia-reperfusion injury in kidney. *PLoS One* 7: e37075, 2012.
39. **Li Y, Yamada H, Kita Y, Suzuki M, Endo Y, Horita S, Yamazaki O, Shimizu T, Seki G, Fujita T.** Arachidonic acid metabolites inhibit the stimulatory effect of angiotensin II in renal proximal tubules. *Hypertens Res* 31: 2155–2164, 2008.
40. **Livak KJ, Schmittgen TD.** Analysis of relative gene expression data using real-time quantitative PCR and the 2(-Delta Delta C(T)) method. *Methods* 25: 402–408, 2001.
41. **Luria A, Weldon SM, Kabcenell AK, Ingraham RH, Matera D, Jiang H, Gill R, Morisseau C, Newman JW, Hammock BD.** Compensatory mechanism for homeostatic blood pressure regulation in Ephx2 gene-disrupted mice. *J Biol Chem* 282: 2891–2898, 2007.
42. **Madhun ZT, Goldthwait DA, McKay D, Hopfer U, Douglas JG.** An epoxygenase metabolite of arachidonic acid mediates angiotensin II-induced rises in cytosolic calcium in rabbit proximal tubule epithelial cells. *J Clin Invest* 88: 456–461, 1991.
43. **Marova EI, Goncharov NP, Kolesnikova GS, Arapova SD, Lapshina AM.** The response of corticotropin and adrenal steroids to desmopressin stimulation in patients with various forms of hypercortisolism. *Hormones* 7: 243–250, 2008.
44. **Monti J, Fischer J, Paskas S, Heinig M, Schulz H, Gosele C, Heuser A, Fischer R, Schmidt C, Schirdewan A, Gross V, Hummel O, Maatz H, Patone G, Saar K, Vingron M, Weldon SM, Lindpaintner K, Hammock BD, Rohde K, Dietz R, Cook SA, Schunck WH, Luft FC, Hubner N.** Soluble epoxide hydrolase is a susceptibility factor for heart failure in a rat model of human disease. *Nat Genet* 40: 529–537, 2008.
45. **Moss NG, Kopple TE, Arendshorst WJ.** Renal vasoconstriction by vasopressin V_{1a} receptors is modulated by nitric oxide, prostanoids, and superoxide but not the ADP ribosyl cyclase CD38. *Am J Physiol Renal Physiol* 306: F1143–F1154, 2014.

46. **Mutig K, Paliege A, Kahl T, Jons T, Muller-Esterl W, Bachmann S.** Vasopressin V_2 receptor expression along rat, mouse, and human renal epithelia with focus on TAL. *Am J Physiol Renal Physiol* 293: F1166–F1177, 2007.
47. **Nofziger C, Brown KK, Smith CD, Harrington W, Murray D, Bisi J, Ashton TT, Maurio FP, Kalsi K, West TA, Baines D, Blazer-Yost BL.** PPARγ agonists inhibit vasopressin-mediated anion transport in the MDCK-C7 cell line. *Am J Physiol Renal Physiol* 297: F55–F62, 2009.
48. **Oguro A, Fujita N, Imaoka S.** Regulation of soluble epoxide hydrolase (sEH) in mice with diabetes: high glucose suppresses sEH expression. *Drug Metab Pharmacokinet* 24: 438–445, 2009.
49. **Okada H, Suzuki H, Kanno Y, Saruta T.** Effect of nonpeptide vasopressin receptor antagonists on developing, and established DOCA-salt hypertension in rats. *Clin Exp Hypertens* 17: 469–483, 1995.
50. **Ostrowski NL, Young WS, 3rd Knepper MA, Lolait SJ.** Expression of vasopressin V_{1a} and V_2 receptor messenger ribonucleic acid in the liver and kidney of embryonic, developing, and adult rats. *Endocrinology* 133: 1849–1859, 1993.
51. **Paliege A, Roeschel T, Neymeyer H, Seidel S, Kahl T, Daigeler AL, Mutig K, Mrowka R, Ferreri NR, Wilson BS, Himmerkus N, Bleich M, Bachmann S.** Group VIA phospholipase A_2 is a target for vasopressin signaling in the thick ascending limb. *Am J Physiol Renal Physiol* 302: F865–F874, 2012.
52. **Paliege A, Rosenberger C, Bondke A, Sciesielski L, Shina A, Heyman SN, Flippin LA, Arend M, Klaus SJ, Bachmann S.** Hypoxia-inducible factor-2α-expressing interstitial fibroblasts are the only renal cells that express erythropoietin under hypoxia-inducible factor stabilization. *Kidney Int* 77: 312–318, 2010.
53. **Pan YJ, Tao ZF, Wang Q, Lu M, Guan YF, Zhu Y, Wang Y.** [Expression and role of soluble epoxide hydrolase in renal tissue of two kidneys one clip hypertension rats model]. *Beijing Da Xue Xue Bao* 43: 820–826, 2011.
54. **Pietranera L, Saravia FE, McEwen BS, Lucas LL, Johnson AK, De Nicola AF.** Changes in Fos expression in various brain regions during deoxycorticosterone acetate treatment: relation to salt appetite, vasopressin mRNA and the mineralocorticoid receptor. *Neuroendocrinology* 74: 396–406, 2001.
55. **Pinot F, Grant DF, Spearow JL, Parker AG, Hammock BD.** Differential regulation of soluble epoxide hydrolase by clofibrate and sexual hormones in the liver and kidneys of mice. *Biochem Pharmacol* 50: 501–508, 1995.
56. **Rieg T, Tang T, Murray F, Schroth J, Insel PA, Fenton RA, Hammond HK, Vallon V.** Adenylate cyclase 6 determines cAMP formation and aquaporin-2 phosphorylation and trafficking in inner medulla. *J Am Soc Nephrol* 21: 2059–2068, 2010.
57. **Roman RJ.** P-450 metabolites of arachidonic acid in the control of cardiovascular function. *Physiol Rev* 82: 131–185, 2002.
58. **Roman RJ, Maier KG, Sun CW, Harder DR, Alonso-Galicia M.** Renal and cardiovascular actions of 20-hydroxyeicosatetraenoic acid and epoxyeicosatrienoic acids. *Clin Exp Pharmacol Physiol* 27: 855–865, 2000.
59. **Sarkis A, Ito O, Mori T, Kohzuki M, Ito S, Verbalis J, Cowley AW Jr, Roman RJ.** Cytochrome P-450-dependent metabolism of arachidonic acid in the kidney of rats with diabetes insipidus. *Am J Physiol Renal Physiol* 289: F1333–F1340, 2005.
60. **Sarmiento JM, Ehrenfeld P, Anazco CC, Reyes CE, Troncoso S, Figueroa CD, Muller-Esterl W, Gonzalez CB.** Differential distribution of the vasopressin V receptor along the rat nephron during renal ontogeny and maturation. *Kidney Int* 68: 487–496, 2005.
61. **Schmelzer KR, Kubala L, Newman JW, Kim IH, Eiserich JP, Hammock BD.** Soluble epoxide hydrolase is a therapeutic target for acute inflammation. *Proc Natl Acad Sci USA* 102: 9772–9777, 2005.
62. **Sinal CJ, Miyata M, Tohkin M, Nagata K, Bend JR, Gonzalez FJ.** Targeted disruption of soluble epoxide hydrolase reveals a role in blood pressure regulation. *J Biol Chem* 275: 40,504–40,510, 2000.
63. **Sladek CD, Blair ML, Sterling C, Mangiapane ML.** Attenuation of spontaneous hypertension in rats by a vasopressin antagonist. *Hypertension* 12: 506–512, 1988.
64. **Staudinger R, Escalante B, Schwartzman ML, Abraham NG.** Effects of epoxyeicosatrienoic acids on 86Rb uptake in renal epithelial cells. *J Cell Physiol* 160: 69–74, 1994.
65. **Sun P, Lin DH, Wang T, Babilonia E, Wang Z, Jin Y, Kemp R, Nasjletti A, Wang WH.** Low Na intake suppresses expression of CYP2C23 and arachidonic acid-induced inhibition of ENaC. *Am J Physiol Renal Physiol* 291: F1192–F1200, 2006.
66. **Tahara A, Tsukada J, Tomura Y, Wada K, Kusayama T, Ishii N, Yatsu T, Uchida W, Taniguchi N, Tanaka A.** Alterations of renal vasopressin V_{1A} and V_2 receptors in spontaneously hypertensive rats. *Pharmacology* 67: 106–112, 2003.
67. **Turner MR, Pallone TL.** Vasopressin constricts outer medullary descending vasa recta isolated from rat kidneys. *Am J Physiol Renal Physiol* 272: F147–F151, 1997.
68. **Ulu A, Davis BB, Tsai HJ, Kim IH, Morisseau C, Inceoglu B, Fiehn O, Hammock BD, Weiss RH.** Soluble epoxide hydrolase inhibitors reduce the development of atherosclerosis in apolipoprotein e-knockout mouse model. *J Cardiovasc Pharmacol* 52: 314–323, 2008.
69. **Walkowska A, Skaroupkova P, Huskova Z, Vanourkova Z, Chabova VC, Tesar V, Kramer HJ, Falck JR, Imig JD, Kompanowska-Jezierska E, Sadowski J, Cervenka L.** Intrarenal cytochrome P-450 metabolites of arachidonic acid in the regulation of the nonclipped kidney function in two-kidney, one-clip Goldblatt hypertensive rats. *J Hypertens* 28: 582–593, 2010.
70. **Weichert W, Paliege A, Provoost AP, Bachmann S.** Upregulation of juxtaglomerular NOS1 and COX-2 precedes glomerulosclerosis in fawn-hooded hypertensive rats. *Am J Physiol Renal Physiol* 280: F706–F714, 2001.
71. **Welker P, Bohlick A, Mutig K, Salanova M, Kahl T, Schluter H, Blottner D, Ponce-Coria J, Gamba G, Bachmann S.** Renal Na^+-K^+-Cl^- cotransporter activity and vasopressin-induced trafficking are lipid raft-dependent. *Am J Physiol Renal Physiol* 295: F789–F802, 2008.
72. **Williams TD, Lightman SL, Leadbeater MJ.** Hormonal and cardiovascular responses to DDAVP in man. *Clin Endocrinol* 24: 89–96, 1986.
73. **Yang T, Schnermann JB, Briggs JP.** Regulation of cyclooxygenase-2 expression in renal medulla by tonicity in vivo and in vitro. *Am J Physiol Renal Physiol* 277: F1–F9, 1999.
74. **Yoshida M, Ueda S, Soejima H, Tsuruta K, Ikegami K.** Effects of prostaglandin E_2 and I_2 on renal cortical and medullary blood flow in rabbits. *Arch Int Pharmacodyn Ther* 282: 108–117, 1986.
75. **Yu Z, Davis BB, Morisseau C, Hammock BD, Olson JL, Kroetz DL, Weiss RH.** Vascular localization of soluble epoxide hydrolase in the human kidney. *Am J Physiol Renal Physiol* 286: F720–F726, 2004.
76. **Yu Z, Huse LM, Adler P, Graham L, Ma J, Zeldin DC, Kroetz DL.** Increased CYP2J expression and epoxyeicosatrienoic acid formation in spontaneously hypertensive rat kidney. *Mol Pharmacol* 57: 1011–1020, 2000.
77. **Zhang MZ, Sanchez Lopez P, McKanna JA, Harris RC.** Regulation of cyclooxygenase expression by vasopressin in rat renal medulla. *Endocrinology* 145: 1402–1409, 2004.
78. **Zhao X, Yamamoto T, Newman JW, Kim IH, Watanabe T, Hammock BD, Stewart J, Pollock JS, Pollock DM, Imig JD.** Soluble epoxide hydrolase inhibition protects the kidney from hypertension-induced damage. *J Am Soc Nephrol* 15: 1244–1253, 2004.

4.2. Group VIA phospholipase A_2 is a target for vasopressin signaling in the thick ascending limb

Am J Physiol Renal Physiol 302: F865–F874, 2012.
First published January 4, 2012; doi:10.1152/ajprenal.00222.2011.

Group VIA phospholipase A_2 is a target for vasopressin signaling in the thick ascending limb

A. Paliege,[1] T. Roeschel,[1] H. Neymeyer,[1] S. Seidel,[1] T. Kahl,[1] A. L. Daigeler,[1] K. Mutig,[1] R. Mrowka,[2] N. R. Ferreri,[3] B. S. Wilson,[4] N. Himmerkus,[5] M. Bleich,[5] and S. Bachmann[1]

[1]*Department of Anatomy, Charité Universitätsmedizin-Berlin, Berlin;* [2]*KIM3-Experimentelle Nephrologie, Universitätsklinikum Jena, Jena;* [3]*Department of Pharmacology, New York Medical College, Valhalla, New York;* [4]*Department of Pathology, University of New Mexico Health Sciences Center, Albuquerque, New Mexico; and* [5]*Department of Physiology, Christian-Albrechts-University, Kiel, Germany*

Submitted 21 April 2011; accepted in final form 29 December 2011

Paliege A, Roeschel T, Neymeyer H, Seidel S, Kahl T, Daigeler AL, Mutig K, Mrowka R, Ferreri NR, Wilson BS, Himmerkus N, Bleich M, Bachmann S. Group VIA phospholipase A_2 is a target for vasopressin signaling in the thick ascending limb. *Am J Physiol Renal Physiol* 302: F865–F874, 2012. First published January 4, 2012; doi:10.1152/ajprenal.00222.2011.—Na^+-K^+-$2Cl^-$ cotransporter (NKCC2)-mediated NaCl reabsorption in the thick ascending limb (TAL) is stimulated by AVP via V2 receptor/PKA/cAMP signaling. This process is antagonized by locally produced eicosanoids such as 20-HETE or prostaglandin E_2, which are synthesized in a phospholipase A_2-dependent reaction cascade. Using microarray-based gene expression analysis, we found evidence for an AVP-dependent downregulation of the calcium-independent isoform of PLA_2, $iPLA_2\beta$, in the outer medulla of rats. In the present study, we therefore examined the contribution of $iPLA_2\beta$ to NKCC2 regulation. Immunoreactive $iPLA_2\beta$ protein was detected in cultured mTAL cells as well as in the entire TAL of rodents and humans with the exception of the macula densa. Administration of the V2 receptor-selective agonist desmopressin (5 ng/h; 3 days) to AVP-deficient diabetes insipidus rats increased outer medullary phosphorylated NKCC2 (pNKCC2) levels more than twofold in association with a marked reduction in $iPLA_2\beta$ abundance (-65%; $P < 0.05$), thus confirming microarray results. Inhibition of $iPLA_2\beta$ in Sprague-Dawley rats with FKGK 11 (0.5 μM) or in mTAL cells with FKGK 11 (10 μM) or (*S*)-bromoenol lactone (5 μM) for 1 h markedly increased pNKCC2 levels without affecting total NKCC2 expression. Collectively, these data indicate that $iPLA_2\beta$ acts as an inhibitory modulator of NKCC2 activity and suggest that downregulation of $iPLA_2\beta$ may be a relevant step in AVP-mediated urine concentration.

thick ascending limb; eicosanoids; vasopressin

STIMULATION OF THICK ASCENDING limb (TAL) transport by AVP is an established element for the normal function of the urine concentrating mechanism. In the TAL, AVP stimulates transepithelial NaCl transport by increasing the abundance, phosphorylation, and surface expression of the type 2 Na^+-K^+-$2Cl^-$ cotransporter (NKCC2). This effect is mediated by the AVP V2 receptor and involves an increase in intracellular cAMP concentration leading to subsequent activation of protein kinase A and probably also other protein kinases (2, 20). The activation of NKCC2 is counteracted by locally produced arachidonic acid derivatives such as 20-HETE, 14,15-epoxyeicosatrienoic acid (14,15-EET), or PGE_2 (2, 10, 18). Impairment of this response may cause Na^+ retention and hypertension (19).

The common, rate-limiting step in the biosynthesis of all eicosanoids is the release of arachidonic acid from membrane glycerophospholipids by PLA_2 isoenzymes (7). At present, over 30 different enzymes with PLA_2 activity have been cloned and grouped according to sequence homologies or biochemical properties (30, 37). Characteristically, these enzymes differ with respect to their dependence on ionized calcium. As an ample source of eicosanoids, the kidney expresses both calcium-dependent and calcium-independent PLA_2 activity (23), and the calcium-dependent PLA_2 group IVA has been shown to be involved in the regulation of the renal urine concentrating mechanism (11). Currently, six proteins with calcium-independent PLA_2 activity ($iPLA_2$) have been identified and designated as $iPLA_2$ group VIA to VIF (37). The isoforms $iPLA_2$-VIA and -$iPLA_2$-VIB, more recently termed $iPLA_2\beta$ and $iPLA_2\gamma$, respectively, have been studied in detail (1). They were shown to be activated by ATP and inhibited by bromoenol lactone (BEL), and their functions included phospholipid remodeling, regulation of cell proliferation and apoptosis, activation of storage-operated calcium channels, regulation of vascular tone, and the release of arachidonic acid from membrane phospholipids (1). Apart from data on a calcium-independent PLA_2 isoform mediating the inhibitory effects of dopamine on TAL transport (16), little is currently known about the distribution and effects of renal $iPLA_2$ isoenzymes.

Microarray studies from our group suggested that outer medullary $iPLA_2\beta$ mRNA levels were reduced after treatment with the V2 receptor-selective agonist 1-desamino-8-D-Arg vasopressin (desmopressin; dDAVP; 5 ng/h; 3 days) whereas other $iPLA_2$ isoforms were not affected. This prompted us to study the role of $iPLA_2\beta$ in TAL in more detail. We have shown that *1*) $iPLA_2\beta$ is expressed in the TAL of mouse, rat, and human kidneys; *2*) $iPLA_2\beta$ expression in the outer medulla is inhibited by chronic exposure to the AVP V2 receptor agonist dDAVP; and *3*) pharmacological inhibition of $iPLA_2\beta$ activity increases the abundance of phosphorylated NKCC2 in cultured medullary TAL cells (mTAL cells) and rat outer medulla. Our results suggest that $iPLA_2\beta$ is an effective inhibitory regulator of TAL transport activity. Downregulation of $iPLA_2\beta$ by AVP may therefore be essential for sustained activation of the urine concentrating mechanism.

MATERIALS AND METHODS

Animal studies and tissue preservation. Adult male Sprague-Dawley (SD) rats ($n = 6$), Brattleboro rats with a hereditary central

Address for reprint requests and other correspondence: A. Paliege, Dept. of Anatomy, Charité Universitätsmedizin-Berlin, Philippstr. 12, D-10115 Berlin, Germany (e-mail: alexander.paliege@charite.de).

Table 1. *Effect of dDAVP treatment on mRNA abundance of TAL PLA$_2$ isoenzymes*

Gene Title	Gene Symbol	mRNA Accession	Probe Set ID	x-Fold of Control	P
Phospholipase A$_2$, group IVA (cytosolic, calcium-dependent)	Pla2 g4	NM_133551	Rn.10162_at	1.98	1E-19
HRAS-like suppressor 3	Pla2 g16	NM_017060	Rn.11377_at	1.2	0.3
Lysophospholipase 3	Pla2 g15	NM_001004277	Rn.93631_at	1.12	7E-05
Phospholipase A2, group XIIA	Pla2 g12a	NM_001108565	Rn.137418_at	1.06	0.7
Patatin-like phospholipase domain containing 2	Pnpla2	NM_001108509	Rn.19196_at	1.0	0.9
Phospholipase A$_2$, group VIB	Pnpla8	NM_001108020	Rn.23073_at	0.95	0.5
Neuropathy target esterase-like 1	Pnpla7	NM_144738	Rn.162643_at	0.93	0.06
Peroxiredoxin 6	Prdx6	NM_053576	1367969_at	0.88	0,01
Phospholipase A$_2$, group VIA	Pla2 g6	NM_001005560	Rn.44692_at	0.77	7E-04

PLA$_2$ isoenzymes with significant expression in the thick ascending limb of Henle's loop (TAL) were identified from http://dir.nhlbi.nih.gov/papers/lkem/mtaltr/Default.aspx. Microarray analysis of outer medullary tissue samples of diabetes insipidus rats treated with 1-desamino-8-D-Arg vasopressin (desmopressin; dDAVP) or vehicle revealed 2 significantly regulated products: iPLA$_2$β (PLA2 g6) and the calcium-sensitive PLA$_2$ group IVA (PLA2 g4). mRNA levels of the remaining enzymes including iPLA$_2$γ (Pnpla8) remained unaffected.

diabetes insipidus (40) (DI; originally obtained from Harlan Winkelmann, Borchen, Germany; $n = 16$), and C57/BL6 mice ($n = 6$) were bred in the local animal facility (Charité, Berlin, Germany) and kept on a standard diet and tap water. All animal studies were performed according to National Institutes of Health guidelines and were approved by the Berlin council on animal care (permission numbers G006-02/05 and G0285/10). For microarray studies, young (8 wk) adult male Brattleboro rats were randomly divided into two groups ($n = 3$/group) and treated for 3 days with either dDAVP (5 ng/h; Sigma-Aldrich, Hamburg, Germany) or vehicle via an osmotic minipump (Alzet minipump, model 2001, Charles River, Sulzfeld, Germany). At the end of the treatment period, the animals were euthanized and their kidneys were removed. The outer medulla was isolated and used for cDNA generation and subsequent microarray analysis. For localization studies, SD rats and mice ($n = 3$) were anesthetized by isoflurane (Abbott, Wiesbaden, Germany) inhalation followed by an injection of pentobarbital sodium (0.06 mg/g body wt ip, Fagron, Barsbüttel, Germany). The abdominal cavity was opened, and kidneys were fixed with 3% paraformaldehyde (PFA; Merck, Darmstadt, Germany) in PBS via retrograde perfusion of the abdominal aorta. After perfusion, kidneys were carefully removed and processed for paraffin embedding or cryostat sectioning using routine methodology. Additional animals ($n = 3$) were euthanized after deep isoflurane anesthesia; kidneys were removed and processed for protein biochemistry or cDNA generation. To determine the intrarenal distribution of iPLA$_2$β variants, different zones of rat kidneys were separated using sterile razor blades. Human kidney samples ($n = 3$) were derived from tumor nephrectomy specimens after written consent of the patients. Samples from the healthy parts of the kidneys were fixed by immersion in 3% PFA in PBS and processed for immunohistochemistry (31). The effects of chronic AVP treatment on renal iPLA$_2$β expression was verified in additional male Brattleboro rats ($n = 8$/group). Treatment with dDAVP was performed as described above. At the end of the treatment period, animals (4/group) were euthanized and their kidneys were removed. The outer medulla was isolated and used for cDNA generation or protein biochemistry. The remaining animals were perfusion fixed and processed for histological studies as described above. To test the relevance of iPLA$_2$β for the regulation of NKCC2 in vivo, we employed the novel iPLA$_2$β-specific inhibitor 1,1,1,2,2-pentafluoro-7-phenyl-3-heptanone (FKGK 11; Cayman Chemical, Tallin, Estonia) (5). Young male SD rats ($n = 10$) were randomly divided into two groups. FKGK 11 was administered by intraperitoneal injection of 250 μl of a 2 mM solution of FKGK 11 dissolved in PBS supplemented with 5% Tween 80 (Sigma-Aldrich) as previously described (27). Control animals were injected with vehicle. After 1 h, animals were perfusion fixed and processed for immunoperoxidase staining as detailed above.

Microarray studies. Gene expression profiling was performed in the microarray facility of the Zentrum für Medizinische Forschung of the University of Mannheim (Mannheim, Germany). Total RNA was isolated from the outer medulla of dDAVP- and vehicle-treated Brattleboro rats using a Qiagen RNeasy minikit following the manufacturer's instructions (Qiagen, Hilden, Germany). cDNA and cRNA were prepared according to the Affymetrix standard labeling protocol. Hybridization to Affymetrix rat genome 230 2.0 arrays was performed with GeneChip Hybridization oven 640. Chips were subsequently dyed in GeneChip Fluidics Station 450 and thereafter scanned with GeneChip Scanner 3000. All equipment was from Affymetrix (Affymetrix, High Wycombe, UK). Data were analyzed using commercial software (JMP Genomics version 4, SAS, Cary, NC). Custom CDF Version 9 with Unigene-based gene definitions was used to annotate the arrays (http://brainarray.mbni.med.umich.edu/Brainarray/Database/CustomCDF/CDF_download_v9.asp). The raw fluores-

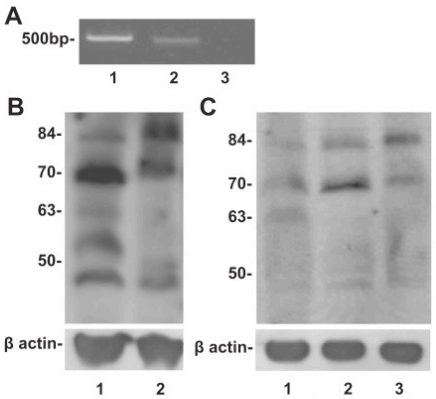

Fig. 1. Expression of calcium-independent isoform of PLA$_2$ (iPLA$_2$β) in rat kidney and cultured medullary thick ascending limb of Henle's loop (mTAL) cells. *A*: PCR amplification of iPLA$_2$β cDNA from total rat kidney (*lane 1*) and mTAL cell (*lane 2*) cDNA shows products at 500 bp. The control reaction without cDNA shows no PCR product (*lane 3*). *B*: Western blot analysis of total rat kidney homogenate (*lane 1*) shows iPLA$_2$β-immunoreactive products with a dominant (70 kDa) and several weaker bands (84, 63, 52, and 48 kDa). In cultured mTAL cell homogenate (*lane 2*), 84-, 70-, and 48-kDa bands appear. β-Actin signal (*bottom*) serves as a loading control. *C*: Western blot of the zonal distribution of iPLA$_2$β variants shows a weak expression in the cortex (*lane 1*). In the outer medulla, there is abundant expression of the 70-kDa band whereas the remaining variants are less abundant (*lane 2*). In the inner medulla, the 84-kDa variant is more abundant than the 70-kDa variant (*lane 3*). The abundance of β-actin (*bottom*) was determined simultaneously to ensure equal loading.

cence intensity values were normalized by applying quantile normalization. Raw and normalized data were deposited in the Gene Expression Omnibus database (http://www.ncbi.nlm.nih.gov/geo/; GEO accession number: GSE34225). To elucidate the effects of AVP treatment on PLA$_2$ isoenzymes expressed in the TAL, we combined a comprehensive list of mammalian enzymes with PLA$_2$ activity (30) with information from a published database on the transcriptome of microdissected mTALs (http://dir.nhlbi.nih.gov/papers/lkem/mtaltr/Default.aspx) (43). The effect of AVP treatment on the identified enzymes was determined by microarray.

Cell culture experiments. For cell culture experiments, we used a rat medullary TAL cell line generated by Eng et al. (12). Cells were grown to confluence in renal epithelial cell growth medium (PromoCell, Heidelberg, Germany) and processed for immunofluorescence staining, cDNA generation, or protein biochemistry as previously described (31, 41). To study the effects of iPLA$_2$ inhibition on NKCC2 phosphorylation and protein abundance, cells were treated with BEL (5 μM; Sigma-Aldrich), (R)-BEL, and (S)-BEL (5 μM; Cayman Chemical) for 1 h. The concentration for BEL treatment has been previously shown to inhibit rat iPLA$_2$β and -γ by 100 and 80%, respectively (21). In addition, cells were treated for 1 h with either the novel iPLA$_2$β inhibitor FKGK 11 (10 μM; Cayman Chemical), with the nonspecific PLA$_2$ inhibitor methyl arachidonyl fluoro-phosphate (MAFP; 100 μM; Cayman Chemical), or the inhibitor of phosphatidate phosphohydrolase (PAPH) propranolol (250 μM; Sigma Aldrich) (3, 5, 25). After treatment, cells were either collected for protein biochemistry or processed for immunofluorescence as previously described (31, 41).

Conventional and real-time PCR. Total mRNA was isolated as described above. After digestion of genomic DNA by DNase 1 treatment (Qiagen), cDNA was generated by RT using an Applied Biosystems cDNA synthesis kit (Applied Biosystems, Darmstadt, Germany). The expression of iPLA$_2$β and iPLA$_2$γ in rat kidney and mTAL cells was detected by conventional PCR using a forward primer from exon 13 (5′-CCGGCCAATGGACGCTTCT-3′) and a reverse primer from exon 16 (TGGACAAGCTTCTGGAACTC) for iPLA$_2$β and (5′-GAAGGCCGGGCAGGCTGATG-3′) and (5′-AGTCCCTTGGGAGCAGAAGTGC-3′) for iPLA$_2$γ. PCR without the addition of cDNA served as a negative control. TaqMan quantitative RT-PCR for NKCC2 and iPLA$_2$β was performed using the Applied Biosystems probes Rn.01485101 for NKCC2 and Rn.01504428 for iPLA$_2$β and the 7500 Fast Real-Time PCR system (Applied Biosystems) following the manufacturer's instructions. The mRNA levels of GAPDH were determined in parallel and served as a loading control (catalog no. 4352338E, Applied Biosystems). The probe for iPLA$_2$β was directed against the transition of exons 5 and 6, which is present in all known iPLA$_2$β splice variants. Expression levels were calculated according to the $2^{-\Delta\Delta CT}$ method and expressed as % of control (26).

Western blot analysis. Samples were homogenized in sucrose-triethanolamine buffer (41). Nuclei were removed by centrifugation at 800 *g* for 10 min at 4°C, and supernatant protein concentration was determined by a bicinchoninic acid protein assay reagent kit (Thermo Fisher Scientific, Bonn, Germany). Samples were subsequently separated by SDS-PAGE in a 10% gel (50 μg protein/lane) and electrophoretically transferred to nitrocellulose membranes. Equity in protein loading and blotting was verified by membrane staining using 0.1% Ponceau red stain. Nonspecific protein binding sites were blocked by immersion in 5% nonfat dry milk in PBS. Membranes were subsequently incubated with the respective primary antibody. For detection

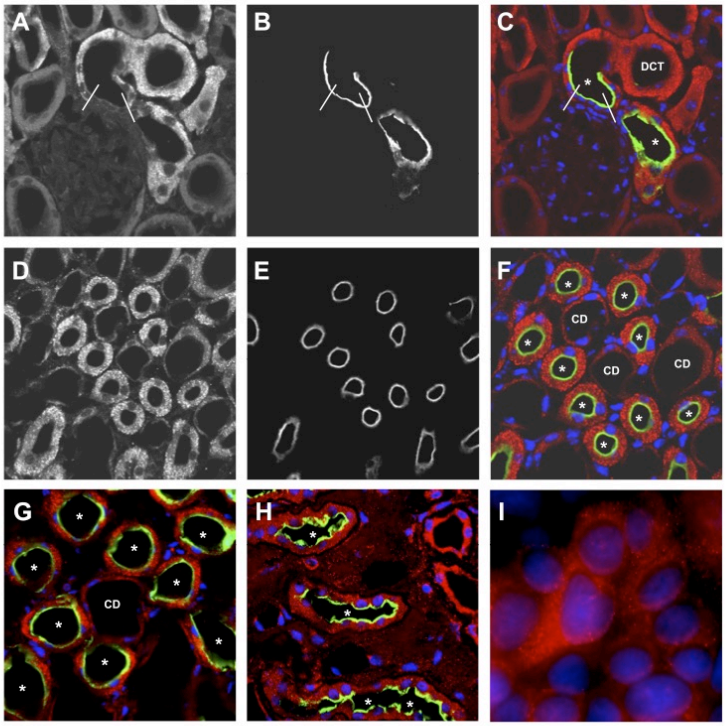

Fig. 2. Immunofluorescence localization of iPLA$_2$β protein in the thick ascending limb. Double labeling was done of mouse (*A–F*), rat (*G*), and human (*H*) kidney sections with rabbit anti-iPLA$_2$β antibody (*A*, *D*, and *G–I*) and guinea pig anti-Na^+-K^+-$2Cl^-$ cotransporter (NKCC2) antibody (*B*, *E*, *G*, and *H*). In the merged color images (*C*, *F*, *G–I*), the red signal indicates iPLA$_2$β and the green signals mark NKCC2 (*C*, *F*, *G*, *H*). Blue signals mark 4,6-diamidino-2-phenylindole (DAPI)-stained nuclei. TAL profiles of all examined species show a coexpression of iPLA$_2$β and NKCC2, thus demonstrating the presence of iPLA$_2$β in the entire TAL. iPLA$_2$β staining is absent from the cells of the macula densa (between flanking lines in *A–C*). Cultured mTAL cells (*I*) show strong, granular staining in scattered groups of cells. Immunofluorescence staining; original magnification ×400 for *A–H*; ×630 for *I*. *Marks profiles of TAL, DCT marks profile of a distal convoluted tubule, and CD marks profiles of collecting ducts.

of iPLA$_2$β, we used an affinity-purified rabbit anti iPLA$_2$β antibody (1:500, HPA001171, Sigma-Aldrich). This antibody is directed against amino acids 100–250 of human iPLA$_2$β protein and thus recognizes all described splice variants of the enzyme. The homologies toward the murine and rat proteins are 90 and 91%, respectively. Total NKCC2 protein abundance was evaluated using either a mouse monoclonal antibody against the COOH-terminal part of NKCC1 which cross-reacts with NKCC2 (T4 antibody developed by Lytle and Forbush III; Developmental Studies Hybridoma Bank, University of Iowa, Iowa City, IA) or a guinea pig anti NKCC2 antibody against the N-terminal part of the protein to detect total NKCC2 (28, 31). Phosphorylated NKCC2 was detected using a rabbit anti-pNKCC2 antibody as previously described (31). Membranes were incubated with the primary antibodies for 1 h at room temperature followed by an overnight incubation at 4°C. Bound antibody was detected using the respective horseradish peroxidase-conjugated secondary antibody and chemiluminescence. Developed X-ray films were scanned and densitometrically evaluated using AlphaImager software (Cell Biosciences, Santa Clara, CA). Expression levels were normalized to the expression of the housekeeping gene β-actin using a well-characterized monoclonal antibody (1:20 000, Sigma-Aldrich) and expressed as % of control.

Immunostaining. Immunostaining for iPLA$_2$β was performed using rabbit anti-iPLA$_2$β antibody in a 1:50 dilution. Identification of iPLA$_2$β-expressing nephron segments was achieved by double labeling with the segment-specific markers guinea pig anti-thiazide-sensitive Na^+-Cl^- cotransporter (NCC; 1:100) for distal convoluted tubule, goat anti-calbindin-D$_{28k}$ (1:1,000) for distal convoluted tubule and connecting tubule, and goat anti-aquaporin-2 (1:100, sc-9882, Santa Cruz Biotechnology, Heidelberg, Germany) for connecting tubule and collecting duct as previously described (31). Total NKCC2 and pNKCC2 were detected using well-characterized antibodies against the nonphosphorylated (guinea pig anti-NKCC2; 1:500) and the phosphorylated N-terminal part of NKCC2 (rabbit anti-pNKCC2;

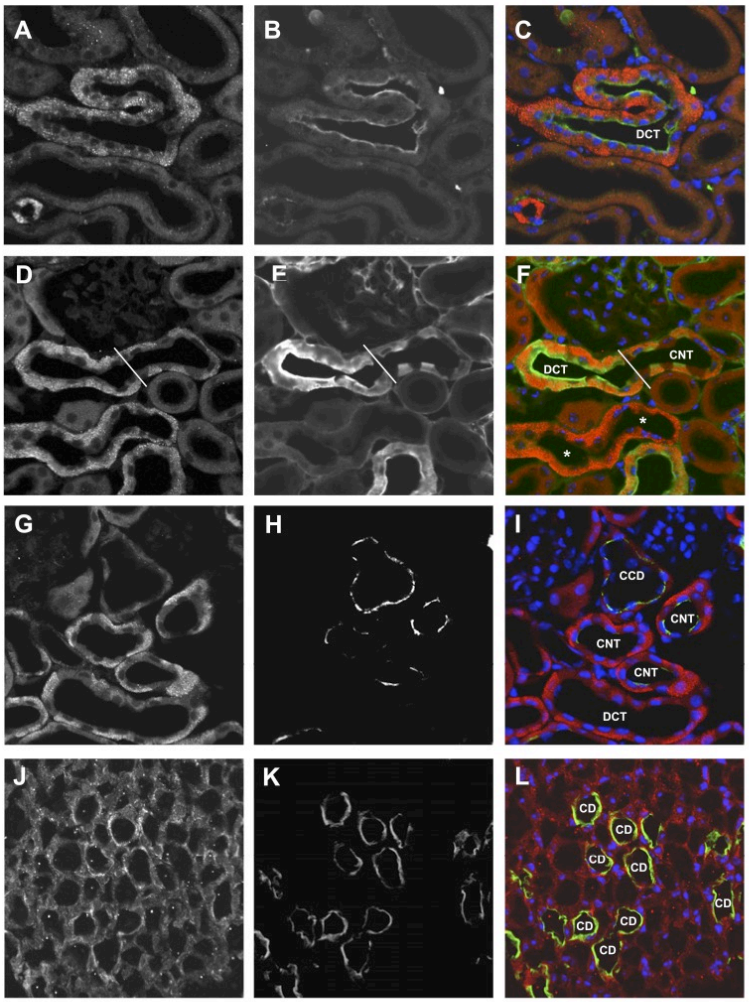

Fig. 3. Immunofluorescence localization of iPLA$_2$β protein in DCT and medullary CD. Double labeling was done of mouse kidney sections with rabbit anti-iPLA$_2$β antibody (*A*, *D*, *G*, and *J*) and guinea pig anti-NCC antibody (*B*), goat anti-calbindin-D$_{28k}$ antibody (*E*) or goat anti-aquaporin-2 (AQP2) antibody (*H* and *K*). In the merged color images (*C*, *F*, *I*, and *L*), red signal indicates iPLA$_2$β, and green signals mark thiazide-sensitive Na^+-Cl^- cotransporter (NCC; *C*), calbindin-D$_{28k}$ (*F*), or AQP2 (*I* and *L*). Blue signals mark DAPI-stained nuclei. Profiles of DCT show coexpression of iPLA$_2$β with NCC (*A–C*) and calbindin-D$_{28k}$ (*D–F*), thus demonstrating the presence of iPLA$_2$β in the DCT and the connecting tubule (CNT). Lines in (*D–F*) mark the transition between DCT and CNT characterized by the decreased calbindin-D$_{28k}$ abundance and the ample presence of intercalated cells which do not express calbindin-D$_{28k}$ or iPLA$_2$β. Profiles of CNT in the cortex (*G–I*) and CD in the inner medulla (*J–L*) show coexpression of iPLA$_2$β and AQP2 whereas abundance of iPLA$_2$β in the cortical CD was low (*G–I*). Immunofluorescence staining; original magnification ×400 for *A–L*. *Marks profiles of TAL, DCT marks profiles of distal convoluted tubules, CNT of connecting tubules; CCD marks the profile of cortical, and CD the profiles of inner medullary collecting ducts.

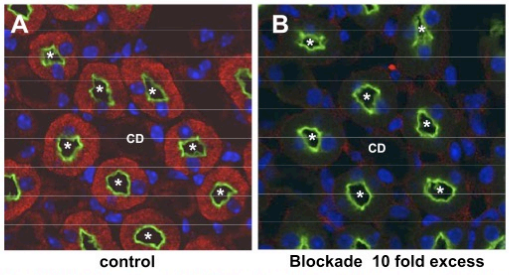

Fig. 4. Characterization of iPLA$_2$β antibody. Immunofluorescence labeling of mouse kidney sections with rabbit anti-iPLA$_2$β antibody (red) and guinea pig anti-NKCC2 antibody (green). Blue signals mark DAPI-stained nuclei. TAL profiles in the outer medulla show coexpression of iPLA$_2$β and NKCC2 (*A*). iPLA$_2$β staining was abolished after preincubation of iPLA$_2$β antibody with a 10-fold excess of immunizing peptide (*B*). Immunofluorescence staining; original magnification ×400 for *A* and *B*. *Marks profiles of TAL, and CD marks profiles of collecting ducts.

1:20,000) as previously described (31). Nuclei were stained with 4′-6-diamidino-2-phenylindole (DAPI). For all antibodies, control experiments were conducted in which the primary antibody was omitted.

Verification of iPLA$_2$β antibody. Antibody specificity was further verified by peptide blockade. To this end, immunizing peptide was obtained from the antibody manufacturer (Atlas Antibodies, Stockholm, Sweden). iPLA$_2$β antibody was diluted in 5% nonfat dry milk in PBS and incubated for 30 min with different amounts of blocking peptide before application to mouse kidney sections. Immunostaining was performed as described above. For Western blotting, rat total kidney homogenates were separated by SDS-PAGE in a 10% gel and electrophoretically transferred to nitrocellulose membranes as described above. iPLA$_2$β antibody was incubated with a 10-fold excess of blocking peptide for 30 min and added to the membranes. Signal generation was achieved as described above.

Rip-flip immunoelectron microscopy. Preparation of plasma membrane sheets was performed as previously described (42). Briefly, mTAL cells were grown to confluence on glass coverslips and treated with 5 μM (S)-BEL or vehicle as described above. After 1 h, cells were fixed for 15 min using 0.5% PFA in PBS. After fixation, cells were washed multiple times in PBS and subsequently inverted on nickel electron microscopy grids that had been coated with formvar and carbon and, on the day of the experiment, glow-discharged and floated on poly-L-lysine (0.8 mg/ml for 30 min, followed by 10-s rinsing in distilled H_2O and air drying). Pressure was applied to the coverslip for 15 s using a fine pair of forceps. The coverslips were subsequently lifted, leaving sections of the upper cell surface adherent to the poly-L-lysine-coated grid. Membranes were subsequently fixed in 2% PFA for 20 min at room temperature. Labeling of pNKCC2 was performed by sequential incubation with pNKCC2 antibody (1:150) and gold-conjugated secondary antibody (1:50, Abcam, Cambridge, UK); to this end, grids were placed into droplets. Samples were then postfixed in 2% glutaraldehyde in PBS and processed for 10 min in 1% aqueous tannic acid and 10 min with 1% aqueous uranyl acetate separated by washing with dH_2O. Grids were air-dried and examined by transmission electron microscope (Zeiss E905, Zeiss, Oberkochen, Germany).

Statistical analysis. All values are given as means ± SE of 4 animals/group. Statistical analysis was performed using an unpaired Student's *t*-test. A null hypothesis has been excluded when P was <0.05.

RESULTS

Gene expression analysis of dDAVP effects on TAL PLA$_2$ isoenzymes. A comprehensive list of 31 mammalian enzymes with PLA$_2$ enzyme activity was obtained from a recent review (30). Nine of these were expressed in the TAL as revealed by the mTAL transcriptome database (43), and two of the enzymes were significantly altered following AVP treatment. Regulated enzymes included the calcium sensitive PLA$_2$ group IVA (+98%) and iPLA$_2$β (−23%) (Table 1).

Expression of iPLA$_2$β in rat kidney and mTAL cells. Analysis of iPLA$_2$β mRNA accumulation in SD rat kidney and cultured mTAL cells showed a product of the expected size of 500 bp by conventional PCR (Fig. 1*A*). iPLA$_2$γ mRNA was expressed in both sources as well (data not shown). In Western blot analysis from rat kidney extracts, a dominant iPLA$_2$β-immunoreactive band at ~70 kDa and additional, weaker bands at 84, 63, 52, and 48 kDa were detectable (Fig. 1*B*). mTAL cells only showed the 84-, 70-, and 48-kDa bands; here, the 84- and 70-kDa bands were equally abundant (Fig. 1*B*). In

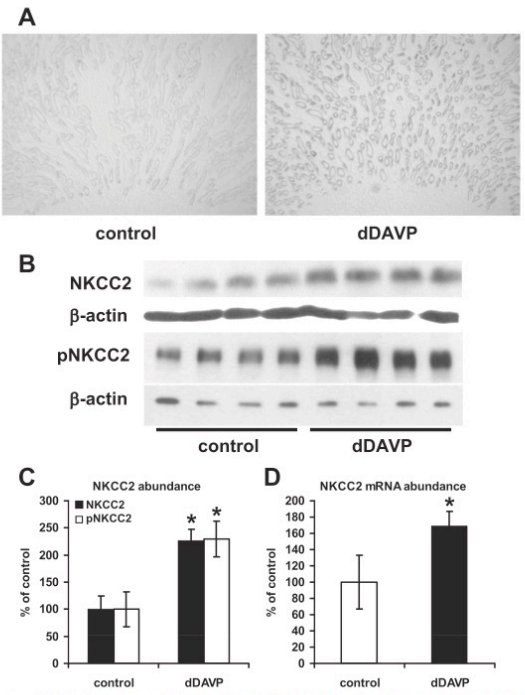

Fig. 5. Chronic vasopressin V2 receptor activation stimulates outer medullary NKCC2 in diabetes insipidus (DI) rats. *A*: low-power micrographs show immunoreactive phosphorylated NKCC2 (pNKCC2) in DI rat kidney medulla after vehicle (control) or 1-desamino-8-D-Arg vasopressin (desmopressin; dDAVP) treatment (5 ng/h for 3 days); pNKCC2 is enhanced in TALs of the treated group. Immunoperoxidase staining; original magnification ×100. *B*: Western blot of outer medullary tissue extracts from DI rats treated with vehicle (*lanes 1–4*) or dDAVP (*lanes 5–8*) showing increased pNKCC2 (open bars) and total NKCC2 (filled bars) signals; β-actin served as a loading control. *C*: densitometric analysis of the signal. *D*: real-time PCR of NKCC2 mRNA abundance in outer medullary tissue extracts. *$P < 0.05$.

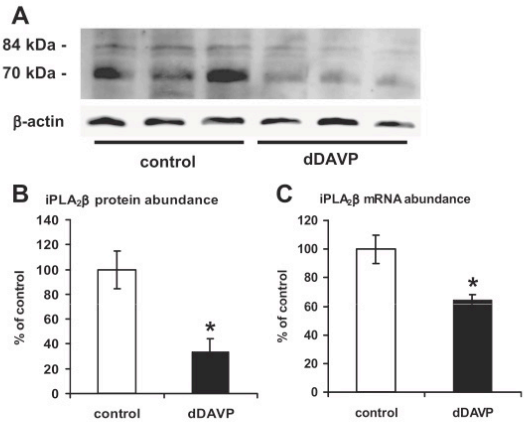

Fig. 6. Chronic dDAVP treatment reduces outer medullary iPLA$_2$β in DI rats. *A*: Western blot of outer medullary tissue extracts from DI rats treated with vehicle (control; *lanes 1–3*) or dDAVP (5 ng/h for 3 days; *lanes 4–6*) showing reduced iPLA$_2$β-immunoreactive bands in the treated animals; β-actin served as a loading control. *B*: densitometric analysis of the blot. *C*: real-time PCR of iPLA$_2$β mRNA abundance in outer medullary tissue. $*P < 0.05$.

the kidney cortex, iPLA$_2$β signals were weaker than in the medulla; in the outer medulla, the 70-kDa band was dominant, whereas in the inner medulla the 84-kDa variant was stronger (Fig. 1*C*).

Localization of iPLA$_2$β in kidney and mTAL cells. Distribution of iPLA$_2$β was analyzed by immunofluorescence in rodent and human kidney samples and cultured mTAL cells. Strong iPLA$_2$β immunoreactivity was found in the distal nephron of all examined species. Cellular staining was distributed throughout the cytoplasm, with some scattered, particulate signals. In the glomeruli, podocytes showed weak but consistent iPLA$_2$β immunoreactivity. Proximal tubules and the renal vasculature were devoid of staining. Double labeling with anti-NKCC2 in rat, mouse, and human kidneys revealed that iPLA$_2$β was expressed along the entire medullary and cortical TAL with the exception of the macula densa (Fig. 2). In addition, iPLA$_2$β was expressed in distal convoluted and connecting tubules as revealed by coexpression with NCC or calbindin-D$_{28k}$ (Fig. 3), respectively. Calbindin-D$_{28k}$-negative intercalated cells were also negative for iPLA$_2$β (Fig. 3). In cultured mTAL cells, particulate iPLA$_2$β signals of varying strength were found in scattered groups of cells (Fig. 2*I*). Double labeling of murine kidney sections with iPLA$_2$β and aquaporin-2 demonstrated colocalization of the two products in inner medullary collecting ducts whereas cortical collecting ducts were devoid of immunoreactive iPLA$_2$β protein (Fig. 3).

Characterization of iPLA$_2$β antibody. Specificity of the iPLA$_2$β antibody was verified by peptide blockade. Preincubation of the iPLA$_2$β antibody with iPLA$_2$β peptide caused a dose-dependent decrease in signal intensity in immunofluorescence (Fig. 4) and Western blotting (data not shown). Blockade of signal was maximal at a 10-fold excess of peptide (Fig. 4*B*).

Effect of chronic dDAVP treatment on NKCC2 and iPLA$_2$β. To study the effect of a chronic activation of TAL transport on iPLA$_2$β expression, Brattleboro rats were treated with the AVP V2 receptor analog dDAVP for 3 days using osmotic minipumps. This resulted in a significant drop in urine flow ($-94 \pm 24\%$ compared with controls; $P < 0.05$) and a major increase in outer medullary immunoreactive pNKCC2 protein (Fig. 5*A*). Analysis of the outer medulla confirmed induction of pNKCC2 abundance ($+130 \pm 32\%$ compared with controls; Western blotting; $P < 0.05$; Fig. 5, *B* and *C*). Total NKCC2 protein and mRNA abundance were increased as well ($+130 \pm 7\%$ compared with controls; Western blotting; $P < 0.05$; Fig. 5, *B* and *C*, and $+70 \pm 5\%$ compared with controls; real-time PCR; $P < 0.05$; Fig. 5*D*). These results document an activation of NKCC2 in the TAL of the treated animals, thus confirming previous findings (31). Concomitantly, immunoreactive levels of the 84- and the 70-kDa variants of iPLA$_2$β were diminished (Fig. 6A). Quantification of the 70-kDa variant revealed a reduction of $-65 \pm 7\%$ compared with controls ($P < 0.05$; Fig. 6*B*). iPLA$_2$β mRNA accumulation was reduced as well ($-30 \pm 3\%$ compared with controls; $P < 0.05$; Fig. 6*C*).

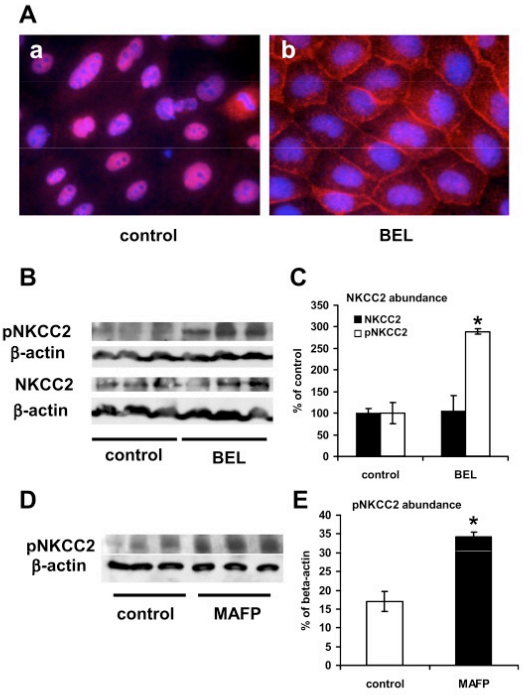

Fig. 7. Inhibition of iPLA$_2$ increases NKCC2 phosphorylation in mTAL cells. *A*: representative micrographs from control (*a*) and bromoenol lactone (BEL; 5 μM, 1 h)-treated mTAL cells (*b*) showing increased abundance and membrane localization of immunoreactive pNKCC2 (red staining) in the treated cells. Blue signals mark DAPI-stained nuclei. Immunofluorescence staining; original magnification ×400. *B*: Western blots of mTAL homogenates from control (*lanes 1–3*) and BEL (5 μM, 1 h)-treated samples (*lanes 4–6*) showing increased pNKCC2 (open bars) but unchanged total NKCC2 (filled bars) signals; β-actin served as a loading control. *C*: densitometric analysis of the blots in *B*. $*P < 0.05$. *D*: Western blot of mTAL cell treated with methyl arachidonyl fluorophosphonate (MAFP; 100 μM, 1 h, *lanes 4–6*) or vehicle (*lanes 1–3*) showing increased pNKCC2 signals in the treated cells. *E*. Densitometric analysis of the blots in *D*. $*P < 0.05$.

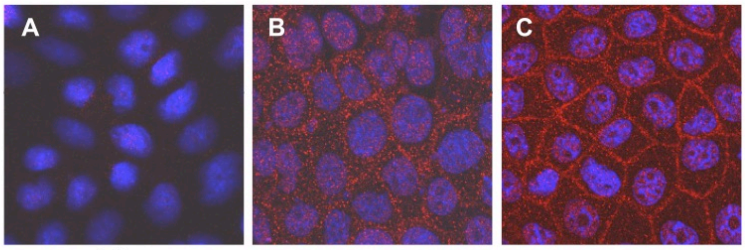

Fig. 8. NKCC2 phosphorylation is preferentially increased after (S)-BEL compared with (R)-BEL treatment. BEL enantiomers enhance pNKCC2 immunoreactivity (red staining) in cultured mTAL cells; (S)-BEL effects (*C*) are much stronger than the effects of (R)-BEL (*B*). Blue signals mark DAPI-stained nuclei. Immunofluorescence staining; original magnification ×400.

Effect of BEL on NKCC2 phosphorylation. The effect of iPLA$_2$ on NKCC2 phosphorylation was studied in mTAL cells using the established iPLA$_2$ inhibitor BEL (5 μM, 1 h). This caused a rapid and pronounced increase in the amount of immunoreactive pNKCC2 as determined by immunofluorescence (Fig. 7*A*) and Western blotting (+189 ± 6% compared with controls; $P < 0.05$; Fig. 7, *B* and *C*). Total NKCC2 levels remained unchanged (Fig. 5, *B* and *C*). BEL-treated mTAL cells revealed increased immunoreactive levels of phospho-NKCC2 (pNKCC2) along the lateral and apical plasma membrane (Fig. 7*A*).

Effect of propranolol and MAFP on NKCC2 phosphorylation. High concentrations of BEL have been shown to inhibit PAPH in addition to iPLA$_2$ (4, 13). To rule out an involvement of PAPH in the regulation of NKCC2, we treated mTAL cells with the PAPH inhibitor propranolol or the nonspecific phospholipase inhibitor MAFP (25). Treatment of mTAL cells with 100 μM MAFP for 1 h increased the abundance of pNKCC2 to a similar extent as BEL (+102 ± 7.5% compared with controls; $P < 0.05$; Fig. 7, *D* and *E*). In contrast, propranolol had no effect (data not shown). The effect of BEL on NKCC2 phosphorylation is therefore likely due to inhibition of an iPLA$_2$ isoenzyme (3, 13, 25).

Effect of (R)-BEL and (S)-BEL on NKCC2 phosphorylation. To explore the contributions of the major iPLA$_2$ isoforms iPLA$_2$β and iPLA$_2$γ to NKCC2 phosphorylation, we utilized the differential inhibitory effects of BEL enantiomeres on iPLA$_2$ isoforms. Since iPLA$_2$β is known to respond to (S)-BEL, whereas iPLA$_2$γ is preferentially inhibited by (R)-BEL, a resulting significantly larger increase in pNKCC2 signal after (S)-BEL than after (R)-BEL treatment suggested that the isoform involved in the regulation of NKCC2 phosphorylation is iPLA$_2$β (Fig. 8) (21). Increased abundance of pNKCC2 in the apical membrane of (S)-BEL-treated mTAL cells was further specified by immunogold staining of apical membrane sheets (Fig. 9). Here, pNKCC2 signal was localized to electron-dense protein aggregations in the treated cells, whereas signal was absent in the controls.

Effect of FKGK 11 on NKCC2 phosphorylation. To further test the hypothesis that iPLA$_2$β is involved in the regulation of NKCC2 phosphorylation, we made use of FKGK 11, the newly developed specific inhibitor of iPLA$_2$β (5). Short-term treatment of mTAL cells with FKGK 11 increased abundance and membrane presentation of pNKCC2 as determined by immunofluorescence (Fig. 10, *a* and *b*). In vivo experiments in rats confirmed the stimulatory effect of the compound on medullary pNKCC2 levels (Fig. 10, *c* and *d*). Together, these data support a functional link between iPLA$_2$β and NKCC2.

DISCUSSION

We have shown that iPLA$_2$β is localized to the distal nephron, where it acts as an inhibitory regulator of NKCC2 phosphorylation and apical surface expression. AVP-induced activation of NKCC2 was associated with decreased iPLA$_2$β abundance, whereas other members of the iPLA$_2$ family were not affected. We assume that downregulation of iPLA$_2$β is part of the mechanism that provides sustained activation of NKCC2 in response to AVP-V2 receptor signaling.

Mammalian cells of various origins express multiple iPLA$_2$β isoenzymes as a result of alternative splicing and proteolytic processing (4, 24, 34, 39). Using a polyclonal antibody against the N-terminal ankyrin-repeats common to all known splice variants of iPLA$_2$β, we found abundant expression in the kidney of normal rats. Analysis of the zonal distribution of iPLA$_2$β demonstrated the highest relative abun-

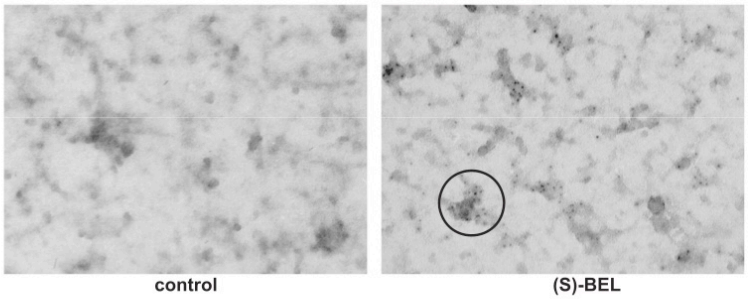

Fig. 9. (S)-BEL increases pNKCC2 abundance in apical membrane sheets of mTAL cells. Apical membrane sheets of mTAL cells treated with vehicle (control)or (S)-BEL (5 μM, 1 h) show pNKCC2 immunogold staining in electron-dense protein aggregations (marked by the circle) of the treated cells. Transmission electron microscopy; original magnification ×27,000.

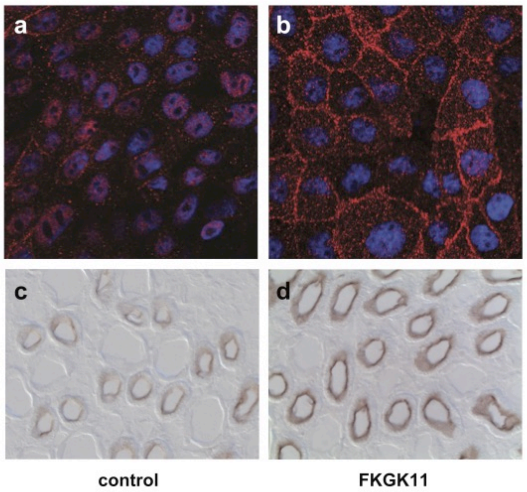

Fig. 10. Inhibition of iPLA$_2$β by FKGK 11 increases pNKCC2 abundance in mTAL cells and rats. Representative micrographs from control and FKGK 11 (10 μM, 1 h)-treated mTAL cells showing increased abundance and membrane localization of immunoreactive pNKCC2 (red staining) in the treated cells. Blue signals mark DAPI-stained nuclei. Treatment of young adult Sprague-Dawley rats with an intraperitoneal injection of FKGK 11 (250 μl of a 2 mM FKGK solution, 1 h, $n = 5$ per group) or vehicle resulted in an increased abundance of pNKCC2 in the outer medulla of the treated animals (*d*) compared with controls (*c*). Immunofluorescence (*a* and *b*) and immunoperoxidase staining (*c* and *d*); original magnification ×400.

dance of the 70-kDa variant of the enzyme in the outer medulla; this variant was also detected in cultured mTAL cells. Weaker bands at 84, 63, 52, and 48 kDa were further detected in rat outer medulla. This pattern agrees with other reports on mammalian iPLA$_2$β protein expression (4, 24, 34, 39). Our findings on the tubular distribution of iPLA$_2$β in mouse, rat, and human kidney along the distal nephron, connecting tubule, and distal collecting duct were novel; macula densa cells were negative for iPLA$_2$β, but expressed the calcium-dependent PLA$_2$ group IV along with cyclooxygenase 2, which may provide active prostaglandin synthesis at this particular site of the kidney (29). Cellular iPLA$_2$β signals within granules and along the basolateral membrane were in agreement with reported data (4, 39). Significant iPLA$_2$ activity has been reported in proximal tubules, with proximal membrane preparations containing iPLA$_2$β. In our hands, however, proximal tubules were negative, eventually owing to a low abundance of the enzyme in this segment, and iPLA$_2$ activity in proximal tubules may also reflect contributions by iPLA$_2$γ and lysophospholipase 1 (22, 33, 44). Another site of joint iPLA$_2$β and iPLA$_2$γ expression has been reported from podocytes, and iPLA$_2$γ was implicated in podocyte injury upon complement activation (9). In our hands, podocytes showed a weak but consistent iPLA$_2$β staining as well.

The significant expression of iPLA$_2$β along the TAL suggested that the enzyme may interfere with TAL transepithelial NaCl cotransport, consistent with earlier data on BEL-induced inhibition of iPLA$_2$ ameliorating dopamine-induced reduction of transport in TAL (16). Here, the nonselective PLA$_2$ inhibitor MAFP and the more selective iPLA$_2$ inhibitor BEL showed that iPLA$_2$ has an inhibitory effect on NKCC2 phosphorylation and surface expression. Since the pNKCC2 level was preferentially increased by S-BEL compared with R-BEL, identity of the iPLA$_2$ isoform involved in the regulation of NKCC2 activity was likely iPLA$_2$β. We were aware that BEL and its enantiomers are not specific for iPLA$_2$β but also affect other enzymes such as PAPH, which may interfere with eicosanoid synthesis as well (3, 13). We therefore applied the PAPH inhibitor propranolol but saw no effect on NKCC2 phosphorylation. In aggregate, these data suggest that iPLA$_2$β has an inhibitory effect on NKCC2 phosphorylation and surface expression. This conclusion was further supported by our studies with FKGK 11, the newly developed specific inhibitor of iPLA$_2$β.

Since several studies have shown that maneuvers which increase NKCC2 phosphorylation also raise NKCC2 transport activity, our observation of increased pNKCC2 levels along with enhanced surface expression of the transporter upon inhibition of iPLA$_2$β is likely to reflect increased NKCC2 transport activity (14, 15, 31).

The mechanisms by which iPLA$_2$β may regulate TAL transport activity, are not entirely clear. iPLA$_2$β catalyzes the hydrolysis of glycerophospholipids at the sn-2 position, thus generating free fatty acid such as arachidonic acid and a 2-lysophospholipid (LPC). These products have either intrinsic biological activity or can be metabolized to other active molecules (7). Depending on the array of enzymes available, arachidonic acid can be processed to a variety of metabolites such as 20-HETE, EETs, or prostaglandins. All of these have been shown to modulate TAL transepithelial transport (2, 10, 18). In outer medullary cell suspensions, arachidonic acid was preferentially metabolized to omega-hydroxylated eicosatetraenoic acid metabolites such as 20-HETE (8, 38). In agreement with this, cytochrome *P*-450-4A (CYP4A), the enzyme responsible for 20-HETE generation, is expressed in the entire TAL (21), whereas cyclooxygenase 2, the enzyme responsible for prostaglandin synthesis, is restricted to the macula densa and few, scattered TAL cells of the cortex and corticomedullary transition (6, 17, 35, 37). The observed reduction of outer medullary iPLA$_2$β levels in dDAVP-treated DI rats as well as the pharmacologically induced inhibition of iPLA$_2$β in mTAL cells are therefore likely to result in a decrease in 20-HETE, which in turn may cause an activation of NKCC2. In line with this assumption, earlier studies have shown an increased capacity for 20-HETE synthesis in outer medullary tissue preparations from DI rats that was reduced by dDAVP treatment (36).

Another mechanistic aspect may be considered regarding LPC production by iPLA$_2$β during lipid hydrolysis, since LPCs may increase membrane fluidity and facilitate the turnover of membrane rafts (32). We have previously shown that activation of NKCC2 by AVP is associated with its shift into membrane rafts along with enhanced surface expression (41). In our setting, inhibition of iPLA$_2$β therefore may have been instrumental in raising the degree of active, surface-expressed NKCC2 by stabilizing membrane rafts. Since iPLA$_2$β is also involved in membrane-recycling processes (10), impaired endocytosis and consequently increased surface expression of NKCC2 may have contributed to our finding.

In summary, we have shown that iPLA$_2$β, a rate-limiting enzyme for eicosanoid synthesis, is expressed in the distal nephron. Inhibition of iPLA$_2$β raises the activity of NKCC2 in the TAL. AVP, an established activator of TAL transport, causes downregulation of iPLA$_2$β. These results suggest a role for iPLA$_2$β as a negative regulator of NKCC2 and critical part of a mechanism contributing to salt and water homeostasis.

ACKNOWLEDGMENTS

We thank F. Grams, K. Riskowsky, and P. Schrade for their expert technical assistance and P. Schulte for editorial assistance.

GRANTS

These studies were supported by the Deutsche Forschungsgemeinschaft (FOR 667).

DISCLOSURES

No conflicts of interest, financial or otherwise, are declared by the authors.

AUTHOR CONTRIBUTIONS

Author contributions: A.P., T.R., and R.M. provided conception and design of research; A.P., T.R., H.N., S.S., T.K., A.L.D., K.M., N.H., and M.B. performed experiments; A.P., T.R., H.N., S.S., T.K., R.M., N.R.F., B.S.W., N.H., and M.B. analyzed data; A.P., T.R., H.N., N.R.F., B.S.W., N.H., M.B., and S.B. interpreted results of experiments; A.P. prepared figures; A.P. drafted manuscript; A.P., N.R.F., M.B., and S.B. edited and revised manuscript; A.P., T.R., H.N., S.S., T.K., A.L.D., K.M., R.M., N.R.F., B.S.W., N.H., M.B., and S.B. approved final version of manuscript.

REFERENCES

1. **Akiba S, Sato T.** Cellular function of calcium-independent phospholipase A2. *Biol Pharm Bull* 27: 1174–1178, 2004.
2. **Amlal H, Legoff C, Vernimmen C, Paillard M, Bichara M.** Na^+-$K^+(NH_4^+)$-2Cl- cotransport in medullary thick ascending limb: control by PKA, PKC, and 20-HETE. *Am J Physiol Cell Physiol* 271: C455–C463, 1996.
3. **Balsinde J, Dennis EA.** Bromoenol lactone inhibits magnesium-dependent phosphatidate phosphohydrolase and blocks triacylglycerol biosynthesis in mouse P388D1 macrophages. *J Biol Chem* 271: 31937–31941, 1996.
4. **Bao S, Jin C, Zhang S, Turk J, Ma Z, Ramanadham S.** Beta-cell calcium-independent group VIA phospholipase A_2 (iPLA$_2$beta): tracking iPLA$_2$beta movements in response to stimulation with insulin secretagogues in INS-1 cells. *Diabetes* 53, *Suppl* 1: S186–S189, 2004.
5. **Baskakis C, Magrioti V, Cotton N, Stephens D, Constantinou-Kokotou V, Dennis EA, Kokotos G.** Synthesis of polyfluoro ketones for selective inhibition of human phospholipase A2 enzymes. *J Med Chem* 51: 8027–8037, 2008.
6. **Bonvalet JP, Pradelles P, Farman N.** Segmental synthesis and actions of prostaglandins along the nephron. *Am J Physiol Renal Fluid Electrolyte Physiol* 253: F377–F387, 1987.
7. **Bonventre JV.** Phospholipase A2 and signal transduction. *J Am Soc Nephrol* 3: 128–150, 1992.
8. **Carroll MA, Sala A, Dunn CE, McGiff JC, Murphy RC.** Structural identification of cytochrome P450-dependent arachidonate metabolites formed by rabbit medullary thick ascending limb cells. *J Biol Chem* 266: 12306–12312, 1991.
9. **Cohen D, Papillon J, Aoudjit L, Li H, Cybulsky AV, Takano T.** Role of calcium-independent phospholipase A_2 in complement-mediated glomerular epithelial cell injury. *Am J Physiol Renal Physiol* 294: F469–F479, 2008.
10. **Culpepper RM, Andreoli TE.** Interactions among prostaglandin E2, antidiuretic hormone, and cyclic adenosine monophosphate in modulating Cl^- absorption in single mouse medullary thick ascending limbs of Henle. *J Clin Invest* 71: 1588–1601, 1983.
11. **Downey P, Sapirstein A, O'Leary E, Sun TX, Brown D, Bonventre JV.** Renal concentrating defect in mice lacking group IV cytosolic phospholipase A_2. *Am J Physiol Renal Physiol* 280: F607–F618, 2001.
12. **Eng B, Mukhopadhyay S, Vio CP, Pedraza PL, Hao S, Battula S, Sehgal PB, McGiff JC, Ferreri NR.** Characterization of a long-term rat mTAL cell line. *Am J Physiol Renal Physiol* 293: F1413–F1422, 2007.
13. **Fuentes L, Perez R, Nieto ML, Balsinde J, Balboa MA.** Bromoenol lactone promotes cell death by a mechanism involving phosphatidate phosphohydrolase-1 rather than calcium-independent phospholipase A2. *J Biol Chem* 278: 44683–44690, 2003.
14. **Gimenez I, Forbush B.** Regulatory phosphorylation sites in the NH_2 terminus of the renal Na-K-Cl cotransporter (NKCC2). *Am J Physiol Renal Physiol* 289: F1341–F1345, 2005.
15. **Gimenez I, Forbush B.** Short-term stimulation of the renal Na-K-Cl cotransporter (NKCC2) by vasopressin involves phosphorylation and membrane translocation of the protein. *J Biol Chem* 278: 26946–26951, 2003.
16. **Grider J, Kilpatrick E, Ott C, Jackson B.** Effect of dopamine on NaCl transport in the medullary thick ascending limb of the rat. *Eur J Pharmacol* 342: 281–284, 1998.
17. **Harris RC, McKanna JA, Akai Y, Jacobson HR, Dubois RN, Breyer MD.** Cyclooxygenase-2 is associated with the macula densa of rat kidney and increases with salt restriction. *J Clin Invest* 94: 2504–2510, 1994.
18. **He H, Podymow T, Zimpelmann J, Burns KD.** NO inhibits Na^+-K^+-2Cl- cotransport via a cytochrome *P*-450-dependent pathway in renal epithelial cells (MMDD1). *Am J Physiol Renal Physiol* 284: F1235–F1244, 2003.
19. **Hoagland KM, Flasch AK, Roman RJ.** Inhibitors of 20-HETE formation promote salt-sensitive hypertension in rats. *Hypertension* 42: 669–673, 2003.
20. **Imbert M, Chabardes D, Montegut M, Clique A, Morel F.** Vasopressin dependent adenylate cyclase in single segments of rabbit kidney tubule. *Pflügers Arch* 357: 173–186, 1975.
21. **Jenkins CM, Han X, Mancuso DJ, Gross RW.** Identification of calcium-independent phospholipase A2 (iPLA2) beta, and not iPLA2gamma, as the mediator of arginine vasopressin-induced arachidonic acid release in A-10 smooth muscle cells. Enantioselective mechanism-based discrimination of mammalian iPLA2s. *J Biol Chem* 277: 32807–32814, 2002.
22. **Kinsey GR, Blum JL, Covington MD, Cummings BS, McHowat J, Schnellmann RG.** Decreased iPLA2gamma expression induces lipid peroxidation and cell death and sensitizes cells to oxidant-induced apoptosis. *J Lipid Res* 49: 1477–1487, 2008.
23. **Kuo CF, Cheng S, Burgess JR.** Deficiency of vitamin E and selenium enhances calcium-independent phospholipase A2 activity in rat lung and liver. *J Nutr* 125: 1419–1429, 1995.
24. **Larsson Forsell PK, Kennedy BP, Claesson HE.** The human calcium-independent phospholipase A2 gene multiple enzymes with distinct properties from a single gene. *Eur J Biochem* 262: 575–585, 1999.
25. **Lio YC, Reynolds LJ, Balsinde J, Dennis EA.** Irreversible inhibition of Ca^{2+}-independent phospholipase A2 by methyl arachidonyl fluorophosphonate. *Biochim Biophys Acta* 1302: 55–60, 1996.
26. **Livak KJ, Schmittgen TD.** Analysis of relative gene expression data using real-time quantitative PCR and the 2(-delta delta C(T)) method. *Methods* 25: 402–408, 2001.
27. **Lopez-Vales R, Navarro X, Shimizu T, Baskakis C, Kokotos G, Constantinou-Kokotou V, Stephens D, Dennis EA, David S.** Intracellular phospholipase A_2 group IVA and group VIA play important roles in Wallerian degeneration and axon regeneration after peripheral nerve injury. *Brain* 131: 2620–2631, 2008.
28. **Lytle C, Xu JC, Biemesderfer D, Forbush B 3rd.** Distribution and diversity of Na-K-Cl cotransport proteins: a study with monoclonal antibodies. *Am J Physiol Cell Physiol* 269: C1496–C1505, 1995.
29. **Mangat H, Peterson LN, Burns KD.** Hypercalcemia stimulates expression of intrarenal phospholipase A2 and prostaglandin H synthase-2 in rats. Role of angiotensin II AT1 receptors. *J Clin Invest* 100: 1941–1950, 1997.
30. **Murakami M, Taketomi Y, Miki Y, Sato H, Hirabayashi T, Yamamoto K.** Recent progress in phospholipase A research: from cells to animals to humans. *Prog Lipid Res* 50: 152–192, 2011.
31. **Mutig K, Paliege A, Kahl T, Jons T, Muller-Esterl W, Bachmann S.** Vasopressin V2 receptor expression along rat, mouse, and human renal epithelia with focus on TAL. *Am J Physiol Renal Physiol* 293: F1166–F1177, 2007.
32. **Nakano T, Inoue I, Shinozaki R, Matsui M, Akatsuka T, Takahashi S, Tanaka K, Akita M, Seo M, Hokari S, Katayama S, Komoda T.** A possible role of lysophospholipids produced by calcium-independent

phospholipase A_2 in membrane-raft budding and fission. *Biochim Biophys Acta* 1788: 2222–2228, 2009.

33. **Portilla D, Crew MD, Grant D, Serrero G, Bates LM, Dai G, Sasner M, Cheng J, Buonanno A.** cDNA cloning and expression of a novel family of enzymes with calcium-independent phospholipase A2 and lysophospholipase activities. *J Am Soc Nephrol* 9: 1178–1186, 1998.
34. **Poulsen KA, Pedersen SF, Kolko M, Lambert IH.** Induction of group VIA phospholipase A_2 activity during in vitro ischemia in C2C12 myotubes is associated with changes in the level of its splice variants. *Am J Physiol Cell Physiol* 293: C1605–C1615, 2007.
35. **Rodriguez JA, Vio CP, Pedraza PL, McGiff JC, Ferreri NR.** Bradykinin regulates cyclooxygenase-2 in rat renal thick ascending limb cells. *Hypertension* 44: 230–235, 2004.
36. **Sarkis A, Ito O, Mori T, Kohzuki M, Ito S, Verbalis J, Cowley AW Jr, Roman RJ.** Cytochrome *P*-450-dependent metabolism of arachidonic acid in the kidney of rats with diabetes insipidus. *Am J Physiol Renal Physiol* 289: F1333–F1340, 2005.
37. **Schaloske RH, Dennis EA.** The phospholipase A2 superfamily and its group numbering system. *Biochim Biophys Acta* 1761: 1246–1259, 2006.
38. **Schwartzman M, Ferreri NR, Carroll MA, Songu-Mize E, McGiff JC.** Renal cytochrome P450-related arachidonate metabolite inhibits (Na^+ + K^+)ATPase. *Nature* 314: 620–622, 1985.
39. **Song H, Bao S, Lei X, Jin C, Zhang S, Turk J, Ramanadham S.** Evidence for proteolytic processing and stimulated organelle redistribution of iPLA$_2$beta. *Biochim Biophys Acta* 1801: 547–558, 2010.
40. **Valtin H, Schroeder HA.** Familial hypothalamic diabetes insipidus in rats (Brattleboro strain). *Am J Physiol* 206: 425–430, 1964.
41. **Welker P, Bohlick A, Mutig K, Salanova M, Kahl T, Schluter H, Blottner D, Ponce-Coria J, Gamba G, Bachmann S.** Renal Na^+-K^+-Cl-cotransporter activity and vasopressin-induced trafficking are lipid raft-dependent. *Am J Physiol Renal Physiol* 295: F789–F802, 2008.
42. **Wilson BS, Pfeiffer JR, Raymond-Stintz MA, Lidke D, Andrews N, Zhang J, Yin W, Steinberg S, Oliver JM.** Exploring membrane domains using native membrane sheets and transmission electron microscopy. *Methods Mol Biol* 398: 245–261, 2007.
43. **Yu MJ, Miller RL, Uawithya P, Rinschen MM, Khositseth S, Braucht DW, Chou CL, Pisitkun T, Nelson RD, Knepper MA.** Systems-level analysis of cell-specific AQP2 gene expression in renal collecting duct. *Proc Natl Acad Sci USA* 106: 2441–2446, 2009.
44. **Zhang L, Peterson BL, Cummings BS.** The effect of inhibition of Ca^{2+}-independent phospholipase A2 on chemotherapeutic-induced death and phospholipid profiles in renal cells. *Biochem Pharmacol* 70: 1697–1706, 2005.

4.3. The calcineurin inhibitor tacrolimus activates the renal sodium chloride cotransporter to cause hypertension

LETTERS

nature medicine

The calcineurin inhibitor tacrolimus activates the renal sodium chloride cotransporter to cause hypertension

Ewout J Hoorn[1,6], Stephen B Walsh[2,6], James A McCormick[1], Antje Fürstenberg[2], Chao-Ling Yang[1], Tom Roeschel[3], Alexander Paliege[3], Alexander J Howie[4], James Conley[1], Sebastian Bachmann[3], Robert J Unwin[2,6] & David H Ellison[1,5,6]

Calcineurin inhibitors (CNIs) are immunosuppressive drugs that are used widely to prevent rejection of transplanted organs and to treat autoimmune disease. Hypertension and renal tubule dysfunction, including hyperkalemia, hypercalciuria and acidosis, often complicate their use[1,2]. These side effects resemble familial hyperkalemic hypertension, a genetic disease characterized by overactivity of the renal sodium chloride cotransporter (NCC) and caused by mutations in genes encoding WNK kinases. We hypothesized that CNIs induce hypertension by stimulating NCC. In wild-type mice, the CNI tacrolimus caused salt-sensitive hypertension and increased the abundance of phosphorylated NCC and the NCC-regulatory kinases WNK3, WNK4 and SPAK. We demonstrated the functional importance of NCC in this response by showing that tacrolimus did not affect blood pressure in NCC-knockout mice, whereas the hypertensive response to tacrolimus was exaggerated in mice overexpressing NCC. Moreover, hydrochlorothiazide, an NCC-blocking drug, reversed tacrolimus-induced hypertension. These observations were extended to humans by showing that kidney transplant recipients treated with tacrolimus had a greater fractional chloride excretion in response to bendroflumethiazide, another NCC-blocking drug, than individuals not treated with tacrolimus; renal NCC abundance was also greater. Together, these findings indicate that tacrolimus-induced chronic hypertension is mediated largely by NCC activation, and suggest that inexpensive and well-tolerated thiazide diuretics may be especially effective in preventing the complications of CNI treatment.

We first studied whether tacrolimus was capable of inducing a familial hyperkalemic hypertension (FHHt)-like phenotype in wild-type mice, as most previous studies have used rats[3–5]. Two weeks of tacrolimus administration increased systolic blood pressure (SBP) from 123 ± 3 to 145 ± 3 mm Hg (**Fig. 1a**) and caused renal sodium (**Fig. 1b**) and potassium retention (**Fig. 1c**), as found previously[3,4,6]. A transient SBP rise in both groups on days 1 and 2 was attributable to acclimation to the injections. Although higher SBPs were already present during the first week of treatment with tacrolimus, hypertension did not develop fully until the second week (**Fig. 1a**) and was preceded by a decline in urinary sodium excretion (**Fig. 1b**). The increase in SBP also correlated with the degree of renal sodium retention (**Fig. 1d**). Although reduced food intake with tacrolimus might also explain lower urinary sodium excretion, there was no weight loss in the tacrolimus group, and body weights in the tacrolimus and vehicle-treated mice were similar. In a separate group of mice, we showed that tacrolimus-induced hypertension was salt-sensitive (**Fig. 1e**). Tacrolimus caused a modest increase in plasma aldosterone concentration (**Fig. 1f**), but it is unlikely that this is the main factor causing hypertension. Hypertension was more severe in tacrolimus-treated mice on a high sodium diet (**Fig. 1e**), during which plasma aldosterone concentration was suppressed (**Fig. 1f**), than it was on a normal salt diet. To confirm that the modest rise in plasma aldosterone to 348 ± 20 pg ml^{-1} during tacrolimus treatment was not responsible for the rise in SBP, we infused additional mice with aldosterone for 2 weeks, without tacrolimus. This treatment increased plasma aldosterone concentrations to 1506 ± 614 pg ml^{-1} but did not increase SBP significantly (121 ± 6 mm Hg to 125 ± 5 mm Hg; $P > 0.05$). Although this result indicates that the increase in plasma aldosterone concentration is not responsible for the effect of tacrolimus on SBP, aldosterone could still have a permissive role.

In addition to hypertension, tacrolimus caused hypomagnesemia, hypercalciuria and lowered plasma bicarbonate, with a positive urine anion gap, consistent with renal tubular acidosis (**Supplementary Table 1**); the degree of hypercalciuria was strain-dependent (**Supplementary Fig. 1**). Although tacrolimus did not cause frank hyperkalemia during normal potassium intake, when mice consumed high-potassium chow, blood potassium concentration was higher in tacrolimus-treated mice (5.4 ± 0.2 mmol per liter) than in vehicle-treated mice (4.5 ± 0.3 mmol per liter, $P = 0.02$, **Supplementary Fig. 2**). These results confirm that tacrolimus causes salt-sensitive hypertension, hypercalciuria, renal tubular acidosis and potassium retention in mice, recapitulating the FHHt phenotype.

[1]Division of Nephrology & Hypertension, Oregon Health & Science University, Portland, Oregon, USA. [2]UCL Centre for Nephrology, University College London, London, UK. [3]Department of Anatomy, Charité, Berlin, Germany. [4]Department of Pathology, University College London, London, UK. [5]Veterans Affairs Medical Center, Portland, Oregon, USA. [6]These authors contributed equally to this work. Correspondence should be addressed to D.H.E. (ellisond@ohsu.edu).

Received 1 April; accepted 15 July; published online 2 October 2011; corrected after print 13 January 2012; doi:10.1038/nm.2497

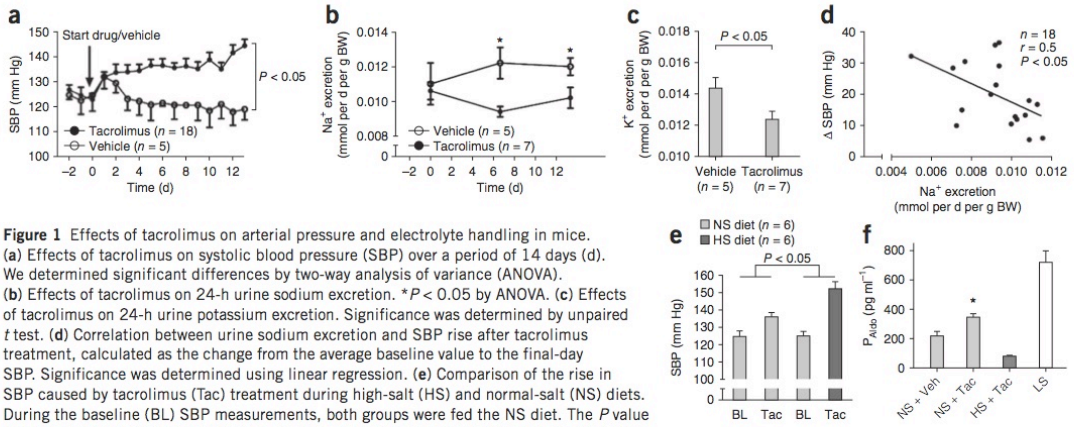

Figure 1 Effects of tacrolimus on arterial pressure and electrolyte handling in mice. (**a**) Effects of tacrolimus on systolic blood pressure (SBP) over a period of 14 days (d). We determined significant differences by two-way analysis of variance (ANOVA). (**b**) Effects of tacrolimus on 24-h urine sodium excretion. $^*P < 0.05$ by ANOVA. (**c**) Effects of tacrolimus on 24-h urine potassium excretion. Significance was determined by unpaired *t* test. (**d**) Correlation between urine sodium excretion and SBP rise after tacrolimus treatment, calculated as the change from the average baseline value to the final-day SBP. Significance was determined using linear regression. (**e**) Comparison of the rise in SBP caused by tacrolimus (Tac) treatment during high-salt (HS) and normal-salt (NS) diets. During the baseline (BL) SBP measurements, both groups were fed the NS diet. The *P* value was obtained using two-way ANOVA to analyze whether the change in SBP in one group was significantly different from the change in SBP in the other group. (**f**) Effect of tacrolimus (Tac, $n = 13$) on plasma aldosterone concentrations (P_{Aldo}), compared with vehicle (Veh) ($n = 5$), during NS diet. HS suppressed plasma aldosterone despite Tac ($n = 5$). To illustrate an activated renin angiotensin system, plasma aldosterone concentrations are also shown in untreated wild-type mice fed a low-sodium diet (LS, $n = 5$). $^*P < 0.05$, compared with NS + Veh. Significance was determined by unpaired *t* test. BW, body weight. Error bars are means ± s.e.m.

Tacrolimus interacts with several binding proteins to exert effects[7]. One of these, FKBP12 (also known as FKBP1a), is essential for its immunosuppressive effects and is widely expressed, including throughout the nephron, where it is prominent along the distal tubule[8]. CNIs inhibit calcineurin (also called protein phosphatase 3, formerly protein phosphatase 2b), a phosphatase believed to have a central role in immunosuppression. Calcineurin comprises a catalytic (A) subunit, with three closely related isoforms (α, β and γ), and a regulatory (B) subunit. Calcineurin A-α is considered to be the dominant isoform in the renal cortex[9], where NCC is expressed[10], and inhibition of calcineurin A-α activity is thought to be responsible for CNI nephrotoxicity[9]. We first confirmed that calcineurin A-α is expressed by cells of the distal convoluted tubule (DCT; **Fig. 2a**). Next, we showed that tacrolimus treatment increased the abundance of phosphorylated (activated) NCC (pNCC; **Fig. 2b**), detected using an antibody specific to phosphothreonine 53 (ref. 10); total NCC abundance was not increased. Tacrolimus treatment also decreased the abundance of the transient receptor calcium channel TRPV5 (**Fig. 2b**), consistent with a previous report that tacrolimus reduces the abundance of TRPV5 messenger RNA in rats[3]. In rats, another CNI, cyclosporine, has been shown to increase NKCC2 abundance[11], but we did not find an effect of tacrolimus on NKCC2 in mice (**Fig. 2b**). Tacrolimus treatment did increase the abundance of WNK3, WNK4 (**Fig. 2c**) and the STE20-related kinase SPAK; it also caused a shift in the electrophoretic mobility of SPAK, indicating its activation[12] (**Fig. 2c**).

As WNK3 and SPAK have been shown to increase NCC activity through effects on NCC trafficking and phosphorylation, they may be involved in tacrolimus-induced NCC activation. The increased WNK4 abundance observed in tacrolimus-treated mice seems at odds with WNK4's proposed role as a negative regulator of NCC[13]; however, WNK4 has been shown to switch to a stimulatory form under some conditions[14], and may also have been induced as a compensatory response. Another group recently reported that cyclosporine treatment increases WNK4 and NCC abundance in rats[15], effects consistent with our observations.

These results point to an effect of tacrolimus on the DCT, the only nephron segment expressing NCC. CNIs might increase the abundance of activated NCC directly, perhaps by inhibiting phosphate removal from the NCC amino terminus. To test for such a direct effect, in the absence of systemic factors, we determined the abundance of NCC and pNCC in stably transfected HEK293 cells. Tacrolimus treatment increased pNCC abundance in these cells (**Fig. 2d**), indicating that systemic factors are not required. Although this result is consistent with tacrolimus inhibiting calcineurin actions on NCC directly, it is also consistent with secondary activation via SPAK or WNK kinases, as HEK293 cells express these kinases endogenously (data not shown). Further work will be required to unravel these possibilities.

These results indicate that tacrolimus stimulates NCC activity *in vivo* and *in vitro*, but do not indicate whether this stimulation is responsible for the effect of tacrolimus on raising SBP. To address this issue, we analyzed the effects of tacrolimus on SBP in NCC-knockout mice and in mice overexpressing NCC. As reported previously[16], we found that NCC-knockout mice had normal SBP under control conditions (**Fig. 3a**). Unlike wild-type mice (**Fig. 1a**), NCC-knockout mice were resistant to the effect of tacrolimus treatment in raising SBP (**Fig. 3a**). Consistent with this result, tacrolimus treatment of these mice also did not affect renal sodium, potassium and calcium excretion, or plasma bicarbonate and magnesium concentrations (**Supplementary Table 2**). The peak plasma tacrolimus concentration was similar in NCC-knockout and wild-type mice (49.8 versus 46.1 ng ml^{-1}, determined from a pooled sample of all animals in each group), indicating that the observed differences were not the result of altered tacrolimus pharmacokinetics. Our results, based on studies in mice, support the suggestion of others on the basis of a clinical observation that NCC has an important role in tacrolimus-induced hypertension[17]: kidney transplantation from a donor with undetected Gitelman syndrome normalized blood pressure and led to hypokalemia in a hypertensive individual, despite ongoing tacrolimus treatment.

Because NCC-knockout mice lack this transporter throughout life, developmental effects due to NCC deficiency may have contributed to

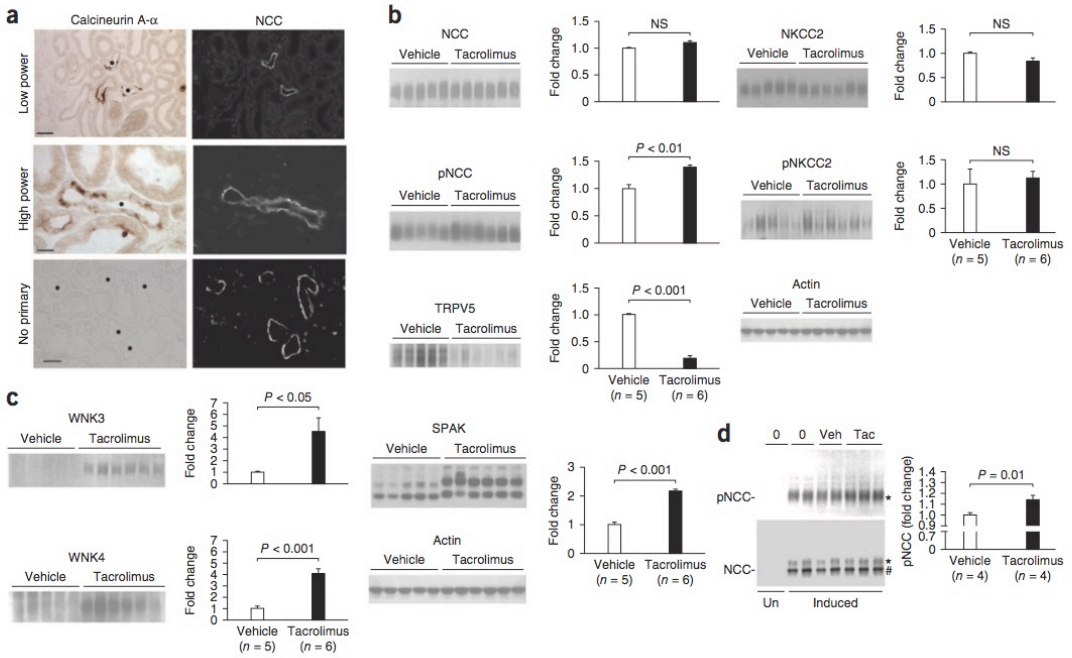

Figure 2 Effects of tacrolimus on transport proteins and kinases in kidney and *in vitro*. (**a**) Localization of calcineurin A-α in kidney; left images show immunohistochemical detection of calcineurin; right images show NCC in the same field delineating distal convoluted tubules. A control without primary antibody is shown for comparison. Dots (•) indicate distal convoluted tubules. Scale bars, 50 μm (top and bottom); 20 μm (middle). (**b**) Immunoblots showing effects of tacrolimus on the sodium chloride cotransporters (NCC and pNCC at ~130 kDa, and NKCC2 and pNKCC2 at ~140 kDa) and on the calcium channel TRPV5 (at ~90 kDa). Densitometry analysis (fold change compared to vehicle, normalized for actin) for each are shown at the right. Significance was determined by unpaired *t* test. (**c**) Immunoblots showing effects of tacrolimus on WNK3 (at ~200 kDa), WNK4 (at ~150 kDa) and SPAK. Densitometry analysis (fold change compared to vehicle, normalized for actin) is shown at the right; densitometry of SPAK was done by averaging all isoforms. Significance was determined by unpaired *t* test. (**d**) Immunoblots showing effects of tacrolimus on HEK293 cells. NCC expression was undetectable when cells were not induced with tetracycline (Un). Induced cells were either untreated (0), or treated with vehicle (Veh) or with tacrolimus (Tac). Bands corresponding to total NCC were detected at ~130 kDa (*) and 110 kDa (#), indicating mature and immature forms, respectively, whereas the band corresponding to pNCC was detected only at 130 kDa. Representative immunoblots are shown. Densitometry was normalized for actin. Significance was determined by unpaired *t* test. NS, not significant. Error bars are means ± s.e.m.

the resistance of these mice to tacrolimus treatment. To exclude this possibility, we showed that hypertension induced in wild-type mice by tacrolimus was reversed by treatment with hydrochlorothiazide, a pharmacological inhibitor of NCC (**Fig. 3b**). A thiazide-induced natriuresis or chloriuresis is often used as a marker of NCC activity in experimental animals and humans[18,19]. Hydrochlorothiazide caused a greater natriuresis in tacrolimus-treated mice than in untreated mice (**Fig. 3c**), supporting the conclusion that increased NCC activity mediates the effects of tacrolimus. Notably, treatment with hydrochlorothiazide for 4 d did not worsen tacrolimus-induced hypomagnesemia in wild-type mice (plasma magnesium 0.72 ± 0.03 versus 0.78 ± 0.08 mmol liter^{-1}; $P = 0.5$), suggesting that tacrolimus treatment of humans may not exacerbate the hypomagnesemia induced by CNIs.

In as much as NCC-knockout mice were resistant to hypertension when treated with tacrolimus, we next tested the effects of tacrolimus on transgenic mice overexpressing NCC. These mice, which our group has recently generated[10], have no overt phenotype at baseline, despite a 70% increase in total NCC abundance compared to wild-type controls; this lack of a phenotype is consistent with the lack of an increase in pNCC abundance. When treated with tacrolimus, mice overexpressing NCC developed more severe hypertension than did their wild-type counterparts (**Fig. 3d**). Notably, the transgenic NCC mice and their wild-type controls had a lower baseline SBP than the mice in the previous experiments, which was attributed to a strain difference (see Online Methods), as reported elsewhere[20]. The more severe hypertension in the transgenic NCC mice receiving tacrolimus was associated with increased pNCC abundance compared to tacrolimus-treated wild-type mice (**Fig. 3e,f**).

To analyze whether these findings in experimental animals extend to humans, we identified CNI-treated recipients of kidney transplants with an FHHt-like phenotype. This was defined as individuals on a CNI with resistant hypertension (requiring two or more antihypertensive agents), hyperkalemia (plasma potassium recurrently >5.5 mmol per liter) or acidosis (serum bicarbonate recurrently <20 mmol per liter, or requiring oral bicarbonate supplements); all had serum creatinine values below 150 μmol per liter (**Supplementary Table 3**). The change in fractional chloride excretion (FE_{Cl}) after a single dose of bendroflumethiazide was taken as a measure of NCC activity. Individuals with CNI-induced hypertension had a significantly ($P = 0.003$) greater change in FE_{Cl} after bendroflumethiazide treatment

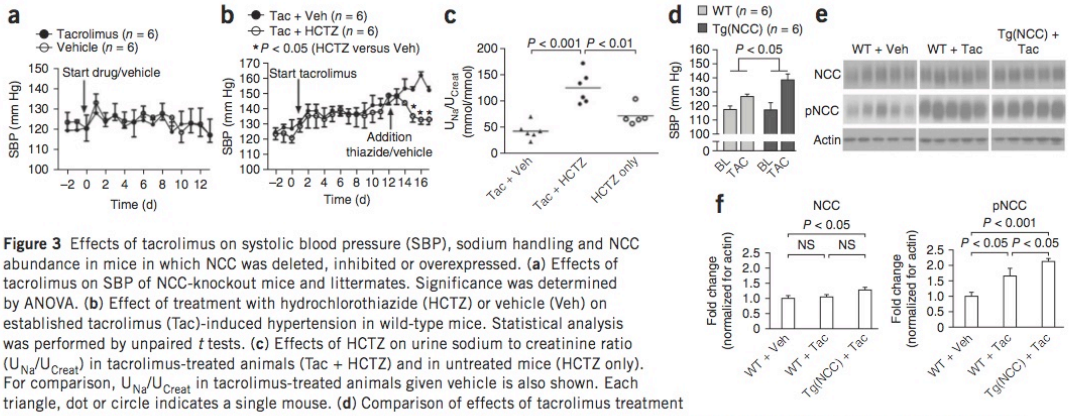

Figure 3 Effects of tacrolimus on systolic blood pressure (SBP), sodium handling and NCC abundance in mice in which NCC was deleted, inhibited or overexpressed. (**a**) Effects of tacrolimus on SBP of NCC-knockout mice and littermates. Significance was determined by ANOVA. (**b**) Effect of treatment with hydrochlorothiazide (HCTZ) or vehicle (Veh) on established tacrolimus (Tac)-induced hypertension in wild-type mice. Statistical analysis was performed by unpaired *t* tests. (**c**) Effects of HCTZ on urine sodium to creatinine ratio (U_{Na}/U_{Creat}) in tacrolimus-treated animals (Tac + HCTZ) and in untreated mice (HCTZ only). For comparison, U_{Na}/U_{Creat} in tacrolimus-treated animals given vehicle is also shown. Each triangle, dot or circle indicates a single mouse. (**d**) Comparison of effects of tacrolimus treatment (TAC) on SBP in wild-type (WT) and transgenic mice overexpressing NCC (Tg(NCC)). Baseline (BL) and final-day SBPs are shown. The *P* value was obtained using two-way ANOVA to analyze whether the change in SBP from BL to the final day in one group was significantly different from the change in SBP in the other group. (**e**) Immunoblots comparing total NCC and pNCC abundances from kidneys of vehicle (Veh)-treated WT mice and tacrolimus (Tac)-treated WT and Tg(NCC) mice. (**f**) Quantification of the effects of tacrolimus (Tac) on NCC and pNCC abundance in WT and TgNCC mice ($n = 5$ in each group). Significance was determined by ANOVA. NS, not significant. Error bars are means ± s.e.m.

than did healthy volunteer controls (**Fig. 4a** and **Supplementary Table 3**). Recipients of kidney transplants who were treated with sirolimus but not a CNI had a significantly smaller ($P = 0.04$) response than did CNI-treated individuals, similar to controls (**Fig. 4a**). Bioimpedance measurements showed that extracellular fluid volume was expanded in the CNI group compared with controls (**Fig. 4b**,**c**), although there was no significant difference in plasma renin activity or plasma aldosterone concentration (**Fig. 4d**,**e**). We examined transplant biopsy samples using immunohistochemistry for NCC and pNCC in individuals treated with CNIs with an FHHt phenotype (**Supplementary Table 4**) and compared them with biopsy samples from after-transplant individuals treated with azathioprine (**Supplementary Table 5**), and with samples from prospective kidney donors (**Supplementary Table 6**). The subjects treated with CNIs had a pronounced increase in NCC and pNCC staining compared with the azathioprine and healthy control groups (**Fig. 4f** shows representative examples; the other biopsy samples are shown in **Supplementary Fig. 3**). Enhanced staining was visible in 10 of 14 biopsy samples from the CNI group but in none of 13 from the azathioprine group ($P < 0.001$, by Fisher's exact test).

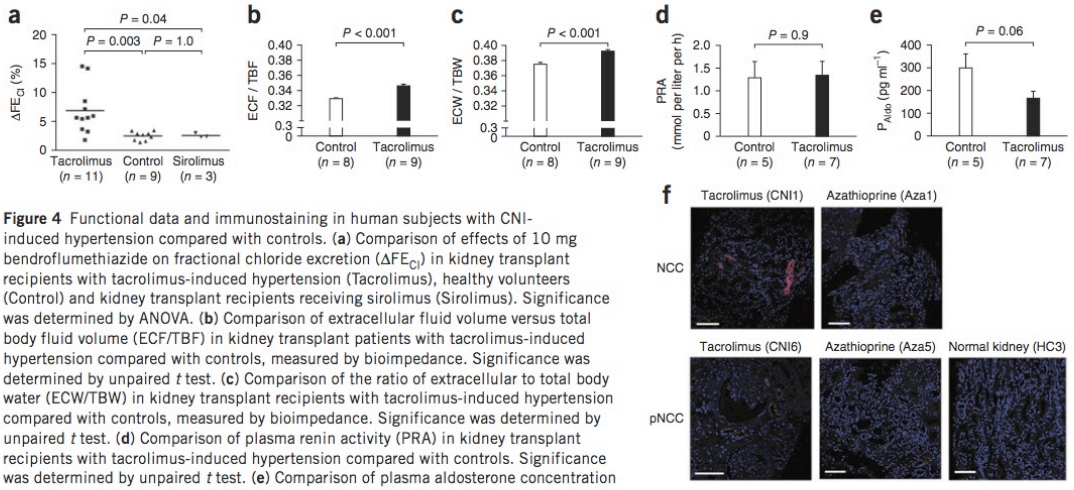

Figure 4 Functional data and immunostaining in human subjects with CNI-induced hypertension compared with controls. (**a**) Comparison of effects of 10 mg bendroflumethiazide on fractional chloride excretion (ΔFE_{Cl}) in kidney transplant recipients with tacrolimus-induced hypertension (Tacrolimus), healthy volunteers (Control) and kidney transplant recipients receiving sirolimus (Sirolimus). Significance was determined by ANOVA. (**b**) Comparison of extracellular fluid volume versus total body fluid volume (ECF/TBF) in kidney transplant patients with tacrolimus-induced hypertension compared with controls, measured by bioimpedance. Significance was determined by unpaired *t* test. (**c**) Comparison of the ratio of extracellular to total body water (ECW/TBW) in kidney transplant recipients with tacrolimus-induced hypertension compared with controls, measured by bioimpedance. Significance was determined by unpaired *t* test. (**d**) Comparison of plasma renin activity (PRA) in kidney transplant recipients with tacrolimus-induced hypertension compared with controls. Significance was determined by unpaired *t* test. (**e**) Comparison of plasma aldosterone concentration (P_{Aldo}) in kidney transplant recipients with tacrolimus-induced hypertension compared with controls. Significance was determined by unpaired *t* test. (**f**) Representative confocal immunofluorescence images of renal tissue showing NCC and pNCC in kidney transplant recipients with tacrolimus-induced hypertension compared with azathioprine-treated kidney transplant recipients and with healthy controls. Scale bars, 100 μm. Images from additional biopsy samples and clinical characteristics are provided in **Supplementary Tables 4–6** and **Supplementary Figure 3**. Error bars are means ± s.e.m.

CNI-induced hypertension has been attributed to a combination of vasoconstriction and renal sodium retention[21,22]. When administered in high doses, especially intravenously, vascular effects predominate[5]. CNIs have been shown to constrict arterioles, an effect that may be both direct and via sympathetic activation. For this reason CNI-induced hypertension is often treated with calcium channel blockers[21]. Calcium channel blockers are mainly vasodilatory drugs, although a natriuretic effect has been demonstrated for some classes[23]. Our results show that activation of the NCC in the DCT is necessary for CNIs to cause sustained hypertension. This does not, however, exclude an important role for vasoconstriction either as a direct effect or as a result of sodium retention. Changes in vasoreactivity occur in association with altered sodium balance; for example, individuals with FHHt have an enhanced response to a 'cold pressor' test[24], whereas subjects with Gitelman syndrome have increased vasodilation[25,26]. In Gitelman syndrome the deleted gene, *SLC12A3*, is expressed in renal but not vascular tissue, indicating that the vasodilation must be the result of kidney dysfunction[25]. According to Guyton's model of whole-body autoregulation, sodium retention will result in a pressure natriuresis and secondary vasoconstriction[27]. Indeed, a role for increased endothelin and reduced nitric oxide has been proposed in CNI-induced hypertension in rats, but only at very high doses ($5\ mg\ kg^{-1}$)[5]; moreover, an endothelin inhibitor does not completely prevent a rise in blood pressure with tacrolimus[5].

The prevalence of the FHHt phenotype, with hypertension, hyperkalemia and acidosis, has been reported to be as high as 16–30% in some series of patients treated with CNIs[28,29]. Hypertension may be less common with tacrolimus compared with cyclosporine, but hyperkalemia seems to be more common[30]. A long-term follow-up study detected hyperkalemia and hypertension in approximately 33% of individuals with liver transplants maintained on tacrolimus[2], suggesting that these complications are relatively common. Our data suggest that thiazide diuretics should be uniquely effective in treating CNI-induced hypertension and hyperkalemia. Although there are concerns about combining CNIs with thiazides because of the tendency of the latter to cause magnesium wasting and glucose intolerance[31], our own data and a previous clinical study[32] indicate that thiazides do not worsen CNI-induced hypomagnesemia.

The contribution of CNIs to decreasing rejection rates after transplantation is undisputed, but this benefit comes at the cost of increasing rates of hypertension, which contribute to long-term kidney damage and chronic allograft nephropathy[33]. Our findings indicate that activation of the NCC has a central role in tacrolimus-induced hypertension and imply that a controlled trial of thiazide diuretics to treat CNI-induced hypertension is justified.

METHODS

Methods and any associated references are available in the online version of the paper at http://www.nature.com/naturemedicine/.

Note: Supplementary information is available on the Nature Medicine website.

ACKNOWLEDGMENTS

For technical assistance, we thank N. Desmerais (animal studies), S. Rogers, K. Risowsky (immunohistochemistry), D. Gannon and A. Bakke (tacrolimus measurements in mice). We thank G. Jones and M. Harber for help in identifying human subjects. We also thank G. Shull (University of Cincinnati) for the NCC-knockout mice, and E. Delpire (Vanderbilt Kennedy Center) for SPAK antibodies. E.J.H. is supported by an Erasmus Medical Center Fellowship and Kolff Junior Postdoc Grant (Dutch Kidney Foundation, KJPB 08.004); J.A.M. is supported by the US National Institutes of Health (NIH) (K01 DK076617); D.H.E. is supported by the NIH (RO1 DK51496), the Department of Veterans Affairs (Merit Review) and the American Heart Association (10 GRNT 2630199). Portions of this work were presented at the High Blood Pressure Research Council Meeting of the American Heart Association, 13–16 October 2010, and the American Society of Nephrology, 15–18 November 2010.

AUTHOR CONTRIBUTIONS

E.J.H. and S.B.W. carried out most of the experiments, analyzed the data and wrote the initial manuscript. J.A.M. generated the mice overexpressing the NCC and participated in animal experiments and analyses. J.C. did the aldosterone infusion experiments. A.F. contributed to the human experiments and, together with A.J.H., to the kidney biopsy tissue staining. C.-L.Y. conducted the cell studies. T.R., A.P. and S.B. carried out the calcineurin immunohistochemistry. R.J.U. and D.H.E. conceived of the study, supervised the work and edited the manuscript. All authors reviewed the manuscript.

COMPETING FINANCIAL INTERESTS

The authors declare no competing financial interests.

Published online at http://www.nature.com/naturemedicine/.
Reprints and permissions information is available online at http://www.nature.com/reprints/index.html.

1. Kim, H.C. *et al.* Primary immunosuppression with tacrolimus in kidney transplantation: three-year follow-up in a single center. *Transplant. Proc.* **36**, 2082–2083 (2004).
2. Jain, A. *et al.* What have we learned about primary liver transplantation under tacrolimus immunosuppression? Long-term follow-up of the first 1000 patients. *Ann. Surg.* **230**, 441–448, discussion 448–449 (1999).
3. Nijenhuis, T., Hoenderop, J.G. & Bindels, R.J. Downregulation of Ca^{2+} and Mg^{2+} transport proteins in the kidney explains tacrolimus (FK506)-induced hypercalciuria and hypomagnesemia. *J. Am. Soc. Nephrol.* **15**, 549–557 (2004).
4. Mohebbi, N., Mihailova, M. & Wagner, C.A. The calcineurin inhibitor FK506 (tacrolimus) is associated with transient metabolic acidosis and altered expression of renal acid-base transport proteins. *Am. J. Physiol. Renal Physiol.* **297**, F499–F509 (2009).
5. Takeda, Y., Miyamori, I., Furukawa, K., Inaba, S. & Mabuchi, H. Mechanisms of FK 506-induced hypertension in the rat. *Hypertension* **33**, 130–136 (1999).
6. Curtis, J.J., Luke, R.G., Jones, P. & Diethelm, A.G. Hypertension in cyclosporine-treated renal transplant recipients is sodium dependent. *Am. J. Med.* **85**, 134–138 (1988).
7. Kang, C.B., Hong, Y., Dhe-Paganon, S. & Yoon, H.S. FKBP family proteins: immunophilins with versatile biological functions. *Neurosignals* **16**, 318–325 (2008).
8. Smith, K.D. *et al.* Delayed graft function and cast nephropathy associated with tacrolimus plus rapamycin use. *J. Am. Soc. Nephrol.* **14**, 1037–1045 (2003).
9. Gooch, J.L., Roberts, B.R., Cobbs, S.L. & Tumlin, J.A. Loss of the alpha-isoform of calcineurin is sufficient to induce nephrotoxicity and altered expression of transforming growth factor-beta. *Transplantation* **83**, 439–447 (2007).
10. McCormick, J.A., Nelson, J.H., Yang, C.L., Curry, J.N. & Ellison, D.H. Overexpression of the sodium chloride cotransporter is not sufficient to cause familial hyperkalemic Hypertension. *Hypertension* published online, doi:10.1161HYPERTENSIONAHA.110.167809 (6 September 2011).
11. Esteva-Font, C. *et al.* Ciclosporin-induced hypertension is associated with increased sodium transporter of the loop of Henle (NKCC2). *Nephrol. Dial. Transplant.* **22**, 2810–2816 (2007).
12. Anselmo, A.N. *et al.* WNK1 and OSR1 regulate the Na^+, K^+, $2Cl^-$ cotransporter in HeLa cells. *Proc. Natl. Acad. Sci. USA* **103**, 10883–10888 (2006).
13. Yang, C.L., Angell, J., Mitchell, R. & Ellison, D.H. WNK kinases regulate thiazide-sensitive Na-Cl cotransport. *J. Clin. Invest.* **111**, 1039–1045 (2003).
14. San-Cristobal, P. *et al.* Angiotensin II signaling increases activity of the renal Na-Cl cotransporter through a WNK4-SPAK-dependent pathway. *Proc. Natl. Acad. Sci. USA* **106**, 4384–4389 (2009).
15. Melnikov, S., Mayan, H., Uchida, S., Holtzman, E.J. & Farfel, Z. Cyclosporine metabolic side effects: association with the WNK4 system. *Eur. J. Clin. Invest.* **41**, 1113–1120 (2011).
16. Schultheis, P.J. *et al.* Phenotype resembling Gitelman's syndrome in mice lacking the apical Na^+-Cl^- cotransporter of the distal convoluted tubule. *J. Biol. Chem.* **273**, 29150–29155 (1998).
17. Hu, D.C., Burtner, C., Hong, A., Lobo, P.I. & Okusa, M.D. Correction of renal hypertension after kidney transplantation from a donor with Gitelman syndrome. *Am. J. Med. Sci.* **331**, 105–109 (2006).
18. Colussi, G. *et al.* A thiazide test for the diagnosis of renal tubular hypokalemic disorders. *Clin. J. Am. Soc. Nephrol.* **2**, 454–460 (2007).
19. Madala Halagappa, V.K., Tiwari, S., Riazi, S., Hu, X. & Ecelbarger, C.M. Chronic candesartan alters expression and activity of NKCC2, NCC, and ENaC in the obese Zucker rat. *Am. J. Physiol.* **294**, F1222–F1231 (2008).
20. Feng, M. *et al.* Genetic analysis of blood pressure in 8 mouse intercross populations. *Hypertension* **54**, 802–809 (2009).
21. Koomans, H.A. & Ligtenberg, G. Mechanisms and consequences of arterial hypertension after renal transplantation. *Transplantation* **72**, S9–S12 (2001).
22. Curtis, J.J. Hypertensinogenic mechanism of the calcineurin inhibitors. *Curr. Hypertens. Rep.* **4**, 377–380 (2002).

23. Segal, A.S., Hayslett, J.P. & Desir, G.V. On the natriuretic effect of verapamil: inhibition of ENaC and transepithelial sodium transport. *Am. J. Physiol. Renal Physiol.* **283**, F765–F770 (2002).
24. Paver, W.K. & Pauline, G.J. Hypertension and hyperpotassemia without renal disease in a young male. *Med. J. Aust.* **2**, 305–306 (1964).
25. Calò, L., Davis, P.A. & Semplicini, A. Control of vascular tone in the syndromes of Bartter and Gitelman. *Crit. Rev. Clin. Lab. Sci.* **37**, 503–522 (2000).
26. Calò, L., Davis, P.A. & Semplicini, A. Reduced content of alpha subunit of Gq protein content in monocytes of Bartter and Gitelman syndromes: relationship with vascular hyporeactivity. *Kidney Int.* **61**, 353–354 (2002).
27. Guyton, A.C. Blood pressure control—special role of the kidneys and body fluids. *Science* **252**, 1813–1816 (1991).
28. Adu, D., Michael, J., Turney, J. & McMaster, P. Hyperkalemia in cyclosporine treated renal allograft recipients. *Lancet* **322**, 370–372 (1983).
29. Heering, P.J. *et al.* Aldosterone resistance in kidney transplantation is in part induced by a down-regulation of mineralocorticoid receptor expression. *Clin. Transplant.* **18**, 186–192 (2004).
30. Higgins, R. *et al.* Hyponatraemia and hyperkalaemia are more frequent in renal transplant recipients treated with tacrolimus than with cyclosporin. Further evidence for differences between cyclosporin and tacrolimus nephrotoxicities. *Nephrol. Dial. Transplant.* **19**, 444–450 (2004).
31. Van Laecke, S. *et al.* Posttransplantation hypomagnesemia and its relation with immunosuppression as predictors of new-onset diabetes after transplantation. *Am. J. Transplant* **9**, 2140–2149 (2009).
32. Arthur, J.M. & Shamim, S. Interaction of cyclosporine and FK506 with diuretics in transplant patients. *Kidney Int.* **58**, 325–330 (2000).
33. Schindler, R., Tanriver, Y. & Frei, U. Hypertension and allograft nephropathy—cause, consequence, or both? *Nephrol. Dial. Transplant.* **15**, 8–10 (2000).

ONLINE METHODS

Animal studies. All animal studies were approved by Oregon Health and Science University's Animal Care and Usage Committee (A858). All mice were male littermates (12–16 weeks, 25–30 g) and were fed a normal (0.5%), high-sodium (8%) or high-potassium (5%) diet (Harlan Laboratories), as indicated. All mice had a BALB/c background, except for the transgenic mice and their wild-type controls (C57BL/6;129SV). Our NCC-knockout colony was backcrossed to BALB/c every 10 generations to maintain the genetic background. The NCC transgenic animals were recently generated by our group[10]. Standard PCR, using previously reported primers[16], was used to distinguish NCC-knockout and transgenic mice from wild-type mice. SBPs were measured with tail-cuffs using volumetric pressure recording (CODA-6; Kent Scientific). This method has been validated for SBP measurements in mice, demonstrating excellent correlation with radiotelemetry[34,35]. The mice were first acclimated to the experimental procedure for five consecutive days; baseline SBP was then measured for 3 d, followed by daily measurements before the tacrolimus or vehicle injections. Tacrolimus (Enzo Life Sciences) was dissolved in ethanol, Tween-20 and sterile saline; the vehicle solution contained the same concentrations of the solvents. Tacrolimus or vehicle was administered subcutaneously; the dose of tacrolimus was 1 mg per kg body weight per day.

Blood and urinary measurements in mice. Whole blood was collected via terminal cardiac puncture (under anesthesia) and immediately pipetted into an i-STAT analyzer (Abbott Point of Care). The remainder of the blood was centrifuged to measure plasma magnesium (Pointe Scientific), aldosterone (ELISA; IBL-America) and tacrolimus (~4 h after the last injection; Architect Tacrolimus Reagent Kit; Abbott Laboratories). Metabolic cages were used for collection of spot urine and 24-h urine (under mineral oil); water and food were provided as gel to avoid dilution of urine with drinking water. A 3-h timed urine collection was used for the thiazide response; before this procedure, the animals' bladders were emptied by bladder massage. Urine sodium and potassium concentrations were measured using a dual-channel flame photometer (Cole-Palmer Instrument). Urine chloride, calcium and creatinine were measured using the mercuric thiocyanate, cresolphthalein complexone and modified Jaffé methods, respectively (all from Pointe Scientific).

Generation and culture of human embryonic kidney 293 cells transfected with NCC. Complementary DNA (cDNA) encoding full-length mouse NCC was subcloned into the pcDNA5/FRT/TO vector (Invitrogen). Flp-In 293 host cells (Invitrogen) were cotransfected with the pcDNA5/FRT/TO-NCC construct and pOG44, a plasmid expressing Flp recombinase, resulting in a homologous recombination event. Transfected cells were screened for hygromycin resistance and lack of β-galactosidase activity. The Flp-In T-REx 293 NCC cell line was maintained in high-glucose DMEM containing 10% v/v FBS, 200 μg ml^{-1} hygromycin, 15 μg ml^{-1} blasticidin and penicillin/streptomycin. NCC induction was confirmed by incubating the cells with or without tetracycline (1 μg ml^{-1}), followed by cell lysis and immunoblotting with antibodies specific to NCC and to pNCC.

Human studies. All human studies were approved by the West London Ethics Committee 3, and indivudals gave informed consent for all procedures. Kidney transplant recipients on tacrolimus (all outpatients) were selected with at least two out of three features of the following: resistant hypertension, otherwise unexplained metabolic acidosis or hyperkalemia. They were compared with kidney transplant recipients using sirolimus, azathioprine and with untreated healthy volunteers, as indicated in the Figures. The thiazide sensitivity test was based on one previously described[18]. Urine and plasma electrolytes were measured by ion-selective electrodes, and creatinine by the compensated kinetic Jaffé method (Roche). Plasma renin activity and plasma aldosterone concentration were measured by radioimmunoassay (Diasorin and Siemens). Multifrequency bioelectrical impedance analysis was performed using a tetrapolar eight-point tactile electrode system (Inbody720; Biospace).

Immunoblotting. Mouse kidneys were harvested and snap-frozen in liquid nitrogen. Kidneys were then homogenized on ice in chilled homogenization buffer containing protease and phosphatase inhibitors. Protein (20–80 μg) was separated on 3–8% (wt/vol) Tris acetate gel (Invitrogen) as described[36]. All primary antibodies had been characterized and were specific to the following proteins: NCC, pNCC at threonine-53, WNK3 (**Supplementary Fig. 4**), WNK4 (all developed in our laboratory)[10,36], NKCC2 and pNKCC2 (ref. 37), SPAK[38] and TRPV5 (Santa Cruz Biotechnology, SC-30187)[39]. Densitometry was performed using ImageJ (http://rsbweb.nih.gov/ij/).

Immunofluorescence and immunohistochemistry. For calcineurin and NCC immunohistochemistry and immunofluorescence on mouse kidney sections (**Fig. 2a**), an untreated wild-type BALB/c mouse was perfusion-fixed with 4% (vol/vol) paraformaldehyde in phosphate buffered saline (PBS) via the abdominal aorta and cryoprotected in 800 mOsm per liter sucrose–(PBS). After freezing in liquid nitrogen, 7-μm sections were prepared on a cryostat. Sections were blocked with 5% (wt/vol) skim milk–PBS and incubated with primary antibody at 4 °C overnight, followed by incubation with Cy-3- or horseradish peroxidase–coupled secondary antibody. Secondary antibodies conjugated with horseradish peroxidase were detected using diaminobenzidine. Antibodies specific to calcineurin A-α were obtained from Santa Cruz Biotechnology (sc-6123).

Human kidney sections for NCC and pNCC were stained on paraffin-embedded sections using standard procedures. The sections were blocked with 1% (wt/vol) BSA in PBS and stained with antibodies specific to NCC (1:3,000, The Binding Site) and pNCC (see above). Confocal microscopy was carried out using an Olympus IX81.

Statistical analyses. All values are expressed as mean ± s.e.m. For the animal and human studies, comparisons between two groups were done using the Student's *t* test (paired or unpaired, as indicated in figure legends). Multigroup comparisons were done using one-way ANOVA followed by a *post hoc* test. In animals, SBP data were analyzed using two-way ANOVA to assess whether the changes from average baseline SBP to final-day SBP in the two groups were different.

34. Feng, M. *et al.* Validation of volume-pressure recording tail-cuff blood pressure measurements. *Am. J. Hypertens.* **21**, 1288–1291 (2008).
35. Kurtz, T.W., Griffin, K.A., Bidani, A.K., Davisson, R.L. & Hall, J.E. Recommendations for blood pressure measurement in humans and experimental animals. Part 2: Blood pressure measurement in experimental animals: a statement for professionals from the Subcommittee of Professional and Public Education of the American Heart Association Council on High Blood Pressure Research. *Hypertension* **45**, 299–310 (2005).
36. Yang, C.-L., Zhu, X. & Ellison, D.H. The thiazide-sensitive Na-Cl cotransporter is regulated by a WNK kinase signaling complex. *J. Clin. Invest.* **117**, 3403–3411 (2007).
37. Welker, P. *et al.* Renal Na^+-K^+-Cl^- cotransporter activity and vasopressin-induced trafficking are lipid raft-dependent. *Am. J. Physiol.* **295**, F789–F802 (2008).
38. Piechotta, K., Lu, J. & Delpire, E. Cation chloride cotransporters interact with the stress-related kinases Ste20-related proline-alanine-rich kinase (SPAK) and oxidative stress response 1 (OSR1). *J. Biol. Chem.* **277**, 50812–50819 (2002).
39. Yang, S.S. *et al.* Mechanisms for hypercalciuria in pseudohypoaldosteronism type II–causing WNK4 knock-in mice. *Endocrinology* **151**, 1829–1836 (2010).

5. Lebenslauf von Tom Röschel

Mein Lebenslauf wird aus Datenschutztechnischen Gründen in der elektronischen Version meiner Arbeit nicht veröffentlicht.

Mein Lebenslauf wird aus Datenschutztechnischen Gründen in der elektronischen Version meiner Arbeit nicht veröffentlicht.

6. Publikationsliste

1. Boldt C*, **Roeschel T***, Himmerkus N, Plain A, Bleich M, Labes R, Blum M, Krause H, Magheli A, Giesecke T, Mutig K, Rothe M, Weldon SM, Dragun D, Schunck WH, Bachmann S, Paliege A
   Vasopressin lowers renal epoxyeicosatrienoic acid levels by activating soluble epoxide hydrolase
   Am J Physiol Renal Physiol. 2016;311(6):F1198-F1210.
   Impact Factor: 3,09

2. Paliege A, **Roeschel T**, Neymeyer H, Seidel S, Kahl T, Daigeler AL, Mutig K, Mrowka R, Ferreri NR, Wilson BS, Himmerkus N, Bleich M, and Bachmann S
   Group VIA phospholipase A_2 is a target for vasopressin signaling in the thick ascending limb
   Am J Physiol Renal Physiol. 2012;302(7):F865-F874.
   Impact Factor: 3,09

3. Seidel S, Neymeyer H, Kahl T, **Röschel T**, Mutig K, Flower R, Schnermann J, Bachmann S, Paliege A
   Annexin A1 modulates macula densa function by inhibiting cyclooxygenase 2
   Am J Physiol Renal Physiol. 2012;303(6):F845-F854.
   Impact Factor: 3,09

4. Hoorn EJ, Walsh SB, McCormick JA, Fürstenberg A, Yang CL, **Roeschel T**, Paliege A, Howie AJ, Conley J, Bachmann S, Unwin RJ, Ellison DH
   The calcineurin inhibitor tacrolimus activates the renal sodium chloride cotransporter to cause hypertension
   Nature Medicine. 2011;17:1304–1309.
   Impact Factor: 28,95

7. Danksagung

An dieser Stelle möchte ich mich bei all Denen bedanken, die diese Promotion möglich gemacht haben.

Mein besonderer Dank gilt meinem Doktorvater Prof. Bachmann und meinem Betreuer Dr. Paliege für das wirklich schöne Projekt.
Danke Alex, für die ganze Unterstützung im Labor, beim Studium und danach; danke für die Geduld und das Vertrauen; vor Allem danke, dass du immer ein offenes Ohr für mich hattest. Immer wenn ich die Physiologie der Niere verstanden geglaubt habe, wurde ich zügig eines Besseren belehrt.

Ich möchte der ganzen Arbeitsgruppe für die vielen Ratschläge, Tipps und die nette Atmosphäre im Labor danken, insbesondere meinen Mitdoktoranten Dr. Saritas, Dr. Seidel und Dr. Boldt. Vielen Dank auch an die immer hilfreichen MTAs: Frau Grams, Frau Riskowsky und Frau Schindler.

Zum Schluss möchte ich noch den wichtigsten Menschen in meinem Leben danken, meiner Familie. Ohne eure Unterstützung wär diese Promotion und vieles Anderes nicht möglich gewesen.